

# **Quantum Annealing With Trigger Hamiltonians**

**Vrinda Mehta**

A thesis presented for the degree of  
Master of Science

Faculty of Mathematics, Computer Science and Natural Sciences,  
Rheinisch-Westfälische Technische Hochschule Aachen

**Prepared in**  
Jülich Supercomputing Center Forschungszentrum Jülich  
**Under the supervision of**  
Prof. Dr. Kristel Michielsen

**Abstract**

Quantum annealing is one of the two standard approaches for devising a quantum computer, where the computation advances from an initial Hamiltonian whose ground state is easy to prepare, to a final Hamiltonian whose ground state encodes the solution to an optimization problem. The aim of this work was to simulate a quantum annealer for 12-Boolean-variable 2-SAT problems having a unique ground state, and a highly degenerate first excited state, and to study the effects of introducing a third Hamiltonian, namely, a trigger Hamiltonian, which vanishes at both the start and the end of the annealing process. For this, two types of trigger Hamiltonians - a ferromagnetic Hamiltonian and anti-ferromagnetic Hamiltonian, were employed. It was found that adding the ferromagnetic trigger always enhanced the performance of quantum annealing by increasing the minimum energy gap between the ground state and the first excited state of the total Hamiltonian. Although adding the anti-ferromagnetic trigger reduced the minimum energy gap for a majority of the problems, the performance was improved for a fraction of the problems as a result of an increase in the number of anti-crossings between the two lowest lying states.

# Contents

<b>1</b>	<b>Introduction</b>	<b>5</b>
<b>2</b>	<b>Theoretical Background</b>	<b>7</b>
2.1	Quantum Computing . . . . .	7
2.2	Optimization Problems and Quantum Annealing . . . . .	8
2.3	Exact Diagonalization . . . . .	9
2.4	Suzuki-Trotter Product Formula . . . . .	10
<b>3</b>	<b>Landau-Zener Tunnelling</b>	<b>13</b>
<b>4</b>	<b>Results for the Original Hamiltonian</b>	<b>19</b>
4.1	The problem set . . . . .	19
4.2	Second-order Suzuki-Trotter Product formula algorithm . . . . .	19
4.3	Selected Problems . . . . .	20
4.4	The Bigger Picture . . . . .	22
<b>5</b>	<b>Results with the Ferromagnetic Trigger</b>	<b>25</b>
5.1	The Selected Problems . . . . .	25
5.2	The Bigger Picture . . . . .	31
<b>6</b>	<b>Results with the Anti-ferromagnetic Trigger</b>	<b>35</b>
6.1	The Selected Problems . . . . .	35
6.2	Trigger Strength $g=0.5$ . . . . .	41
6.3	Trigger strength $g=1$ . . . . .	46
6.4	Trigger Strength $g=2$ . . . . .	57
<b>7</b>	<b>Summary</b>	<b>65</b>
.1	8-spin Problems . . . . .	66
.2	Modelling the energy levels using effective Hamiltonian approach . . . . .	68
.3	Specific 12-spin problems . . . . .	71
	<b>Bibliography</b>	<b>73</b>



# Chapter 1

## Introduction

The idea of quantum computation emerged as early as 1980's with Benioff's proposals for quantum Turing machines and Feynman's suggestion for simulating quantum mechanics [1, 2, 3]. According to Feynman, for describing the full wavefunction for a quantum mechanical system, the number of variables, and hence the computational resources required to simulate the system, pose a limitation for the classical computers. Therefore, a need for a machine that utilizes the effects like superposition and entanglement from the quantum theory arose. A quantum computer is a machine that is expected to be able to utilise the full complexity of a many-particle quantum wavefunction to solve a computational problem [4].

Soon after the conception of a quantum computer, a few algorithms were devised for which quantum computers should offer an advantage over the classical computers, thus motivating the designing of a quantum computer [5]. Some of the well known algorithms are Deutsch-Jozsa algorithm for determining if a given function is constant or balanced [6], Shor's algorithm which can factorise a number only in polynomial time [7], and Grover's search algorithm for finding the unique solution satisfying a unique property [8].

The gate based model for quantum computation, devised by Deutsch in 1989, is considered to be the standard model for quantum computing. In this model every computation is encoded as a sequence of unitary gates, applied to the input state to obtain the desired output, and can, in principle, explore the entire Hilbert space [Albash,Lidar]. A successful implementation of an algorithm usually requires many quantum-bits, and their coherence times to be longer than the time needed for performing the operation. However, the coupling between these quantum-bits and their interaction with the environment, leads to noise in the system, reducing their coherence times. This makes the task of scaling up the number of quantum-bits for implementing any algorithm very challenging [9].

Another standard approach of devising a quantum computer is adiabatic quantum computing, where the computation proceeds from an initial Hamiltonian whose ground state is easy to prepare, to a final Hamiltonian whose ground state encodes the solution to the computational problem [1]. Since in this model, the energy-eigenbasis of the Hamiltonian becomes the relevant basis for computation, quantum adiabatic computation is believed to exhibit a degree of robustness against decoherence [10].

Quantum annealing is a concept related to adiabatic quantum computing which also allows non-ideal situations like non-adiabatic transitions. It has been designed to solve classical optimization problems, with a wide range of applications like classification, quantum chemistry, machine learning, search engine ranking, and protein folding [9].

The focus of this thesis is on simulating a quantum annealer, for solving 12-spin 2-SAT problems, while studying the effects of adding a third term, namely the trigger Hamiltonian, as opposed to two terms (initial and final Hamiltonian) used by D-wave [1, 9, 11, 12, 13].



# Chapter 2

## Theoretical Background

### 2.1 Quantum Computing

Analogous to the digital bits used for classical computation, a quantum computer requires quantum bits, more commonly known as qubits, as the fundamental register. However, unlike the classical bits which can acquire the value of either a 0 or a 1, a qubit state can be a linear superposition of the states  $|0\rangle$  and  $|1\rangle$ , where  $|\rangle$  represents a quantum state in the Dirac notation, i.e.,

$$|\psi\rangle = a_0 |0\rangle + a_1 |1\rangle, \quad (2.1)$$

where  $a_0$  and  $a_1$  are the complex amplitudes such that  $|a_1|^2 + |a_0|^2 = 1$ . According to the principles of quantum mechanics, a measurement of the qubit state then yields either 0, with probability  $|a_0|^2$ , or 1, with probability  $|a_1|^2$ .

In its simplest form, a qubit is therefore a two-level system. A spin-1/2 particle with its two levels being the up spin and the down spin, can naturally be used as a qubit. In this notation, it is conventional to associate the state  $|0\rangle$  with  $|\uparrow\rangle$ , and the state  $|1\rangle$  with  $|\downarrow\rangle$ . The three components of the Pauli matrices corresponding to the spin-1/2 operator  $\mathbf{S}$  spanned by these states are:

$$\sigma_x = \begin{pmatrix} 0 & 1 \\ 1 & 0 \end{pmatrix}, \sigma_y = \begin{pmatrix} 0 & -i \\ i & 0 \end{pmatrix}, \sigma_z = \begin{pmatrix} 1 & 0 \\ 0 & -1 \end{pmatrix},$$

which are then used as the fundamental elements of quantum computing.

For  $N$  such qubits, the basis state is a tensor product of the single-qubit basis states. Since each single state requires two basis vectors, the  $N$ -qubit state comprises of  $L = 2^N$  basis vectors. This constitutes the computational basis  $\{|00\dots0\rangle, |00\dots1\rangle, \dots, |11\dots1\rangle\}$ . Therefore, a general  $N$ -qubit state can be represented as

$$|\psi\rangle = a_0 |00\dots0\rangle + a_1 |00\dots1\rangle + \dots + a_L |11\dots1\rangle, \quad (2.2)$$

which requires  $L$  complex amplitudes for its description.

The computational basis can be more conveniently notated as  $|00\dots0\rangle = |0\rangle$ ,  $|00\dots1\rangle = |1\rangle, \dots, |11\dots1\rangle = |L\rangle$ . In this representation, Eq. (2.2) thus becomes

$$|\psi\rangle = a_0 |0\rangle + a_1 |1\rangle + \dots + a_L |L\rangle. \quad (2.3)$$

Therefore, the Hilbert space spanned by  $N$  qubits is an  $L$ -dimensional space.

Since Pauli matrices, together with the identity operator  $I$ , form a complete basis for the vector space in  $2 \times 2$  matrices, any gate acting on a qubit can be expressed as a linear combination of Pauli matrices. The action of a Pauli matrix,  $\sigma_\alpha$ , where  $\alpha \in \{x, y, z\}$  on the  $j^{th}$  of the  $N$  bits of the basis vector is represented as  $\sigma_\alpha^j$ . Thus, the Pauli operator  $\sigma_\alpha^j$  acting on the general state  $|\psi\rangle$ , given in Eq. (2.2), just acts on the  $j^{th}$  bit of the basis vector, altering the coefficients  $a_0, a_1, \dots, a_L$ . The other bits of the basis vector remain unchanged as a result of being acted upon by identity matrices, given as

$$I = \begin{pmatrix} 1 & 0 \\ 0 & 1 \end{pmatrix}_{i \neq j}.$$

## 2.2 Optimization Problems and Quantum Annealing

Mathematically, an optimization problem comprises of a cost function,  $f_0(\mathbf{x})$  involving  $N$  variables  $x_1, x_2, x_3, \dots, x_N$ , such that  $\mathbf{x} = (x_1, \dots, x_N)$ . The cost function is subjected to multiple constraints  $f_i(x) \leq b_i$ . The goal is then to find a solution  $\mathbf{x}_0$  that minimises (or maximises) the cost function, while satisfying all the constraints.

For satisfiability problems the cost function is written as a Boolean expression in the form of conjunction (a Boolean AND operation) of  $r$  clauses, where each clause is a disjunction (a Boolean OR operation) of  $k$  variables or their negations ( $k$ -SAT problems)[14, 15, 16]. A 2-SAT instance is thus formulated as a Boolean expression where each clause is a disjunction of two literals. The literals,  $L_{i,j}$ , are Boolean variables or their negations. The task is then to find a truth assignment to the Boolean variables that makes the formula  $G = (L_{1,1} \vee L_{1,2}) \wedge (L_{2,1} \vee L_{2,2}) \wedge \dots \wedge (L_{r,1} \vee L_{r,2})$  true. If  $G=1$  then the 2-SAT instance is satisfiable.

Many physically inspired approaches have been adopted to find the solution for the optimization problems. One of the widely used techniques is to encode the problem into the couplings of Ising Hamiltonians [13]. The ground state of this Hamiltonian, corresponding to the state of the minimum energy, then represents the optimal solution of the problem. At low enough temperatures, the system state should eventually relax to the ground state, yielding the required solution.

For finding the optimal solution, the whole spectrum of the Hamiltonian needs to be explored. This requires that the system should be able to escape from a local minimum, if it gets trapped in one, during the course of annealing. The presence of multiple local minima thus makes the determination of the optimal solution harder [17].

The method of simulated annealing was therefore utilised [18], where adding thermal fluctuations to the cost function, keeps the system from getting trapped in the local minima. Yet if the potential barrier becomes very high, this approach may fail. It was in this spirit that the technique of quantum annealing was first employed by B.Apolloni, C.Carvalho and D.de Falco in 1988 [19], wherein quantum fluctuations were used in place of thermal fluctuations. By making use of the quantum tunnelling effect, this approach can still allow for the search of global minima as the system state can tunnel between the local minima [1].

The cost function is mapped onto the Ising model, making use of the external magnetic field  $h_i^z$  and the spin couplings  $J_{ij}^z$  of the model, and thus has the following form:

$$H_P = - \sum_{i=1}^N h_i^z \sigma_i^z - \sum_{\langle i,j \rangle} J_{ij}^z \sigma_i^z \sigma_j^z, \quad (2.4)$$

where  $\sigma_i^z$  denotes the z component of Pauli-spin matrix acting on the  $i^{th}$  spin, and the set  $\langle i,j \rangle$  represents the set of pairwise couplings.

The recipe for the annealing algorithm consists of starting with an initial Hamiltonian  $H_I$ , whose ground state can be easily determined and realised. Most commonly used is the transverse field Hamiltonian:

$$H_I = - \sum_{i=1}^N h_i^x \sigma_i^x. \quad (2.5)$$

The ground state of  $H_I$  is therefore the uniform superposition state:

$$|\psi\rangle = \frac{1}{(\sqrt{2})^N} (|0\rangle + |1\rangle)_1 \otimes (|0\rangle + |1\rangle)_2 \otimes \dots \otimes (|0\rangle + |1\rangle)_N. \quad (2.6)$$

The Hamiltonian is then slowly swept towards the problem Hamiltonian, with the means of an annealing parameter, say  $s$ , defined as  $s(t) = t/T_A$ , where  $t$  is the instantaneous time, and  $T_A$  is the total annealing time. The Hamiltonian,  $H(t)$ , corresponding to the most straightforward annealing scheme, is then given by:

$$H(t) = (1 - s(t))H_I + s(t)H_P. \quad (2.7)$$

Therefore, the Hamiltonian transitions from the initial Hamiltonian,  $H(t = 0) = H_I$  to the final Hamiltonian,  $H(t = T_A) = H_P$ .

According to the **quantum adiabatic theorem**, the instantaneous state of the system stays close to the ground state of the Hamiltonian  $H(t)$ , if one starts with the ground state of the initial Hamiltonian and if the driving from

the initial Hamiltonian to the problem Hamiltonian is slow enough, which is determined by the minimum energy gap,  $\Delta_{min}$ , between the ground state and the first excited state of the Hamiltonian  $H(t)$  during the course of annealing [20, 21]. Mathematically, adiabatic theorem of evolution holds when

$$T_A \gg \Delta_{min}^{-2}, \quad (2.8)$$

where  $T_A$  is the total annealing time. Therefore, the performance of quantum annealing depends strongly on the minimum energy gap.

Thus, the problem of finding the optimal solution reduces to the problem of solving the time dependent Schrödinger equation for the resulting  $H(t)$  (see Eq. 2.7):

$$i \frac{\partial}{\partial t} |\psi\rangle = H(t) |\psi\rangle. \quad (2.9)$$

However, the process of evolution, starting from the trivial ground state of the initial Hamiltonian and going to a non-trivial ground state of the problem Hamiltonian, may be accompanied by a quantum phase transition. Such a transition is characterized by a vanishing energy gap in the thermodynamic limit. For the problems which are considered to be difficult, the minimum gap is found to close exponentially as a function of the system size, i.e.,  $\Delta_{min} \propto e^{-cN}$ , for a positive constant  $c$  and  $N$  number of spins. This suggests that the annealing time required to ascertain that the evolution is adiabatic also grows exponentially,  $T_A \propto e^{2cN}$ . On the other hand, if the gap closes polynomially ( $\Delta_{min} \propto N^{-l}$ , for a positive constant  $l$ ), the computation time is also polynomial,  $T_A \propto N^{2l+1}$ , and the problem is considered easy [9].

Therefore, the dependence of the minimum energy gap on the size of the system determines the annealing time required to make the evolution of the state of the system to be adiabatic. Thus, one method of improving the performance of quantum annealers is by controlling the closing of the gap. Altering the annealing scheme is believed to be one of the ways by which this can be achieved [1, 9, 11, 12, 13]. In this work we aim to achieve the same by including a third Hamiltonian, a trigger Hamiltonian -  $H_T$  in the time dependent Hamiltonian  $H(t)$  (see Eq. 2.7)[1, 11, 12, 13]. The trigger Hamiltonian should vanish at both the start and end of the annealing process, so that one can still start with the easily realizable ground state of the initial Hamiltonian, and the resulting state of the problem Hamiltonian remains unaffected. The Hamiltonian thus takes the form:

$$H(t) = (1 - s(t))H_I + gs(t)(1 - s(t))H_T + s(t)H_P, \quad (2.10)$$

where parameter  $g$  controls the strength of the added trigger.

In this thesis we deal with two types of trigger Hamiltonians - a ferromagnetic trigger (F) and an anti-ferromagnetic trigger (A)[13], defined as

$$H_T^F = - \sum_{\langle i,j \rangle} \sigma_i^x \sigma_j^x, \quad (2.11)$$

and

$$H_T^A = + \sum_{\langle i,j \rangle} \sigma_i^x \sigma_j^x, \quad (2.12)$$

with the same pairwise coupling set  $\langle i,j \rangle$  as for the problem Hamiltonian. Equivalently, the trigger can also be chosen to have the form  $\pm \sum_{\langle i,j \rangle} \sigma_i^y \sigma_j^y$ . As will be seen in the following chapters, adding these triggers alters the energy spectrum considerably, which in turn affects the overlap of the final state with the ground state in different ways.

The following sections focus on two approaches that have been used in this work to solve the time-dependent Schrödinger equation. The Suzuki-Trotter product formula has been adopted to track the evolution of the state, and to compute the overlap of the final state with the already determined ground state of the problem Hamiltonian. The full diagonalization method, on the other hand, has been used to calculate the errors involved in using the Suzuki-Trotter approximation, and to determine the energy spectra and minimum gaps for  $H(t)$  for  $t \in [0, T_A]$ , where  $T_A$  is the total annealing time.

## 2.3 Exact Diagonalization

This method consists of determining the eigenvalues and eigenvectors of the Hamiltonian matrix, which is an  $L \times L$  ( $2^N \times 2^N$ ) matrix, at each time step.

For constructing the Hamiltonian matrix at time step  $t \in [0, T_A]$ , all the basis vectors in the computational basis are acted upon by the instantaneous Hamiltonian, given by Eq. (2.10). The action of the Hamiltonian on the  $i^{th}$  basis vector corresponds to the  $i^{th}$  column of the Hamiltonian matrix, e.g. for  $|\psi\rangle = (1, 0, \dots, 0)^T$ ,  $H|\psi\rangle$  gives the first column of the Hamiltonian matrix.

The resulting matrix is then diagonalized to obtain the eigenvalues  $\Lambda$ , and unitary matrix of the eigenvectors,  $V$ . Since  $V^\dagger H V = \Lambda$ , the unitary evolution operator  $U(t) = e^{-itH} = V e^{-it\Lambda} V^\dagger$ .

This approach, however, has some serious limitations. First, the memory requirement to store the Hamiltonian matrix grows as  $\mathcal{O}(2^{2N})$  with the number of qubits  $N$ . Additionally, full diagonalization takes  $\mathcal{O}(2^{3N})$  floating-point operations [22]. Therefore, this method is rendered impractical for solving the time dependent Schrödinger equation for systems more than 20 qubits.

## 2.4 Suzuki-Trotter Product Formula

For solving the TDSE (see Eq. 2.9), one needs to evaluate the unitary matrix exponentials of the evolution operator,  $U(t)$  given as:

$$U(t) = e^{-itH} = e^{-it(H_1 + \dots + H_K)} = \lim_{m \rightarrow \infty} \left( \prod_{k=1}^K e^{-itH_k/m} \right)^m. \quad (2.13)$$

In this work, the Lie-Trotter-Suzuki product formula [22, 23, 24] is employed to construct unitary approximations to the evolution operator. Defining  $\tau$  as  $t/m$ , to be the time step at which the evolution operator is applied, a repeated application of  $U(\tau)$  yields  $U(t)$ . For a sufficiently small time step  $\tau$ , the first order approximation for  $U(t)$  in Eq. (2.13) is

$$\tilde{U}_1(\tau) = e^{-i\tau H_1} \dots e^{-i\tau H_K}, \quad (2.14)$$

which holds good if  $\tau \|H_i\| \ll 1$  for all  $i=1, \dots, K$ .

For an improved accuracy, a second order approximation is made to  $U(t)$  in Eq. (2.13), using  $\tilde{U}_1(\tau)$  from Eq. (2.14):

$$\tilde{U}_2(\tau) = \tilde{U}_1^\dagger(-\tau/2)\tilde{U}_1(\tau/2) = e^{-i\tau H_K/2} \dots e^{-i\tau H_1/2} e^{-i\tau H_1/2} \dots e^{-i\tau H_K/2}. \quad (2.15)$$

Since  $\tilde{U}_1(\tau)$  is unitary, as all  $H_k$  in Eq. (2.13) are Hermitian,  $\tilde{U}_2(\tau)$  is also unitary. The measure of error, calculated using the 2-norm of the difference between  $U(\tau)$  and  $\tilde{U}_2(\tau)$ , grows cubically in  $\tau$  [22, 25, 26], i.e.

$$\|U(\tau) - \tilde{U}_2(\tau)\| \leq c\tau^3 \quad (2.16)$$

for a positive constant  $c$ . Since the whole annealing process requires  $m$  such time steps, the involved error becomes

$$\|U(t) - \tilde{U}_2(m\tau)\| \leq mc\tau^3. \quad (2.17)$$

Since  $m\tau = t$ , (2.17) is equivalent to

$$\|U(t) - \tilde{U}_2(m\tau)\| \leq ct\tau^2. \quad (2.18)$$

The Hamiltonian  $H(t)$  is then decomposed as follows:

$$H = H_{single} + H_x + H_y + H_z, \quad (2.19)$$

where  $H_{single} = -(1-s)\sum_{i=1}^N (h_i^x \sigma_i^x) - s(\sum_{i=1}^N \sigma_i^z)$ ,  $H_x = \mp(1-s)(\sum_{\langle i,j \rangle} \sigma_i^x \sigma_j^x)$ ,  $H_y = \mp(1-s)(\sum_{\langle i,j \rangle} \sigma_i^y \sigma_j^y)$ , and  $H_z = -s(\sum_{\langle i,j \rangle} \sigma_i^z \sigma_j^z)$ . In general, we have

$$e^{i\mathbf{v} \cdot \boldsymbol{\sigma}} = \cos(v)I + i\frac{\sin(v)}{v}\mathbf{v} \cdot \boldsymbol{\sigma}, \quad (2.20)$$

where  $I$  represents the identity matrix, and  $v = \sqrt{v_x^2 + v_y^2 + v_z^2}$ . Then,

$$e^{-itH_{single}} = \prod_{i=1}^N e^{it[(1-s)\sum_i h_i^x \sigma_i^x + s\sum_i h_i^z \sigma_i^z]} = \prod_{i=1}^N \begin{pmatrix} \cos(th_i) + i\frac{sh_i^z}{h_i} \sin(th_i) & i\frac{(1-s)h_i^x}{h_i} \sin(th_i) \\ i\frac{(1-s)h_i^x}{h_i} \sin(th_i) & \cos(th_i) - i\frac{sh_i^z}{h_i} \sin(th_i) \end{pmatrix} \quad (2.21)$$

where  $h_i = \sqrt{(1 - s(t))^2 h_i^{x^2} + s(t)^2 h_i^{z^2}}$ .

The computational basis states are the eigenstates of the Pauli-z operator,  $\sigma_z^i$ . Thus  $e^{-itH_z}$  is a diagonal matrix in the computational basis, and its action on the input state changes the phase of each of the basis vectors. As  $H_z$  is a sum of pair interactions, it is trivial to implement this operation [22].

The same approach can be adopted for implementing  $H_x$  operations as well, by using the rotation operators  $Y_j$  as follows. Writing  $Y = \prod_{i=1}^N Y_i$ , we obtain

$$e^{-itH^x} = \bar{Y} Y e^{-itH^x} \bar{Y} Y = \bar{Y} e^{it \sum_{\langle i,j \rangle} J_{ij}^x \sigma_i^x \sigma_j^x} Y. \quad (2.22)$$

This completes the specifications required to solve the TDSE.



# Chapter 3

## Landau-Zener Tunnelling

The Landau-Zener model describes the response of the magnetization of a 2-level spin system, under the action of a slowly reversing external magnetic field at zero temperature [27, 28, 29]. Consider, the following single spin-1/2 Hamiltonian as an example:

$$H_{LZ}(t) = -\Gamma\sigma_x - ct\sigma_z, \quad (3.1)$$

where  $\Gamma$  sets the scale of the splitting between the two energy levels, and  $c$  is the sweep rate of the applied magnetic field, i.e  $H(t) = ct$ . Thus for a field switching its value from  $-H_0$  to  $H_0$  in time  $T$ ,  $c = \Delta H/T = 2H_0/T$ .

Now, for large negative times  $t$ , and  $|H(t)| \geq |\Gamma|$ ,  $H_{LZ}(t) \approx ct\sigma_z$ . Thus, the spin-down state,  $|\downarrow\rangle$ , is close to the ground state of the Hamiltonian, as  $ct\sigma_z|\downarrow\rangle = -ct|\downarrow\rangle$ . As  $t$  goes to infinity,  $H_{LZ}(t) \approx -ct\sigma_z$ , so that the ground state now lies close to the spin up state,  $|\uparrow\rangle$ , as  $-ct\sigma_z|\uparrow\rangle = -ct|\uparrow\rangle$ . According to the quantum adiabatic theorem, the state of the system should always lie close to the instantaneous ground state of the Hamiltonian  $H(t)$ , if one starts with the ground state and if the field is changed slowly enough. However, there is a finite probability that the state transits to a higher excited level during the sweep. The probability,  $p'$ , for this non-adiabatic transition (Landau-Zener tunnelling), as given by the Landau-Zener formula, is

$$p' = \exp\left(\frac{-\pi\Gamma^2}{c}\right). \quad (3.2)$$

Therefore, the probability,  $p$ , that the state of the system follows the instantaneous ground state of the Hamiltonian adiabatically, by changing the magnetization state of the system, in accordance to the reversing field,  $H(t)$ , is [27, 28, 29, 30].

$$p = 1 - p' = 1 - \exp\left(\frac{-\pi\Gamma^2}{c}\right). \quad (3.3)$$

If the minimum energy splitting between the ground state and the first excited state of the Hamiltonian at the anti-crossing is denoted by  $\Delta_{min}$ , then it can be observed that  $\Delta_{min} = 2\Gamma$ . Thus, in terms of  $\Delta_{min}$ , Eq. (3.4) becomes

$$p = 1 - \exp\left(\frac{-\pi\Delta_{min}^2}{4c}\right). \quad (3.4)$$

The deviation from the ground state occurs at  $H \approx 0$ , with a probability  $p'$ , and is accompanied by a step in the magnetization. This step depends on both the energy splitting  $\Delta_{min}$ , and the sweep rate  $c$  [29].

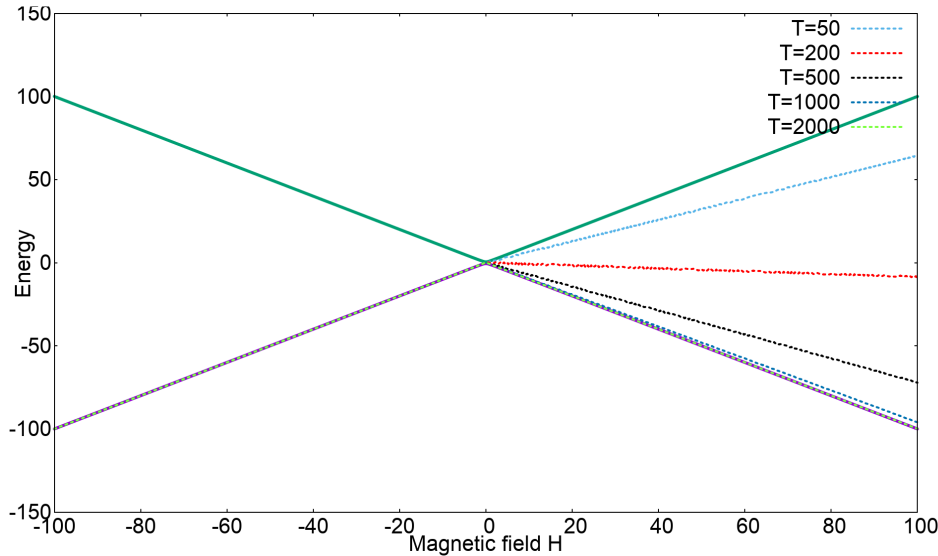


Figure 3.1: Energy spectrum for single qubit Hamiltonian in Eq. (3.1), with energy expectation values of the instantaneous state of the system with different sweeping times. The parameters used are  $\Gamma = 0.5$ ,  $H_0 = 100$ .

For a simple 2-level system where  $\Gamma$  is chosen to be 0.5 and the field is swept from a value from -100 to 100, Fig. (3.1) gives the energy spectra for the Hamiltonian in Eq. (3.1). Figure (3.1) also shows the energy expectation values corresponding to the instantaneous state of the system for different times  $T$  chosen for sweeping the field. As is evident from the figure, the probability of the state of the system staying close to the ground state increases with decreasing speed (increasing  $T$ ), as expected from Eq. (3.3). For a sweeping time of  $T=500$ , Fig. (3.2) shows the instantaneous magnetization state of the system.

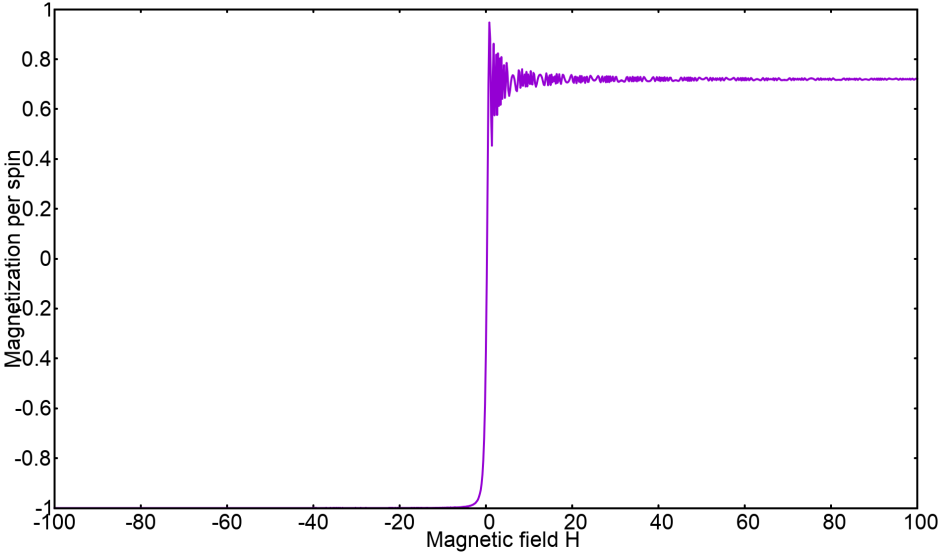


Figure 3.2: Instantaneous magnetization of the system state for  $\Gamma = 0.5$ ,  $H_0 = 100$ ,  $T=500$  and  $c=0.4$ .

Comparing Figs. (3.1) and (3.2), it can be observed that the step in the magnetization corresponds to the position of the anti-crossing between the ground state and the first excited state in the energy spectrum.

For verifying Eq. (3.3), the overlap of the resulting state was computed with the ground state of the Hamiltonian, for different sweeping times. Figure (3.3) shows the result obtained.

From Eq. (3.3),  $p = 1 - e^{-aT}$ , where  $a = \pi\Gamma^2/2H_0$ . For the chosen parameters,  $a$  was calculated to be  $3.926 \times 10^{-3}$ . This value was found to be in reasonable agreement with the value  $3.198 \times 10^{-3}$ , obtained for the

fitting parameter in Fig. (3.3). The difference in the two values could be arising due to the magnetic field not being large enough, as is required by the theory.

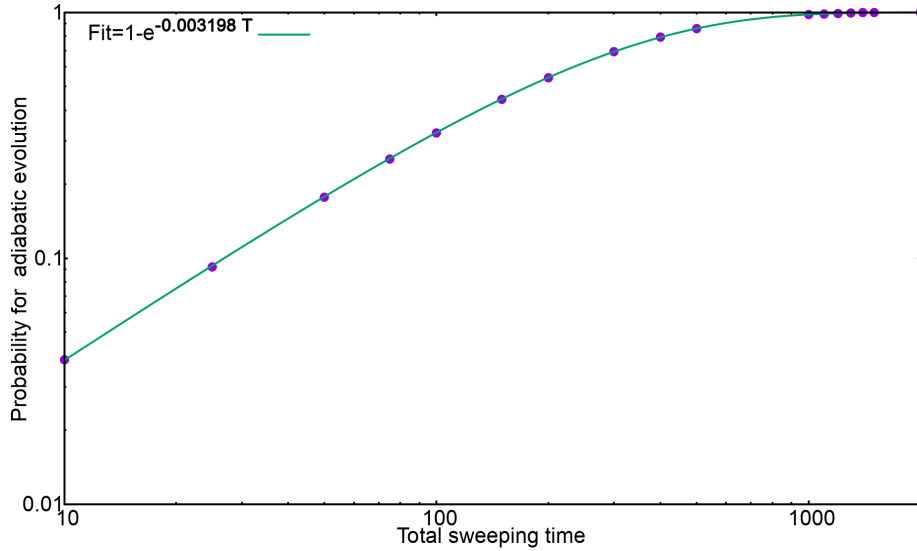


Figure 3.3: Probability for adiabatic evolution as a function of different sweep times for  $\Gamma = 0.5$ .

Although in both Quantum annealing and the Landau-Zener model one deals with time dependent Hamiltonians, and the main task consists of studying the evolution of the state of the system under its action, there are two major points of difference. The Landau-Zener formula is applicable to 2-level systems, and the process of reversing the magnetic field is ideally carried over an infinite amount of time. On the other hand, the Ising Hamiltonian considered for quantum annealing generally consists of more than two energy levels, and the evolution is carried out for a limited time, i.e. from  $s=0$  to  $s=1$  in terms of the annealing parameter:  $s = t/T_A$ , where  $T_A$  is the total annealing time.

Despite these differences, the Landau-Zener formula can be used to predict the probability of an adiabatic evolution for an Ising model, by making use of some approximations [31]. The Ising model in a transverse field involving  $N$  variables is one of the simplest microscopic models for uniaxial magnets. Consider, for example, the Hamiltonian

$$H = -J \sum_{\langle i,j \rangle} \sigma_i^z \sigma_j^z - \Gamma \sum_i \sigma_i^x - H(t) \sum_i \sigma_i^z, \quad (3.5)$$

where set  $\langle i,j \rangle$  defines the interactions between pairs of spins in the cluster. For a uniaxial magnet, only the lowest two levels are important for the adiabatic motion of the ground state. The scattering from the ground state to the first excited state occurs only when these levels come close, at the point of anti-crossing, i.e. around  $H=0$ . The dependence of energy on  $H$  around the anti-crossing is expected to be approximately expressed as the eigenvalue of the two level system:

$$(M_0 H \sigma^z - \Gamma \sigma^x) |\psi\rangle = E(H) |\psi\rangle, \quad (3.6)$$

where  $M_0$  is a saturated magnetization at high field. In the case of a strong uniaxial magnet,  $M_0 = N$ . The probability for the system state to follow the ground state adiabatically then becomes

$$p_N = 1 - \exp\left(\frac{-\pi \Delta_{min}^2}{4Nc}\right). \quad (3.7)$$

Choosing a two spin system, with  $\Gamma = 0.5$ ,  $J = 3$ , and  $H_0 = 100$ , Fig. (3.4) shows the energy spectrum as a function of the magnetic field.

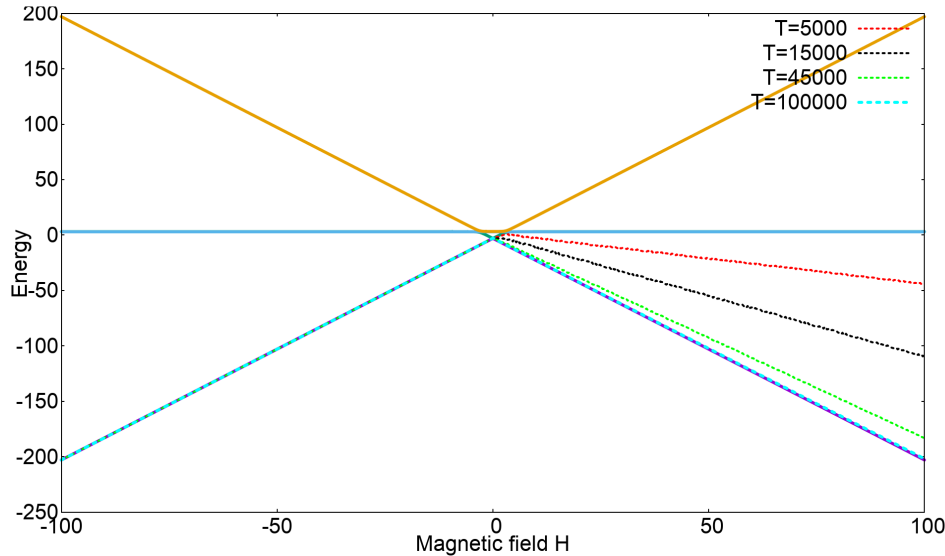


Figure 3.4: Energy spectrum for two spin Hamiltonian in Eq. (3.5), with energy expectation value of the instantaneous state of the system with different sweeping times. The parameters used are  $\Gamma = 0.5$ ,  $J = 3$ ,  $H_0 = 100$ .

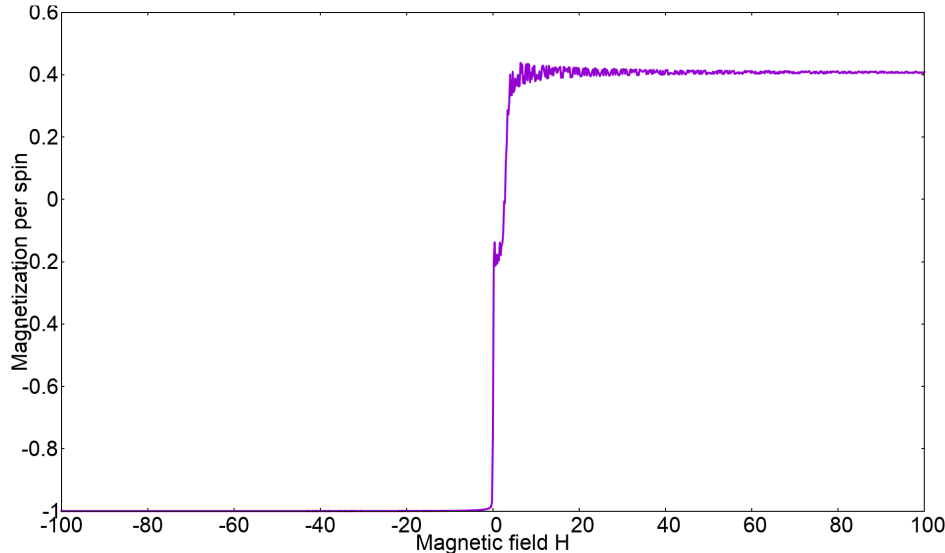


Figure 3.5: Instantaneous magnetization of the system state for  $\Gamma = 0.5$ ,  $H_0 = 100$ ,  $T=10000$  and  $c=0.02$ .

Figures (3.5) and (3.6) show the instantaneous magnetization values for two different sweep rates, corresponding to  $T=10000$  and  $T=20000$  respectively. Similar to the case of a single spin Hamiltonian, the steps in the magnetization values correspond to the position of anti-crossing between the energy levels of the spectrum, in this case as well. Other than the first step in the magnetization at  $H \approx 0$ , in this case, the second step corresponds to the anti-crossing between the first and the second excited state of the Hamiltonian.

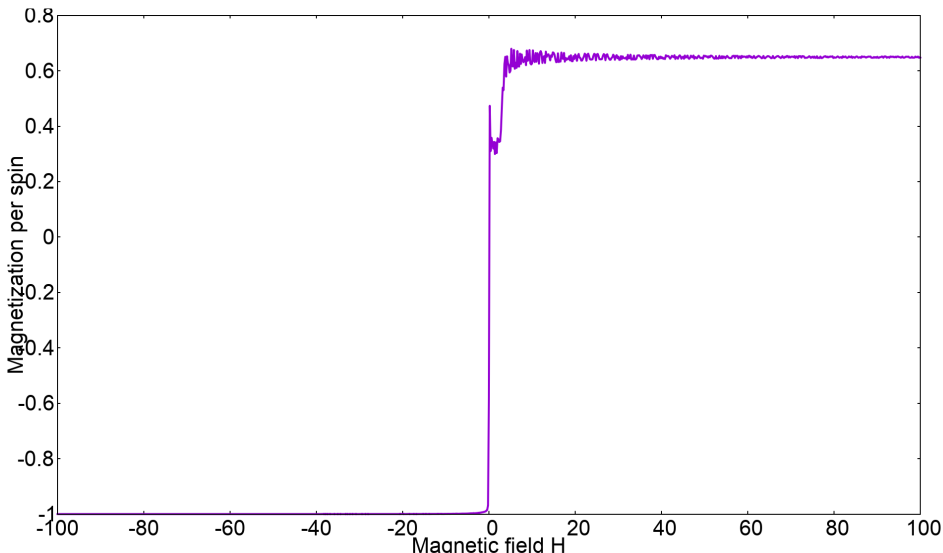


Figure 3.6: Instantaneous magnetization of the system state for  $\Gamma = 0.5$ ,  $H_0 = 100$ ,  $T=20000$  and  $c=0.01$ .

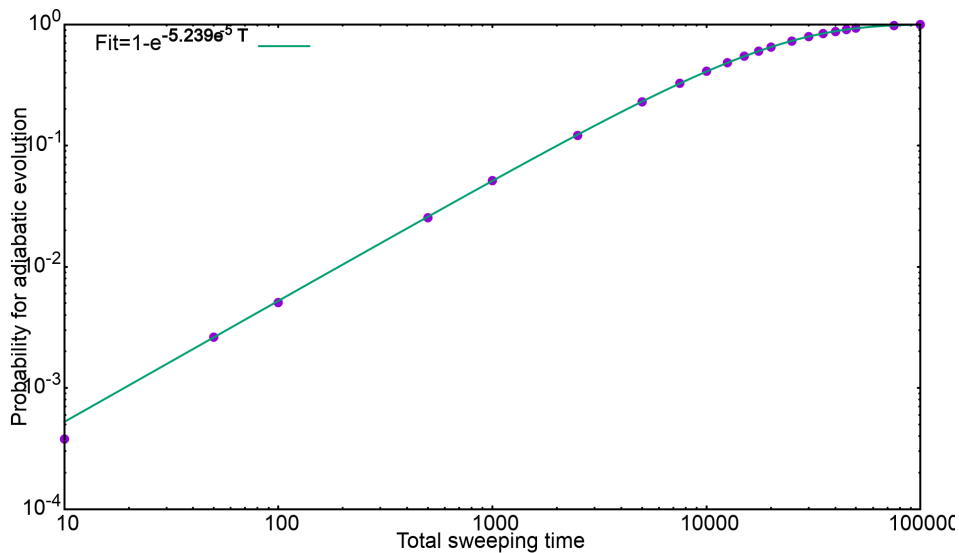


Figure 3.7: Probability for adiabatic evolution as a function of different sweep times for  $\Gamma = 0.5$  and  $J = 3$ .

On increasing the total time for sweeping the field, i.e. decreasing the sweeping speed, the probability of staying in the ground state, by changing the state of magnetization should increase. This can be confirmed by comparing Figs. (3.5) and (3.6).

Finally, for verifying Eq. (3.7) the overlap of the resulting state with the ground state is computed for different times. Results obtained are shown in Fig. (3.7).

The value of the minimum gap,  $\Delta_{min}$  obtained was 0.162, which results in  $a = \pi\Delta_{min}^2/8\Delta H = 5.182 \times 10^{-5}$ . The value of the fitting function obtained in Fig. (3.7) is  $5.239 \times 10^{-5}$ . Thus, the Landau-Zener formula can be extended to the  $N$ -spin Ising Hamiltonian with the approximations.

Equation (3.7) will be used again as a check for adiabatic evolution in the subsequent chapters.



# Chapter 4

## Results for the Original Hamiltonian

### 4.1 The problem set

For this work, we deal with 8-spin and 12-spin 2-SAT problems. The first set had 91 unique problems, while the second set had 1000 such problems. These problems were numbered from 1-1000 in case of the 12-spin problems, and 1-91 in case of the 8-spin problems. All the problems had a predetermined unique ground state, a highly degenerate first excited state, and only one avoided crossing between the ground and the first excited states. All the 8-spin problems had 9 pair-wise couplings, while the 12-spin problems had 13 such couplings. The success probability is then obtained by calculating the overlap between the known ground state and the state resulting from the code performing product evolution. Furthermore, for determining the energy spectra for specific problems, exact diagonalization method was employed.

For every problem belonging to the two sets, three annealing times are chosen to calculate the success probability. These correspond to  $T_A \in \{10, 100, 1000\}$ . This chapter focusses on the results obtained for the original Ising Hamiltonian, i.e. in the absence of any triggers. All the results corresponding to the problems of the 8-spin set are shown in the appendix.

### 4.2 Second-order Suzuki-Trotter Product formula algorithm

Since the Suzuki-Trotter product-formula algorithm is an approximation to solve the TDSE, the numerical error  $\|U(t) - \tilde{U}_2(m\tau)\|$  depends on the time step at which the evolution is computed,  $\tau$  (see Eq. 2.18). Thus, to check if the evolution using the Suzuki-Trotter product formula algorithm is indeed second order, the dependence of the error should be verified to be quadratic in  $\tau$ , in accordance with Eq. (2.18).

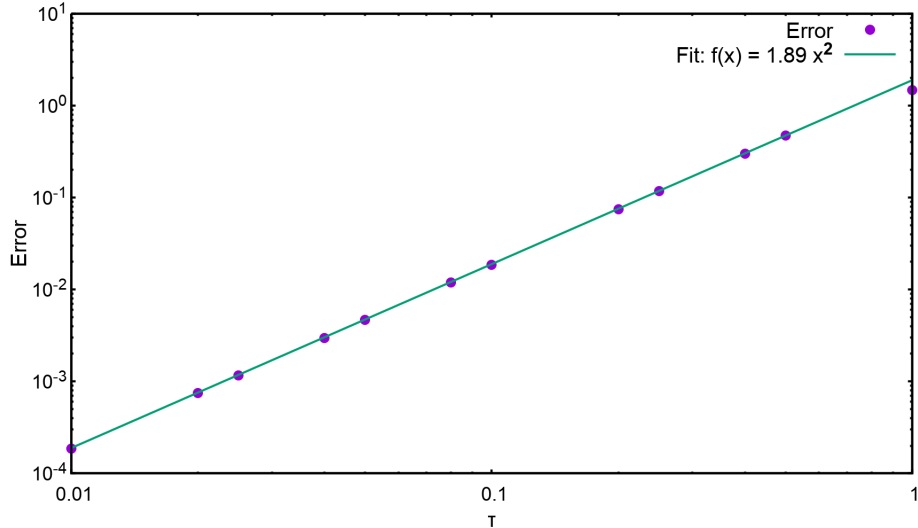


Figure 4.1: The error in the Suzuki-Trotter formula algorithm relative to the full diagonalization method. The involved error grows quadratically in  $\tau$ .

Since the dependence of the error on  $\tau$  can be approximated to be linear in the log scale, as shown in Fig. (4.1), the simulation implementing TDSE can be trusted to be following the second order Suzuki-Trotter product formula algorithm.

### 4.3 Selected Problems

For a fixed  $T_A$ , the success probability is expected to decrease with decreasing  $\Delta_{min}$ , if the evolution of the state is close to adiabatic. In this section, three problems, with distinct minimum energy gaps and success probabilities are selected from the set of 12-spin problems, and their dynamics is studied.

As the first example, considered here is problem number 733, that has a high success probability. Figure (4.2), shows the energy spectrum for this problem.  $\Delta_{min}$  is 0.4407 in this case. Also plotted in the figure are the energy expectation values for the instantaneous state obtained for the three annealing times.

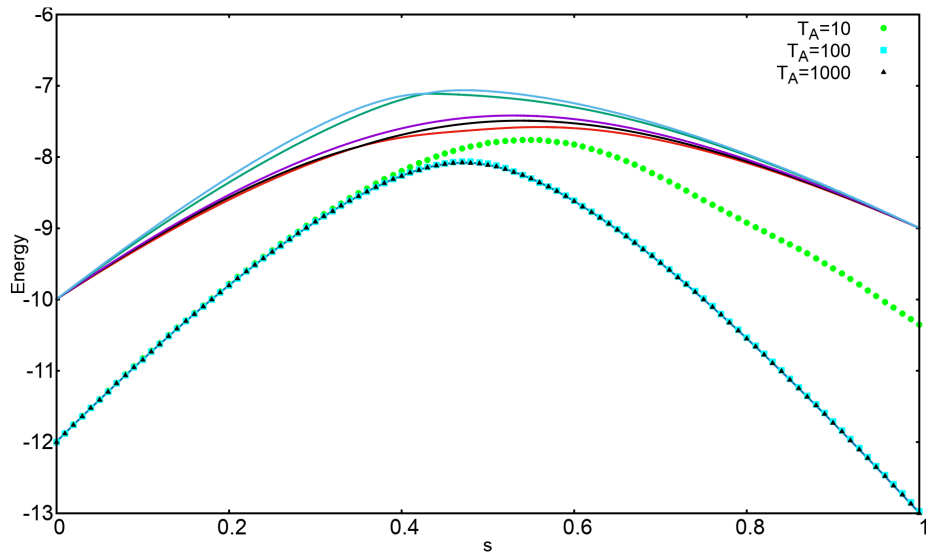


Figure 4.2: The energy spectrum for problem 733, with energy expectation values for the instantaneous state.  $\Delta_{min}$  is found to be 0.4407.

As expected, the overlap of the final state with the ground state of the problem Hamiltonian increases on increasing the total annealing time in Fig. (4.2). Annealing times  $T_A=10, 100, 1000$  yield  $p=0.3444, 0.9944, 0.9999$  respectively.

Secondly, problem number 950, with a small success probability is chosen. Figure (4.3) shows the energy spectrum and the energy expectation values for the instantaneous state corresponding to three annealing times, for this problem. Annealing times  $T_A=10, 100, 1000$  yield  $p=0.0002, 0.0146, 0.1362$  respectively. It should be noted, that the minimum gap for this problem is much smaller than in problem 733, and has a value of  $\Delta_{min} = 0.0312$ . This explains the decrease in success probability for the same annealing times.

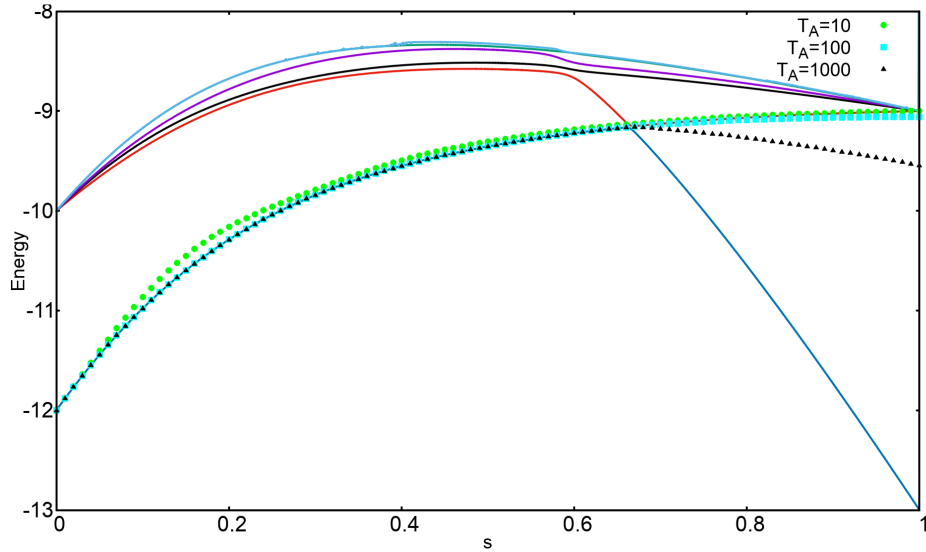


Figure 4.3: The energy spectrum for problem 950, with energy expectation values for the instantaneous state.  $\Delta_{min}$  is found to be 0.0312.

As the final case, problem number 528, with an intermediate success probability is studied. For this case too, the energy spectrum and the energy expectation values for the instantaneous state, corresponding to the three annealing times were determined, as is shown in Fig. (4.4). Annealing times  $T_A=10, 100, 1000$  yield  $p=0.1577, 0.5199, 0.9999$  respectively. The value of the minimum gap is  $\Delta = 0.1573$  for this problem, which is intermediate to the above two cases.

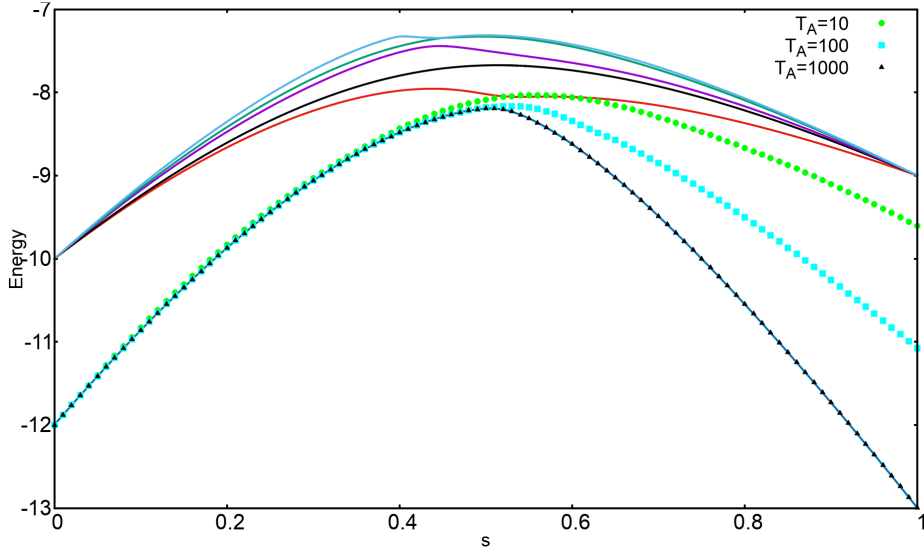


Figure 4.4: The energy spectrum for problem 528, with energy expectation values for the instantaneous state.  $\Delta_{min}$  is found to be 0.1573.

Thus, for all the three problems, the state of the system deviates from the ground state of the Hamiltonian when the annealing time is not long enough as required by the minimum energy gap of the problem for ensuring the evolution of the state to be strictly adiabatic. In all such cases, the system state deviates from the ground state only at the energy anti-crossing between the ground state and first excited state of the Hamiltonian. As the annealing time is increased, the part of the amplitude in the ground state that is shifted to the higher states gets smaller, thus increasing the success probability.

#### 4.4 The Bigger Picture

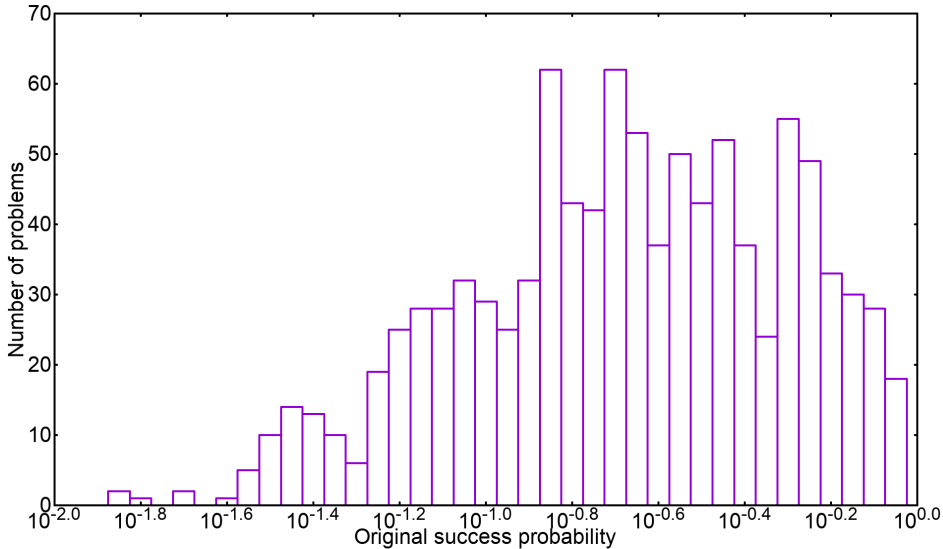


Figure 4.5: Histogram for the success probability of the Hamiltonians without any triggers ( $g=0$ ) for 1000 12-spin problems for  $T_A=100$ .

We now focus on the entire set of the 12-spin problems to understand the performance of the quantum annealing algorithm with the original Hamiltonians (i.e. for  $g=0$ ).

To obtain a rough estimate of the spread of the difficulty of the problems considered in this work, Fig. (4.5) shows a

plot of the distribution of the success probabilities for all the problems in the set. The range of the success probability is from 0.014 for the most difficult cases, to 1 for the relatively easier cases. The mean success probability was found to be 0.208. Finally, Fig. (4.6) shows the success probability of all the 12-spin problems with the corresponding minimum energy gaps.

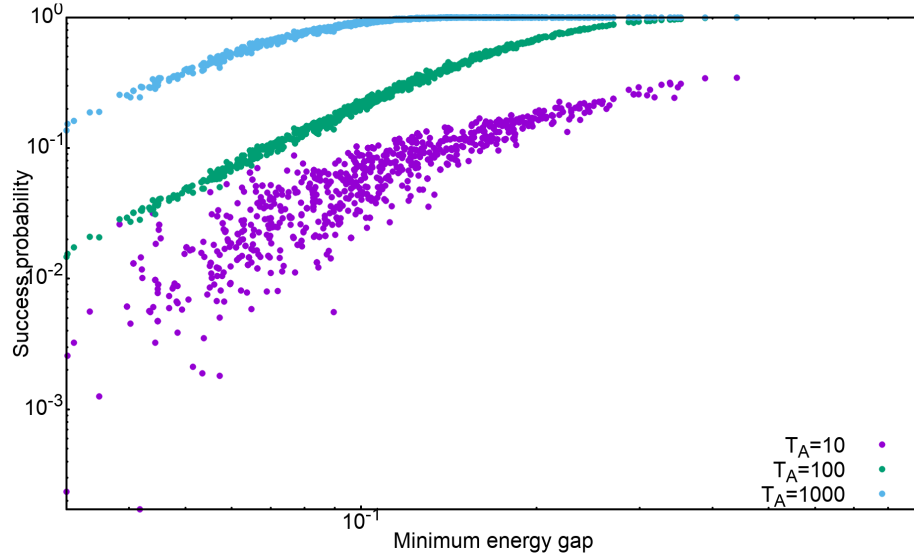


Figure 4.6: Success probability versus minimum energy gaps for all the 12-spin problems for annealing times 10, 100 and 1000.

From Eq. (3.7), the success probability should have the Landau-Zener dependence on the minimum energy gap between the ground and first excited state of the Hamiltonian, if the evolution of the state is close to adiabatic. Since different problems belonging to the set may have different values of  $\Delta_{min}$ , the success probability for each problem, plotted against the respective minimum energy gap for a fixed annealing time, can give an estimate of the fraction of problems undergoing nearly adiabatic evolution. The more is the scattering in the resulting curve, the larger is the fraction of problems involving non-adiabatic mechanisms during the evolution. It can therefore be noted in Fig. (4.6) that for  $T_A=10$ , the scattering is significantly larger than in the other two cases. It should additionally be observed that as the annealing time is increased, the success probability for a specific problem becomes systematically larger. This suggests that as the annealing time is increased, the evolution of the state keeps getting closer to adiabatic, as naively expected.



# Chapter 5

# Results with the Ferromagnetic Trigger

As mentioned in previously, in the course of this thesis we study two trigger Hamiltonians. This chapter focuses on the performance of quantum annealing algorithm upon adding the ferromagnetic trigger,  $H_T^F$  (see Eq. 2.11) to the Ising Hamiltonian.

For the same transverse-field initial Hamiltonian, and each problem from the set of problem Hamiltonians, ferromagnetic trigger was added with three different strengths, i.e. the strength parameter,  $g$  in Eq. (2.10) was chosen to be 0.5, 1 and 2.

We begin by studying the dynamics of the same cases as chosen in the previous chapter, to understand the effects of adding the ferromagnetic trigger. In the subsequent sections, the effects of adding the ferromagnetic trigger with different strengths will be discussed.

## 5.1 The Selected Problems

We start with problem 733 having a large success probability in case of the original Hamiltonian. Figure (5.1) shows the energy spectra for this problem upon adding the ferromagnetic trigger with strengths 0.5, 1 and 2 for all the three annealing times. The corresponding energy expectation values for the instantaneous state have also been included in these plots.

From these figures, it can be noted that compared to the original Hamiltonian, the minimum gap,  $\Delta_{min}$  has increased in all the three cases. Furthermore,  $\Delta_{min}$  becomes larger as the strength of the trigger Hamiltonian is increased from 0.5 to 2.

Secondly, the position of  $\Delta_{min}$  is shifted more rightwards upon increasing the strength. Moreover, all the success probabilities upon adding the trigger are larger than the success probability of the original Hamiltonian, owing to the increase in the minimum gaps. In general, the success probability also increases with increasing the strength of the trigger, though the final overlap also depends on the exact energy spectrum.

Table (5.1) shows a comparison of the minimum energy gaps and success probabilities for problem 733, before and after adding the trigger.

Problem 733	Original Hamiltonian	Trigger=F, $g=0.5$	Trigger=F, $g=1$	Trigger=F, $g=2$
$\Delta_{min}$	0.4407	0.5779	0.6908	0.8333
$p(T_A = 10)$	0.3444	0.4764	0.5298	0.5222
$p(T_A = 100)$	0.9944	0.9996	0.9998	0.9997
$p(T_A = 100)$	0.9999	0.9999	0.9999	0.9999
value of $s$ at $\Delta_{min}$	0.459	0.552	0.629	0.733

Table 5.1: A comparison of the minimum energy gaps and the success probabilities for  $T_A=100$ , between the original Hamiltonian for problem 733 and that after adding the ferromagnetic trigger (F) with different strengths. The minimum gaps become larger as the strength of the ferromagnetic trigger is increased. As a result, the success probabilities are increased. The value of  $s$  corresponding to the position of the minimum gap also becomes larger.

Next, we focus on problem 950, which has a small success probability for the original Hamiltonian. Figure (5.2))

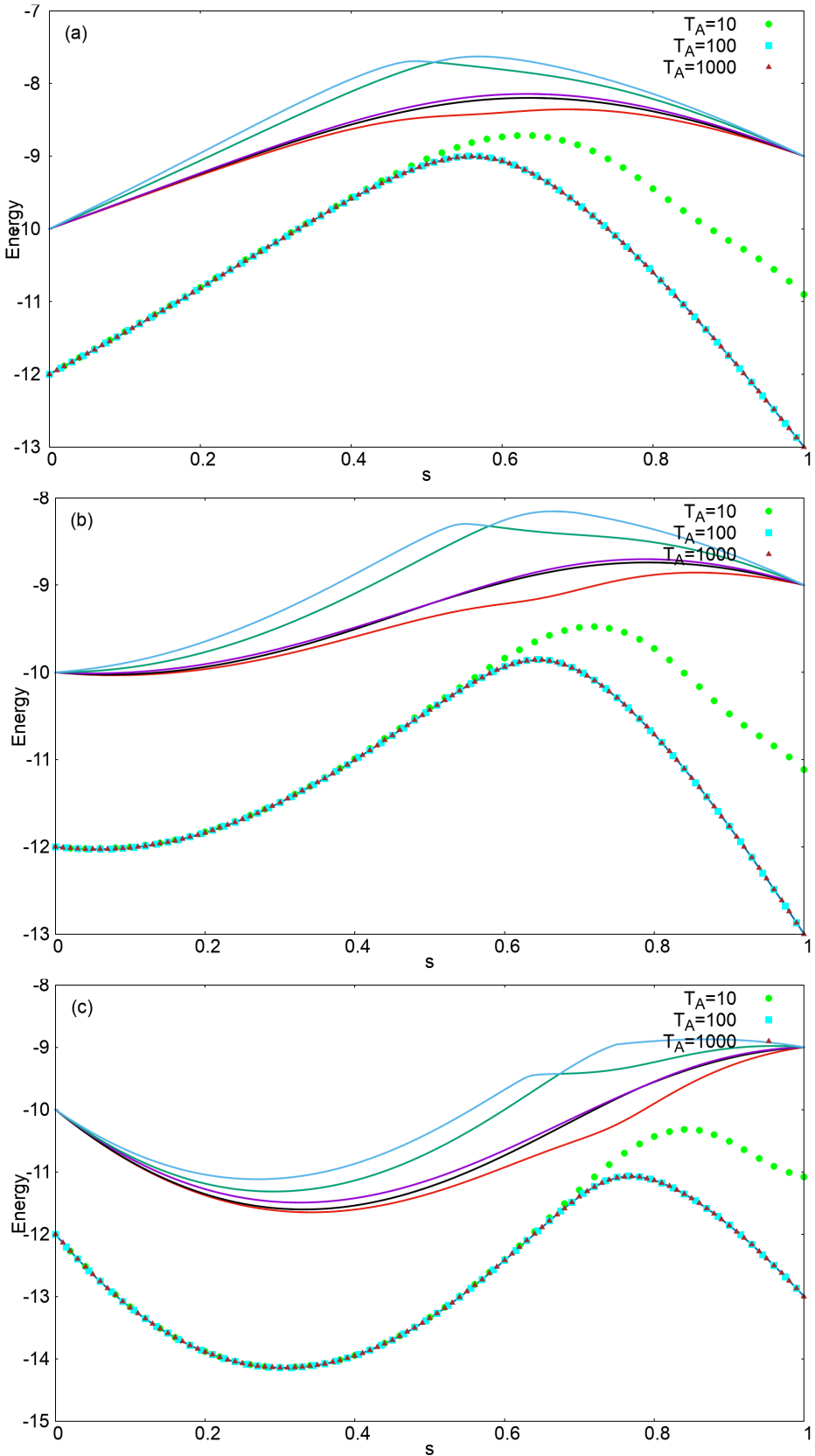


Figure 5.1: The energy spectrum and energy expectation values for the instantaneous state of problem 733, after adding the ferromagnetic trigger. (a):  $g=0.5$ ; (b):  $g=1$ ; (c):  $g=2$ .

shows the energy spectra and the energy expectation values for the instantaneous state, upon adding the ferromagnetic trigger with  $g=0.5, 1$  and  $2$ .

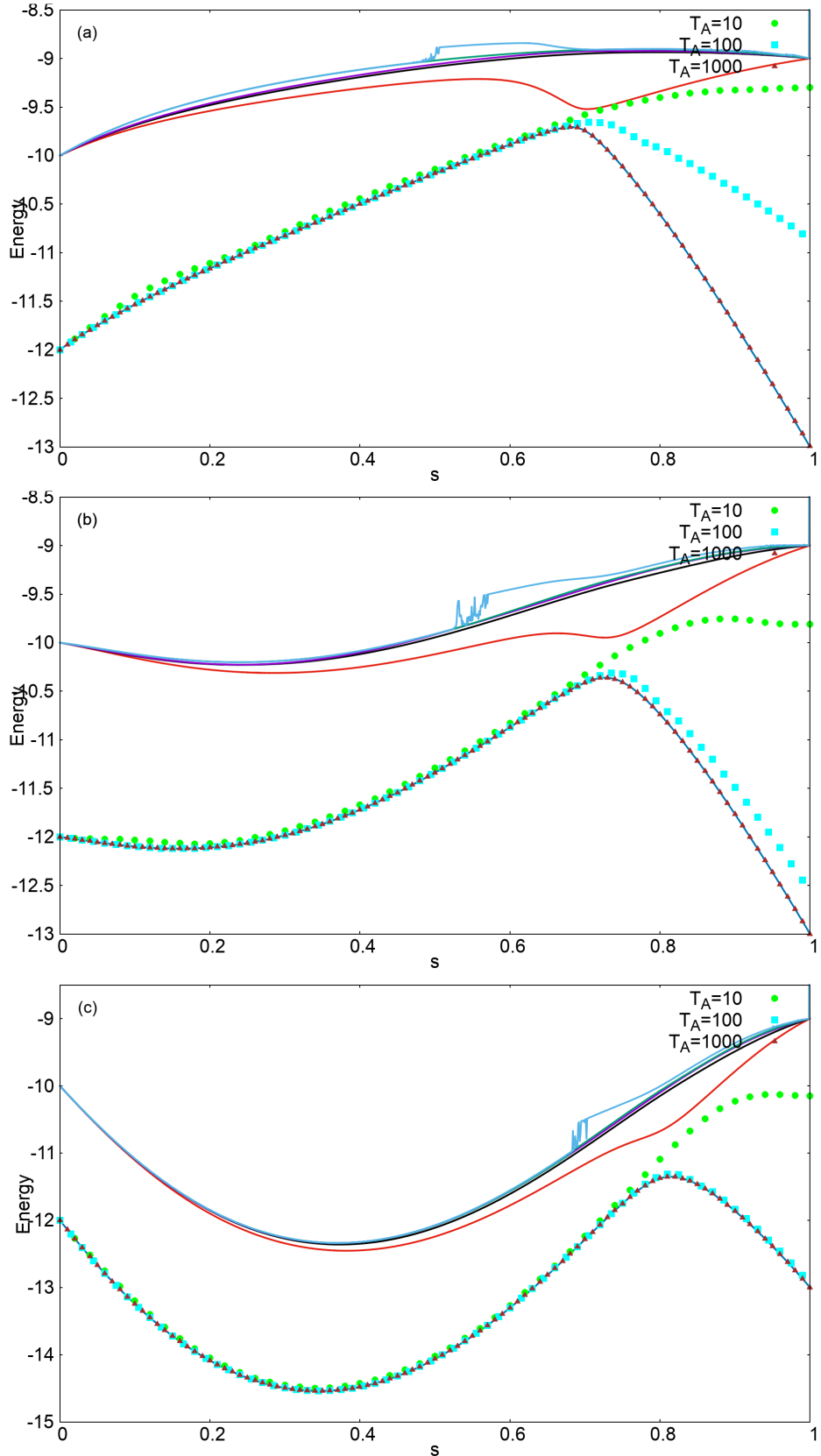


Figure 5.2: The energy spectrum and energy expectation values for the instantaneous state of problem 950, after adding the ferromagnetic trigger. (a):  $g=0.5$ ; (b):  $g=1$ ; (c):  $g=2$ .

For this case too, the minimum energy gaps increase, leading to an improvement in the success probabilities. The improvements can be seen to become larger with increasing the strength of the trigger. The position of the minimum gap was again found to shift rightwards in terms of the annealing parameter  $s$  upon increasing the strength. However, compared to the improvement in the success probability after adding the ferromagnetic trigger to problem 733, the improvement in problem 950 is significantly larger. Defining the relative success probability as the ratio of the success probability of a particular problem after adding the trigger ( $p^F$ ) to the original success probability ( $p^O$ ), for problem 733, the relative success probability at  $T_A=100$  is 1.005 for  $g=2$ , while that for problem 950 is 67.6. In terms of the ratio of the minimum energy gaps, for problem 733,  $\Delta_{min}^F/\Delta_{min}^O=1.89$ , while for problem 950,  $\Delta_{min}^F/\Delta_{min}^O=22.2$ . This can be understood as follows. For the original Hamiltonian in problem 733 and  $T_A=100$ , the system state always stays close to the ground state of the Hamiltonian (see Fig. 4.2), because of the large minimum energy gap. Therefore, although adding the ferromagnetic trigger enlarges the minimum gap, there is not much scope for improvement for increasing the overlap with the ground state further. On the other hand, the original minimum energy gap in problem 950 is rather small. This causes the state of the system to shift most of its amplitude to the first excited state, thereby decreasing the overlap with ground state. Since the ferromagnetic trigger widens the minimum energy gap considerably in this case, the overlap with the ground state increases, resulting in a much larger relative success probability.

In Table 5.2 a comparison of the minimum energy gaps and success probabilities for problem 950, before and after adding the trigger is given.

Problem 950	Original Hamiltonian	Trigger=F, $g=0.5$	Trigger=F, $g=1$	Trigger=F, $g=2$
$\Delta_{min}$	0.0312	0.2074	0.4129	0.6943
$p(T_A = 10)$	0.0002	0.0752	0.2037	0.2914
$p(T_A = 100)$	0.0146	0.4650	0.8889	0.9870
$p(T_A = 1000)$	0.1362	0.9998	0.9999	0.9999
value of $s$ at $\Delta_{min}$	0.665	0.691	0.727	0.793

Table 5.2: A comparison of the minimum gaps and the success probabilities for  $T_A=100$  between the original Hamiltonian for problem 950 and that after adding the ferromagnetic trigger with different strengths. The minimum gaps become larger as the strength of the ferromagnetic trigger (F) is increased. As a result, the success probabilities are increased. The value of  $s$  corresponding to the position of the minimum gap also becomes larger.

Finally, we consider problem 528 with an intermediate success probability for the original Hamiltonian ( $g=0$ ). Figure (5.3) shows the energy spectra and energy expectation values for the instantaneous state after adding the ferromagnetic trigger with strengths 0.5, 1 and 2 respectively.

For this case too, the minimum energy gaps increase, leading to an improvement in the success probabilities. The improvements can be seen to have become larger with increasing strengths of the trigger. The position of the minimum gap shifts rightwards in terms of the annealing parameter  $s$  upon increasing the strength. The relative success ratio for this case is 1.91 , while  $\Delta_{min}^F/\Delta_{min}^O=4.77$  at  $g=2$ . These values are also intermediate to those for problems 733 and 950. Table (5.3) shows a comparison of the success probabilities and the minimum gaps, between the original Hamiltonian ( $g=0$ ) and the Hamiltonian after adding the ferromagnetic trigger with different strengths.

Problem 528	Original Hamiltonian	Trigger=F, $g=0.5$	Trigger=F, $g=1$	Trigger=F, $g=2$
$\Delta_{min}$	0.1573	0.3748	0.5439	0.7512
$p(T_A = 10)$	0.1577	0.2959	0.4036	0.4391
$p(T_A = 100)$	0.5199	0.9577	0.9945	0.9981
$p(T_A = 1000)$	0.9999	0.9999	0.9999	0.9999
value of $s$ at $\Delta_{min}$	0.514	0.595	0.665	0.760

Table 5.3: A comparison of the minimum energy gaps and the success probabilities for  $T_A=100$ , between the original Hamiltonian for problem 528 and that after adding the ferromagnetic trigger (F) with different strengths. The minimum gaps become larger as the strength of the ferromagnetic trigger is increased. The success probabilities are increased as a result. The value of  $s$  corresponding to the position of the minimum gap also becomes larger.

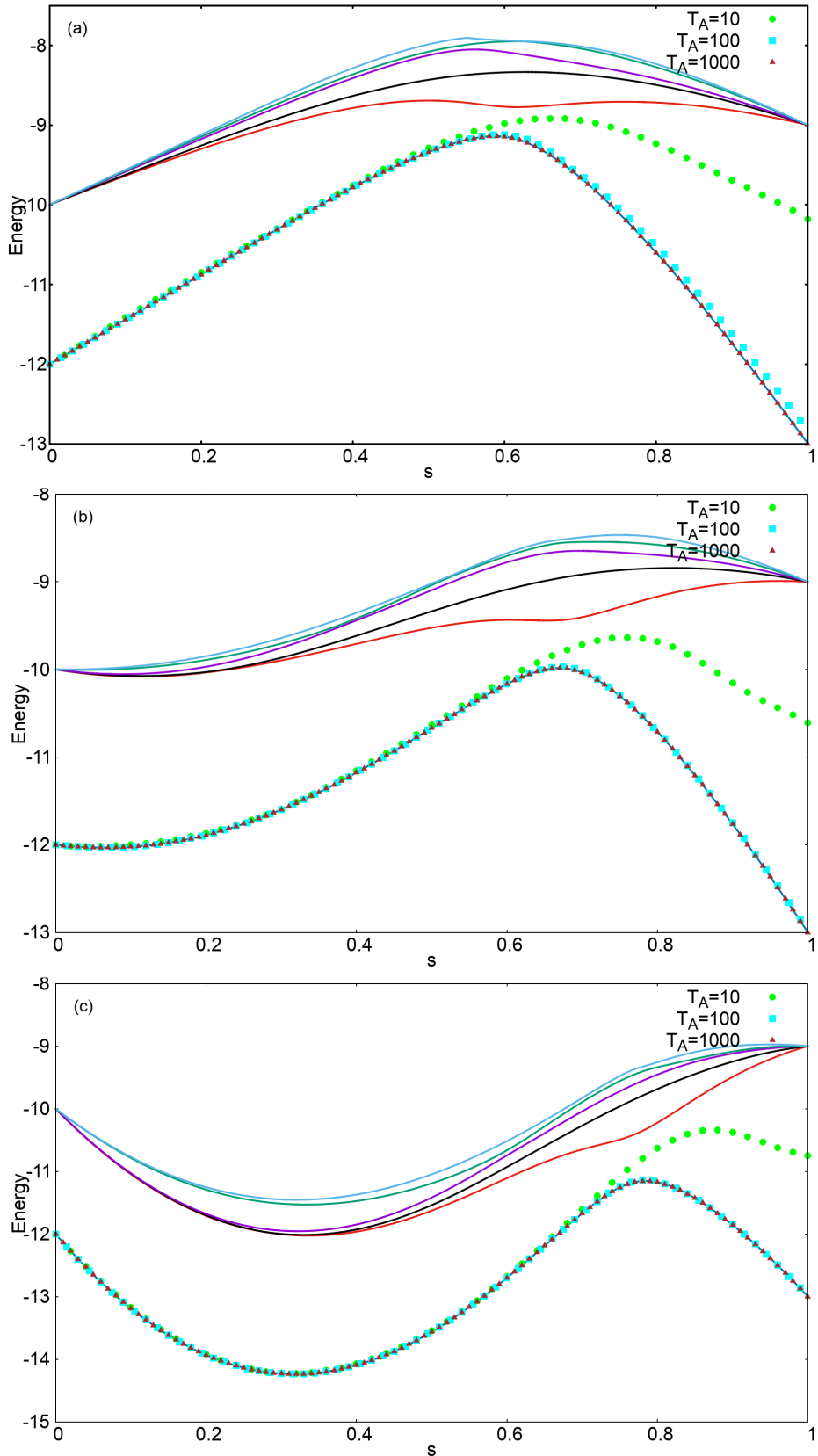


Figure 5.3: The energy spectrum and energy expectation values for the instantaneous state of problem 528, after adding the ferromagnetic trigger. (a):  $g=0.5$ ; (b):  $g=1$ ; (c):  $g=2$ .

In summary, adding the ferromagnetic trigger enlarges the minimum energy gaps, and the resulting success probabilities are larger than the original success probabilities for all the three problems considered here. The same analysis was then done for all the problems belonging to the set to understand the general effects of adding the ferromagnetic trigger.

## 5.2 The Bigger Picture

It was observed that the success probabilities after adding the ferromagnetic trigger improve for all the problems of the set, irrespective of the strength of the trigger or the chosen annealing time. To understand the reasons for the same, the minimum energy gaps were computed for all the problems, before and after adding the trigger with  $g \in \{0.5, 1, 2\}$ .

Figure (5.4) shows the scatter plot of the minimum energy gaps after adding the ferromagnetic trigger with different strengths against the original minimum energy gaps, for all the problems of the set. (The corresponding plot for the problems in the 8-spin set is shown in the appendix as Fig. 1.)

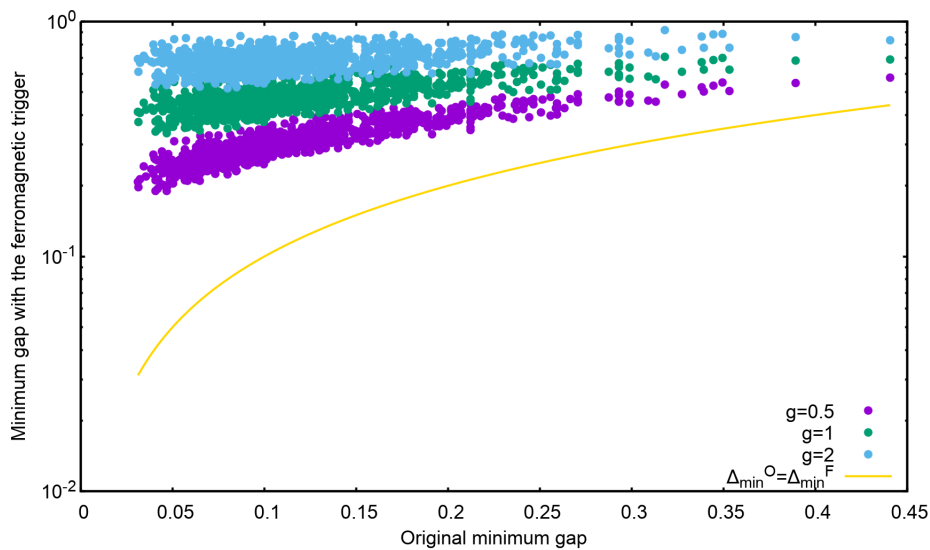


Figure 5.4: Scatter plot of the minimum gaps upon adding the ferromagnetic trigger with  $g \in \{0.5, 1, 2\}$  against the original minimum energy gaps. The points lying above solid line represent the cases with enlarged minimum gaps.

With the ferromagnetic trigger, all the minimum energy gaps are increased, for all the values of  $g$ . Furthermore, for all the problems, the gaps become even larger as the ferromagnetic trigger becomes stronger. It can also be noted that the enhancement in the minimum energy gaps is larger in cases with relatively small original minimum gaps, as was also seen by calculating  $\Delta_{min}^F/\Delta_{min}^O$  for the three chosen problems (733, 950 and 528).

For gauging the performance of the quantum annealing algorithm after adding the ferromagnetic trigger, scatter plots of the success probabilities after adding the ferromagnetic trigger against the original success probabilities have been shown in Fig. (5.5) corresponding to  $g=0.5, 1$  and  $2$ . (See Fig. 3 for the corresponding plot for the 8-spin problems.)

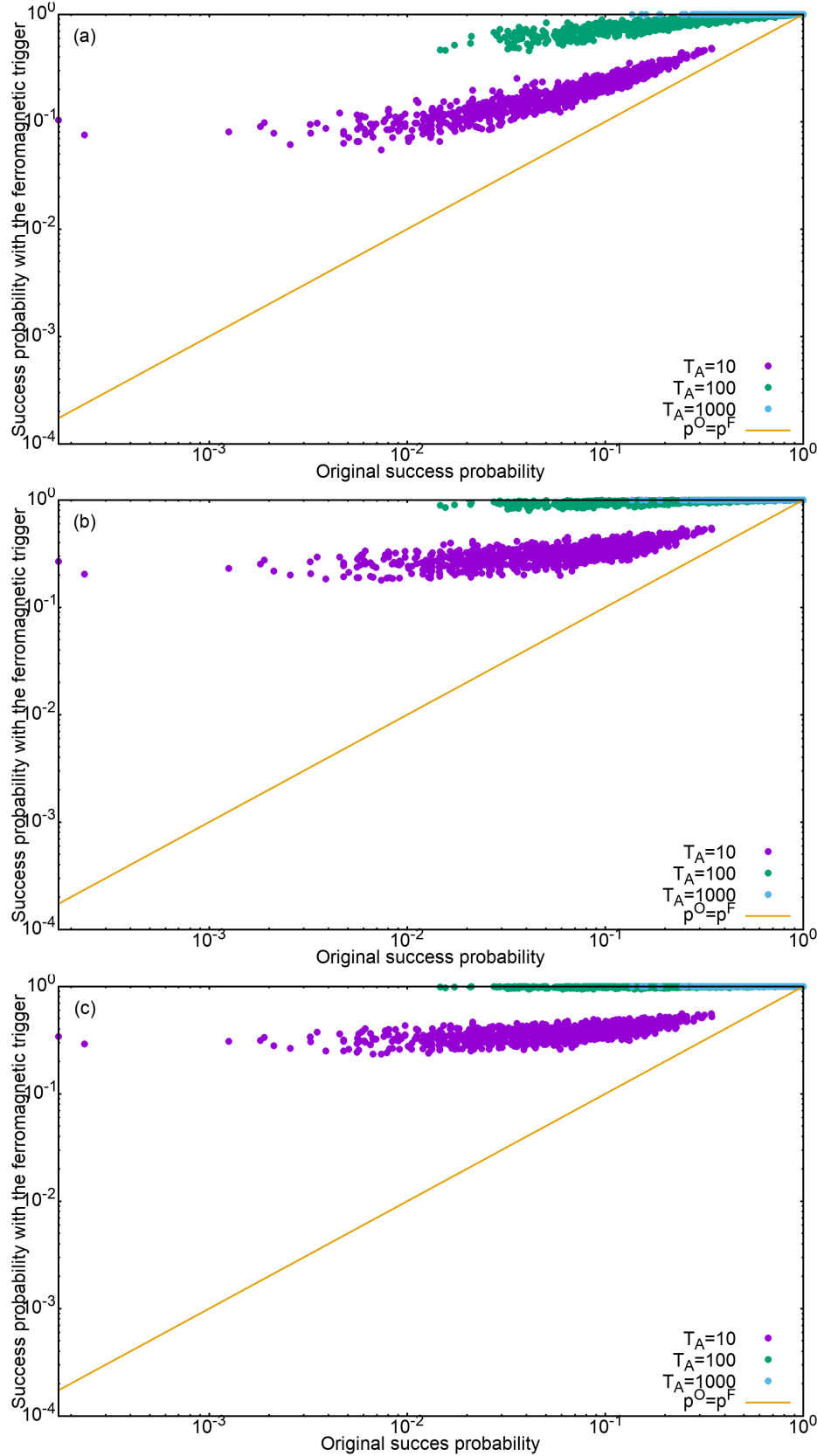


Figure 5.5: Scatter plot for the success probability after adding ferromagnetic trigger against the success probability of the original Hamiltonian, for annealing time  $T_A \in \{10, 100, 1000\}$ . (a):  $g=0.5$ ; (b):  $g=1$ ; (c):  $g=2$ . Points lying above the solid line represent the problems with improved success probability.

For all the three cases, and all the problems in the set, the success probability after adding the trigger is greater than the success probability of the original Hamiltonian. Since in the adiabatic regime, the overlap of the final state with the ground state increases with increasing annealing times, the success probability of the original Hamiltonians for long annealing times ( $T_A=1000$ ) is already large ( $\approx 1$ ). Adding the ferromagnetic trigger can therefore not improve the success probability too much. This explains the confinement of the points representing the success probability for  $T_A=1000$  close to the solid line ( $p^O = p^F$ ) on the upper right corner, for all the three values of the strength parameter. Owing to the same reason, the points corresponding to the success probability for  $T_A=10$  have a much larger spread. For the easy cases (larger  $p^O$ ), the success probability upon adding the trigger ( $p^F$ ) has a similar value. Such points lie close to the line. On the other hand, for more difficult cases (smaller  $p^O$ ) the improvement can be larger, and such points lie away from the line.

Furthermore, since for a given problem, increasing the strength of the ferromagnetic trigger makes the minimum gaps larger, the success probability for that case also becomes larger. This explains the distribution of the points getting successively more flat with increasing strength of the trigger, for all annealing times (see Fig. 5.5).

Finally, we look at the dynamics of the evolution. According to Eq. (3.7), for an adiabatic evolution of the state of the system, the success probability,  $p$ , which is a measure of the overlap of the final state with the ground state of the Hamiltonian, is related to the minimum energy gap,  $\Delta_{min}$  as follows:

$$p = 1 - \exp(-C\Delta_{min}^2), \quad (5.1)$$

for some constant  $C$ . Since different problems belonging to the set may correspond to different minimum energy gaps, a plot of the success probability with these gaps should follow Eq. (3.7) if the evolution of the state for a problem is adiabatic. Moreover, adding the trigger changes the energy spectra, and thereby the minimum energy gaps of these problems. Figure (5.6) shows the success probability versus the minimum energy gap plot for all the problems upon adding the ferromagnetic trigger with three different strengths (0.5, 1 and 2), and for three annealing times (10, 100 and 1000). (See Fig. (5(a)) for the corresponding plot for 8-spin problems.)

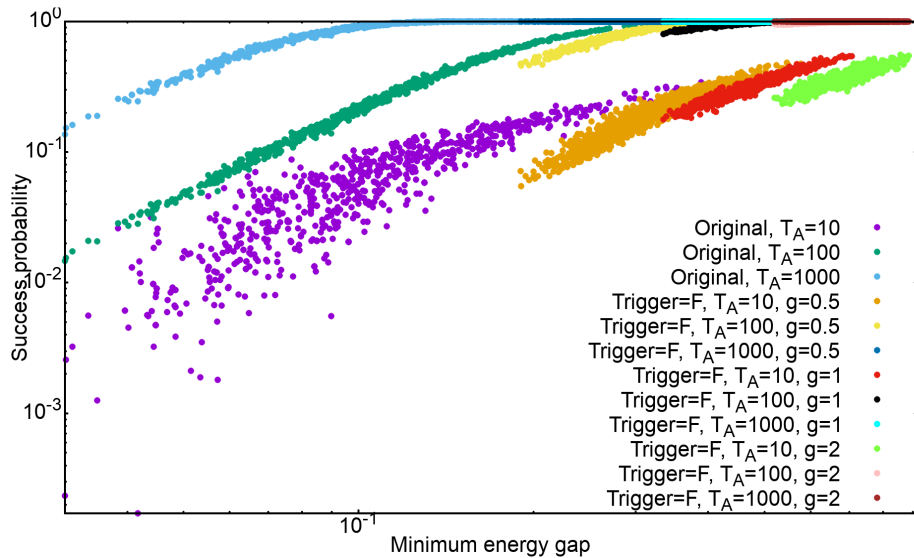


Figure 5.6: Plot of the success probability versus minimum energy gaps for all the problems belonging to the set of the 12-variable 2-SAT problems. The plot shows the effect of adding ferromagnetic trigger to the original Hamiltonian with strengths 0.5, 1 and 2, while the annealing time is chosen to 10, 100 and 1000.

From Fig. (5.6) it can be noted that all the curves roughly follow the Landau-Zener dependence (see Eq. (3.4)) of the success probability on the minimum energy gaps. However, for the original Hamiltonian, and  $T_A=10$ , the scattering is larger compared to the other curves. The scattering of the curves decreases on increasing the annealing times, suggesting that longer annealing times ascertain the evolution of the state to be closer to adiabatic. Since adding the ferromagnetic trigger enlarges the minimum energy gaps, the curves are shifted to the right upon adding the trigger and increasing their strength.



# Chapter 6

## Results with the Anti-ferromagnetic Trigger

This chapter focuses on the effects on the performance of the quantum annealing algorithm upon adding the antiferromagnetic trigger to the original Hamiltonian. Unlike the case of the ferromagnetic trigger, for the anti-ferromagnetic trigger the strength parameter,  $g$  in Eq. (2.10) plays a more decisive role than merely controlling the extent by which the minimum gap is enlarged. The antiferromagnetic trigger alters the energy spectra, the minimum energy gaps, and the number of anti-crossings between the ground and first excited energy state of the Hamiltonian, depending on the strength with which it is added, as well as on the problem itself. We shall begin by observing the effects of adding the antiferromagnetic trigger to the original Hamiltonian, for the three chosen problems. The following sections will then showcase the role that the strength parameter  $g$  plays.

### 6.1 The Selected Problems

Contrary to the systematic effects of adding the ferromagnetic trigger, where adding the trigger always enlarges the minimum energy gap, and both larger minimum energy gaps and longer annealing times result in a higher success probability, the effects of adding the antiferromagnetic trigger are very specific to the problem at hand, and the chosen annealing time. This is a consequence of many non-adiabatic mechanisms involved in improving the success probability as well.

Let us begin by considering problem 733 again, which was found to have a large success probability for the original Hamiltonian.

Table (6.1) shows a comparison of the success probabilities  $p$ , and minimum energy gaps  $\Delta_{min}$  between the original Hamiltonian and the Hamiltonian after adding the antiferromagnetic trigger with different strengths to problem 733. Figure (6.1) shows the energy spectra and the energy expectation values for the instantaneous state corresponding to the three annealing times, after adding the antiferromagnetic trigger to the Hamiltonian with strengths 0.5, 1 and 2.

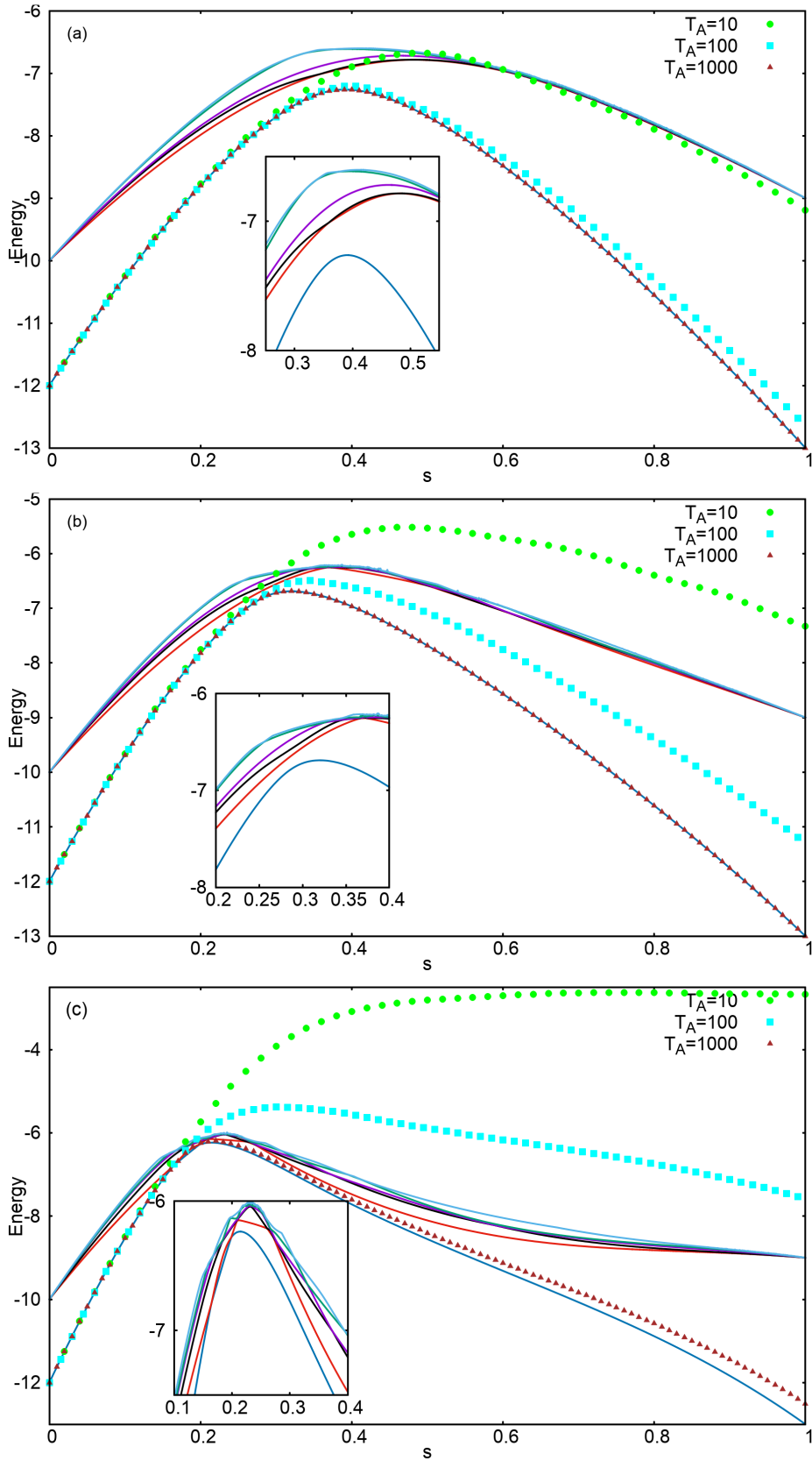


Figure 6.1: The energy spectrum and energy expectation values for the instantaneous state of problem 733, after adding the antiferromagnetic trigger. (a):  $g=0.5$ ; (b):  $g=1$ ; (c):  $g=2$ .

Problem 733	Original Hamiltonian	Trigger=A, g=0.5	Trigger=A, g=1	Trigger=A, g=2
$\Delta_{min}$	0.4407	0.3070	0.1349	0.0020
$p(T_A=10)$	0.3444	0.1446	0.0279	$1.271 \times 10^{-4}$
$p(T_A=100)$	0.9944	0.9117	0.5747	0.0273
$p(T_A=1000)$	0.9999	0.9999	0.9999	0.8761
value of $s$ at $\Delta_{min}$	0.459	0.367	0.282	0.254
Number of anti-crossings	1	1	1	3

Table 6.1: A comparison of the minimum energy gaps and the success probabilities for problem 733, between the original Hamiltonian and the Hamiltonian with antiferromagnetic trigger (A) of different strengths. The minimum gaps become successively smaller as the strength of the antiferromagnetic trigger is increased. The success probabilities are decreased as a result. The value of  $s$  corresponding to the position of the minimum gap also becomes smaller.

As can be noted from the table, the minimum energy gap decreases upon adding the antiferromagnetic trigger, and this decrease becomes larger as the strength of the trigger is increased. Consequently, the success probabilities after adding the trigger are found to be decreasing as well. The value of annealing parameter  $s$  at the position of minimum gap also becomes smaller with increasing strength of the trigger.

Additionally, a new feature observed as a result of adding the antiferromagnetic trigger (compared to the effects of adding the ferromagnetic trigger) is the change in the number of anti-crossings between the ground and the first energy state. For strength  $g=2$ , the number of energy anti-crossings increases to 3, while it remains unchanged for  $g=0.5$  and  $g=1$ . Moreover, when the antiferromagnetic trigger is added with strength 2, the energy spectrum changes significantly (in terms of the number of the energy anti-crossings between the energy levels of the spectrum and the time duration for which the two lowest lying energy levels remain in close proximity) in comparison to the original spectrum (see Fig. 4.2), as can be seen more clearly in the inset of Fig. (6.1(c)).

Next, let us consider problem 950 that had a small success probability in the absence of any triggers. Figure (6.2) shows the energy spectrum and the energy expectation values for the instantaneous state corresponding to the three annealing times, after adding the antiferromagnetic trigger to the Hamiltonian with strengths 0.5, 1 and 2.

For this case, Table (6.2) shows a comparison of the minimum energy gaps, and success probabilities (corresponding to different the antiferromagnetic trigger with different strengths).

annealing times) between the original Hamiltonian and the Hamiltonian upon adding

Problem 950	Original Hamiltonian	Trigger=A, g=0.5	Trigger=A, g=1	Trigger=A, g=2
$\Delta_{min}$	0.0312	0.0130	0.0019	0.1784
$p(T_A=10)$	$2.343 \times 10^{-4}$	0.0567	0.0017	0.0071
$p(T_A=100)$	0.0146	0.0022	0.0239	0.4468
$p(T_A=1000)$	0.1362	0.0228	0.1729	0.9999
value of $s$ at $\Delta_{min}$	0.665	0.644	0.601	0.263
Number of anti-crossings	1	1	2	3

Table 6.2: A comparison of the minimum gaps and the success probabilities for problem 950, between the original Hamiltonian and the Hamiltonian with the antiferromagnetic trigger (A) of different strengths. The minimum gap becomes small for  $g=0.5$ , and even smaller for  $g=1$ , while it becomes even larger than the original minimum energy gap for  $g=2$ . The value of  $s$  corresponding to the position of the minimum gap becomes smaller with increasing strength of the trigger.

The minimum energy gaps decrease with respect to the original minimum gaps, upon adding the trigger with strengths 0.5, and 1. However, the success probability for  $T_A=10$  after adding the antiferromagnetic trigger with

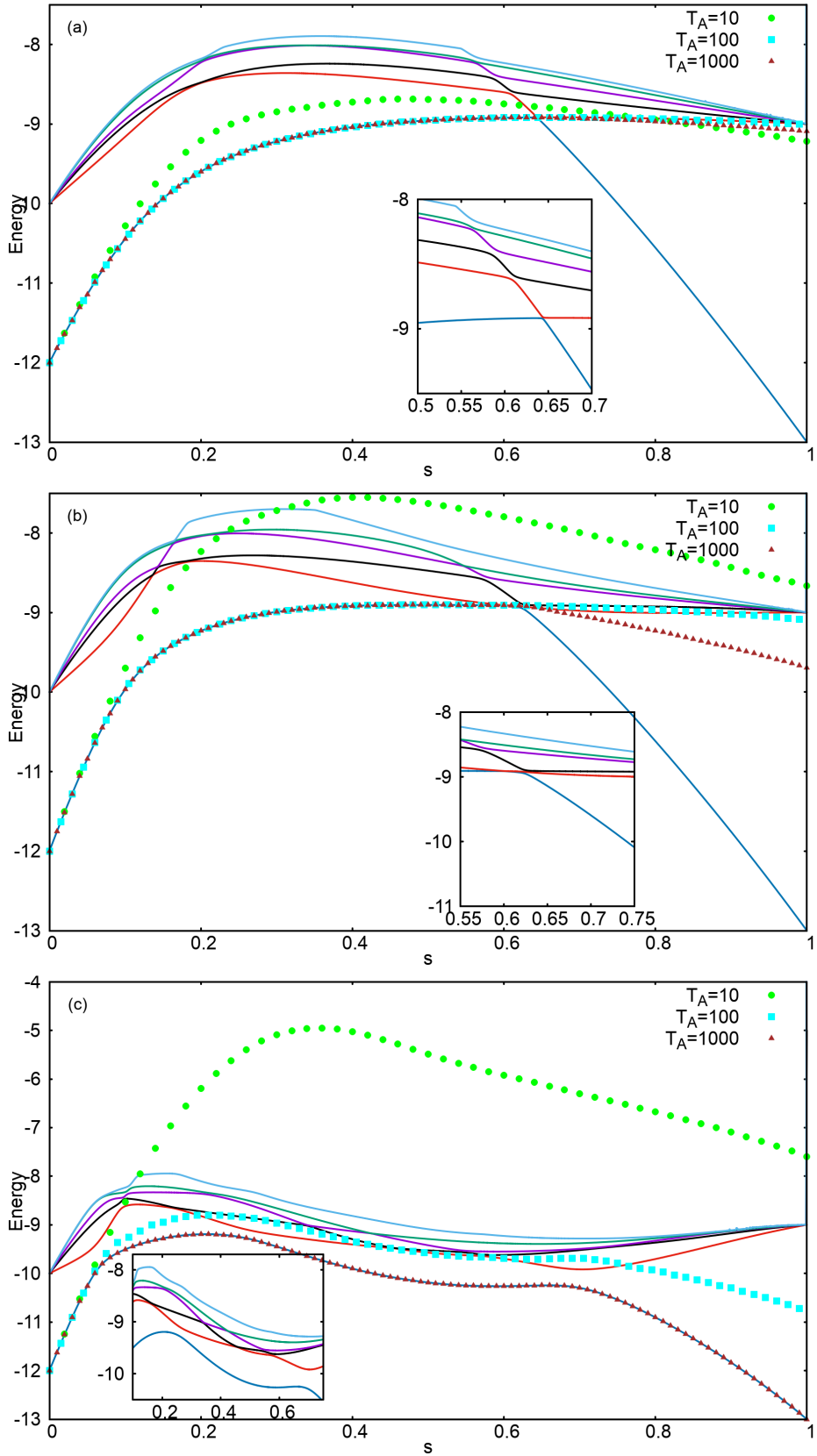


Figure 6.2: The energy spectrum and energy expectation values for the instantaneous state of problem 950, after adding the antiferromagnetic trigger. (a):  $g=0.5$ ; (b):  $g=1$ ; (c):  $g=2$ .

$g=0.5$  and  $g=1$ , is larger compared to that of the original Hamiltonian, owing to different reasons.

Since upon adding the antiferromagnetic trigger with strength 0.5, the minimum energy gap becomes smaller, the annealing time of  $T_A=10$  is so short that the state of the system transits to the first excited state even before the minimum gap anti-crossing. Upon approaching the minimum gap anti-crossing the system state shifts some of the amplitude back to the ground state, increasing the success probability in this case (see Fig. 6.2(a)). However, for the original Hamiltonian the gap is not large enough for  $T_A=10$  for the state to jump to the first excited state before the minimum energy gap (see Fig. 4.3). The state therefore stays close to the first excited state after passing the anti-crossing.

Furthermore, for annealing times  $T_A=100$  and  $T_A=1000$ , the system state transitions only at the minimum gap anti-crossing and closely follows the second and first excited states respectively. The overlap with the ground state decreases, and therefore the success probability in both these cases also reduces.

In case of adding the antiferromagnetic trigger with strength 1, the first energy anti-crossing is small enough for  $T_A=10$  to shift the system state to the first excited state. Quickly after transitioning to the first excited state, the system state shifts to the higher energy levels (see Fig. 6.2(b)). Since the state of the system is a superposition of many energy eigenstates, the final system state has small, yet finite overlap with the ground state. In the original Hamiltonian, however, the system state shifts to the first excited state at the anti-crossing and stays there. Therefore, the overlap with the ground state becomes negligible (see Fig. 4.3).

By choosing the strength to be 2, the minimum energy gap for this problem becomes larger than the original minimum energy gap, while the number of anti-crossings between the ground and the first excited state increases to 3. The success probability in this case is larger than the original success probability for all the annealing times. For  $T_A=10$ , the state of the system shifts to the first excited state at first energy anti-crossing, and then quickly shifts to a superposition state of the higher energy states (due to the proximity of the higher energy levels as result of adding the trigger). In this particular case, this results in a larger overlap with the ground state compared to the case of the state closely following the first excited state after reaching the only energy anti-crossing in case of the original problem (see Fig. 4.3).

Thus, in this case adding the antiferromagnetic trigger with different strengths can decrease or increase the minimum energy gap, thus affecting the success probabilities by different mechanisms.

For  $T_A=100$ , the state starts transitioning to the first excited state only as it approaches the second energy anti-crossing. The state does further shifts to higher energy levels, but comes back to the first excited state before the third energy anti-crossing. At the third anti-crossing some of the amplitude of the wave function shifts to the ground state again, and therefore the success becomes larger than the original problem.

Finally, for  $T_A=1000$ , the annealing time and the minimum energy gap is large enough for the system to always stay close to the ground state, hence the larger success probability.

Lastly, Fig. (6.3) shows the energy spectra and the energy expectation values for the state for problem 528, after adding the antiferromagnetic trigger with strengths 0.5, 1 and 2.

Table (6.3) shows a comparison of the minimum energy gaps, and success probabilities (corresponding to different annealing times) between the original Hamiltonian and the Hamiltonian after adding the antiferromagnetic trigger with different strengths for problem 528.

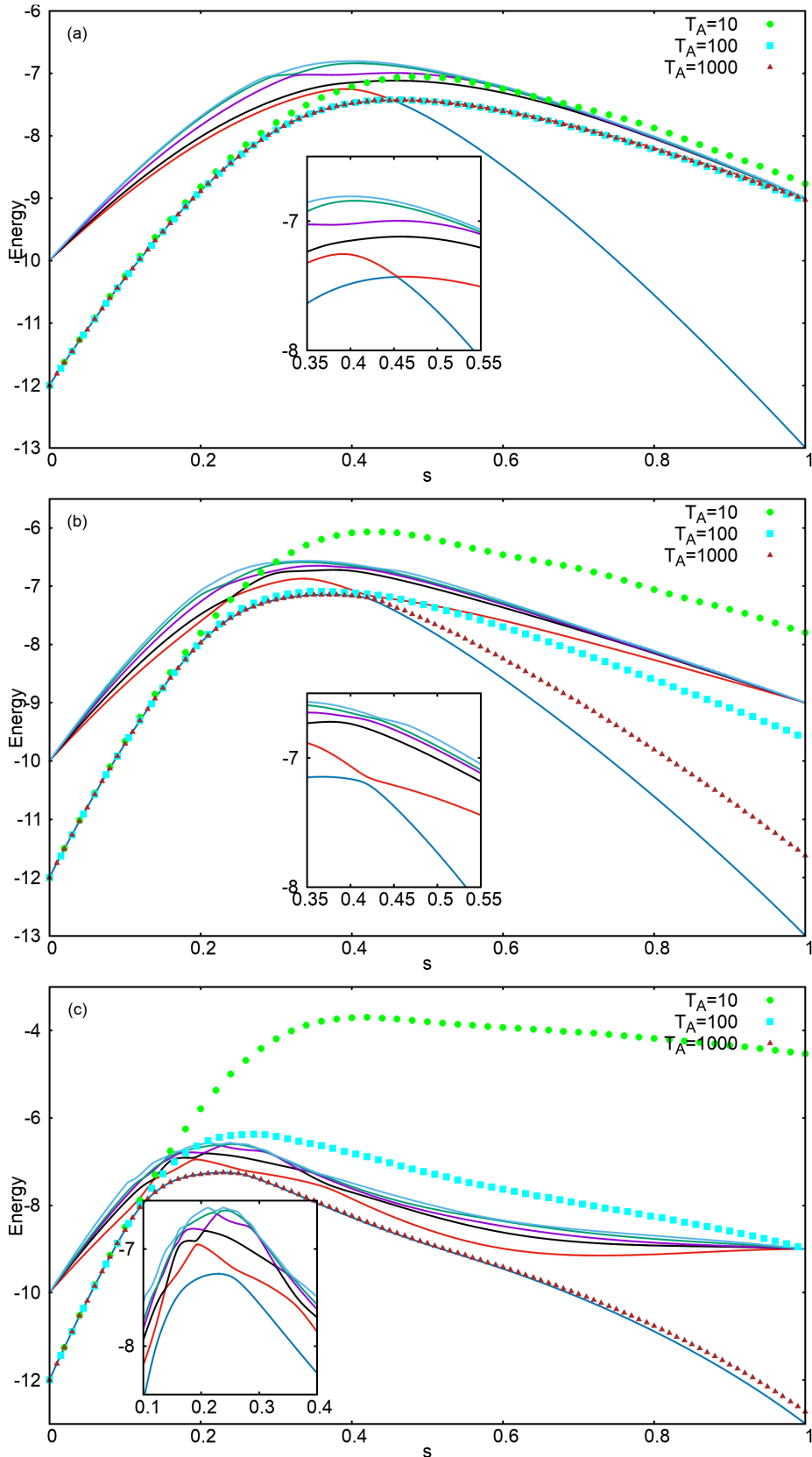


Figure 6.3: The energy spectrum and energy expectation values for the instantaneous state of problem 528, after adding the antiferromagnetic trigger. (a):  $g=0.5$ ; (b):  $g=1$ ; (c):  $g=2$ .

Problem 528	Original Hamiltonian	Trigger=A, g=0.5	Trigger=A, g=1	Trigger=A, g=2
$\Delta_{min}$	0.1573	0.0049	0.0562	0.1008
$p(T_A=10)$	0.1577	0.0573	0.0368	$4.21 \times 10^{-5}$
$p(T_A=100)$	0.5199	0.0120	0.1517	0.0480
$p(T_A=1000)$	0.9992	0.0071	0.6565	0.9313
value of $s$ at $\Delta_{min}$	0.514	0.454	0.418	0.256
Number of anti-crossings	1	1	3	4

Table 6.3: A comparison of the minimum energy gaps and the success probabilities for problem 528, between the original Hamiltonian and and the Hamiltonian with antiferromagnetic trigger (A) of different strengths. The minimum energy gaps after adding the trigger are smaller than the original minimum gap, for all the values of  $g$ . They however become large upon increasing the strength of the antiferromagnetic trigger. The value of  $s$  corresponding to the position of the minimum gap becomes smaller with increasing strength of the trigger.

For this problem, adding the antiferromagnetic trigger makes the minimum energy gaps smaller than the original gap, for all the three  $g$  values. The gaps however increase with increasing the strength of the trigger. The original success probabilities, for all annealing times, are therefore larger than the resulting success probabilities upon adding the triggers with different  $g$ . Additionally, for  $T_A=100, 1000$ , the success probabilities become larger when the antiferromagnetic trigger is added with strength 1 compared to when added with strength 0.5, as the minimum energy gap for the former is larger. For  $T_A=10$ , and both  $g=0.5$  and  $g=1$  cases, the system state transitions to the first excited state prior to the first energy anti-crossing. This is followed by the state shifting to higher energy levels soon after. Since the energy spectrum becomes more complex (in terms of the number of anti-crossings between the higher energy states and their proximity) as the strength of the trigger is increased, the system state shifts farther away from the ground state. For this problem, the state of the system with  $g=0.5$  ends in a superposition state with a higher overlap with the ground state than the final state of the system with  $g=1$ .

Although the gap becomes even larger with  $g=2$ , the success probability in this case is smaller compared to the case with  $g=1$  for  $T_A=10$  and  $T_A=1000$ . This can be explained by observing that adding the antiferromagnetic trigger with  $g=2$  changes the energy spectrum of the Hamiltonian even more drastically. Not only do the number of energy anti-crossings between the ground and the first excited state increase to 4, the higher lying energy levels also become more involved and have a larger number of crossings and anti-crossings. Therefore, as annealing times  $T_A=10$  and  $T_A=100$  are not large enough for the state to stay close to the ground state upon reaching the first energy anti-crossing, the system state settles even farther away from the ground state as compared to the  $g=1$  case. The overlap of the resulting state with the ground state is even smaller and hence, the success probability for  $g=2$  for  $T_A=10$  is negligible. As the annealing time is increased further to  $T_A=1000$ , the minimum energy gap becomes large enough to keep the state of the system close to the ground state, and the success probability becomes comparable to the original success probability.

Thus adding the antiferromagnetic trigger is capable of both enlarging and reducing the minimum energy gap, and therefore capable of improving the success probability by making the evolution more close to adiabatic, or by non-adiabatic mechanisms. It therefore becomes essential to study the effects of the strength parameter on altering the minimum energy gaps, and thereby the choice of the annealing time on the success probability.

## 6.2 Trigger Strength g=0.5

This section will showcase the effects of adding the antiferromagnetic trigger to all the original Hamiltonians from the set of 12 spin problems, with strength 0.5. For each problem, the annealing time was chosen to be 10, 100 and 1000.

As a measure of quantifying the performance with respect to the original Hamiltonian, the relative success probability was defined as the ratio of the success probability upon adding the antiferromagnetic trigger ( $p^A$ ) to the original success probability ( $p^O$ ). Figure (6.4) shows the distribution of the relative success probability for annealing times of 10, 100 and 1000, with the strength of the trigger Hamiltonian chosen to be 0.5.

For an annealing time  $T_A=10$ , 439 problems of the set are improved after including the antiferromagnetic trigger with  $g=0.5$ . On increasing the annealing time to 100 and 1000, the number of cases with improved success

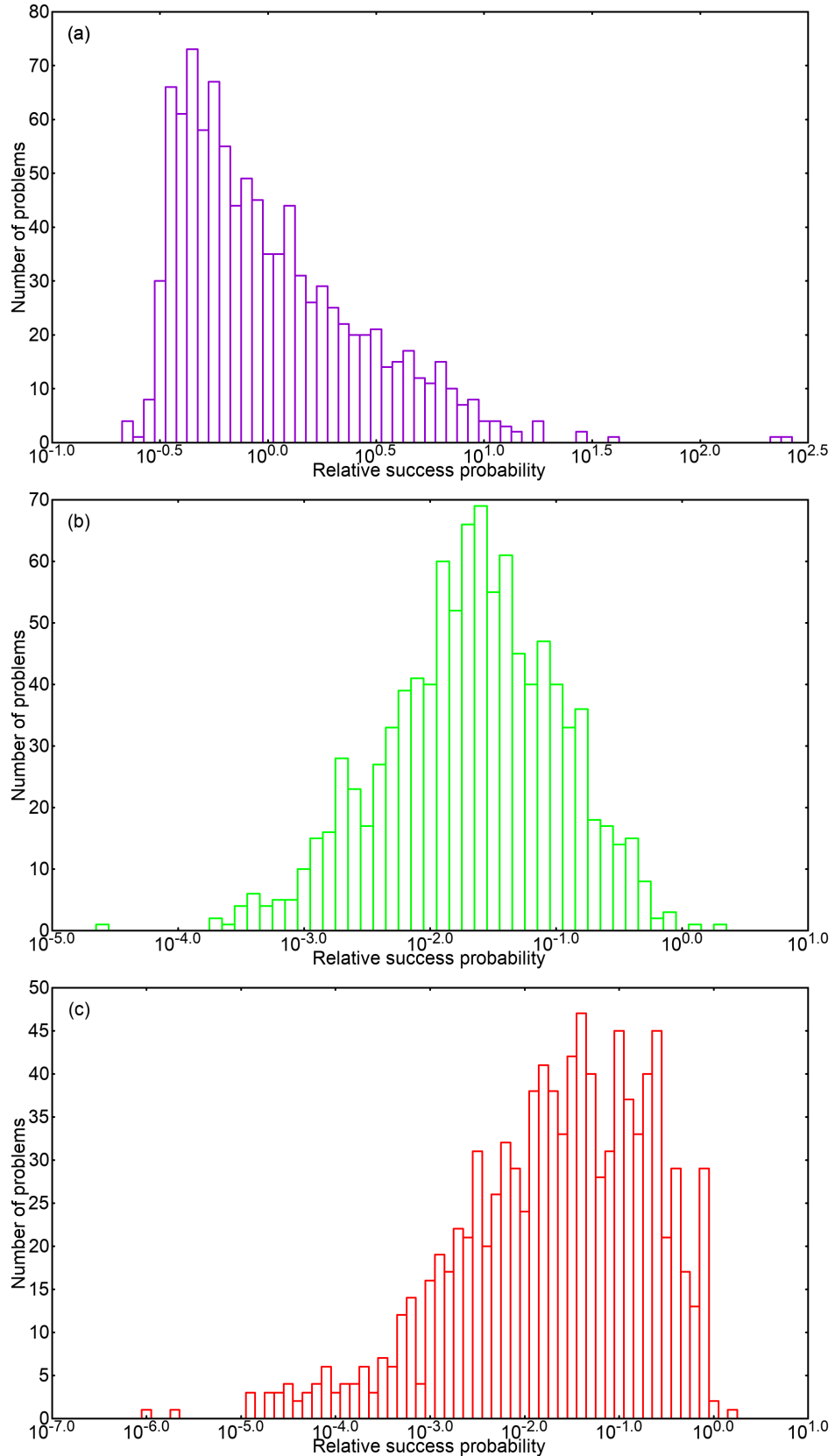


Figure 6.4: Distribution of the relative success probability  $p^A/p^O$  for  $g=0.5$ . (a):  $T_A=10$ ; (b):  $T_A=100$ ; (c):  $T_A=1000$ .

probability drops to 2 for both the cases. Furthermore, the largest value of the relative success ratio is a little more than 250 for  $T_A=10$ , while it reduces to 1.995 for  $T_A=100$ , and to 1.585 for  $T_A=1000$ . In order to understand the reasons for this decrease in the relative success ratio on increasing the annealing time, the minimum energy gaps of all the problems were calculated before and after adding the trigger. Figure (6.5) shows a plot of the minimum energy gaps after adding the antiferromagnetic trigger ( $\Delta_{min}^A$ ) with  $g=0.5$ , against the original minimum energy gaps ( $\Delta_{min}^O$ ). The points lying above the line  $\Delta_{min}^O = \Delta_{min}^A$  represent the problems for which the energy gaps increase after adding the trigger. (See Fig. (2) in the appendix for the similar minimum energy scatter plot for the 8-spin problems for all the values of  $g$ .)

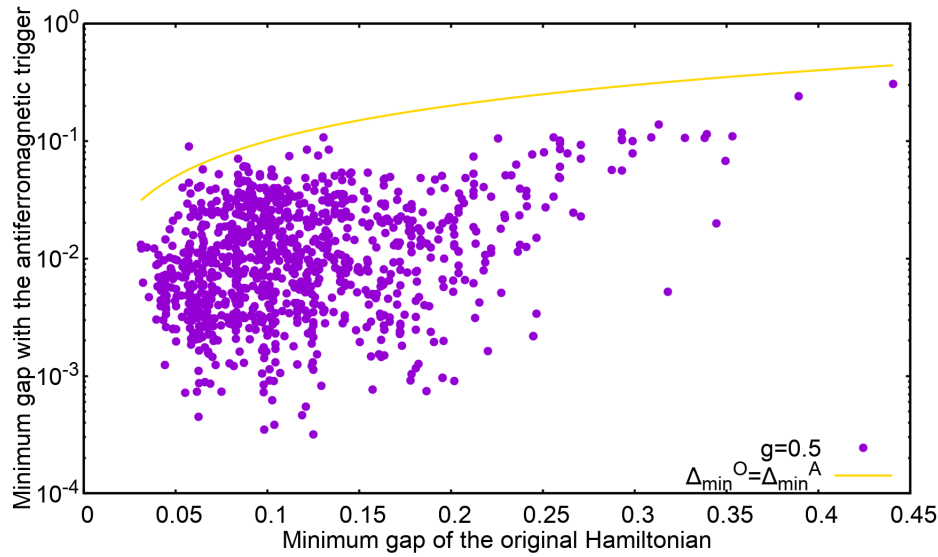


Figure 6.5: A plot of the minimum energy gaps after adding the antiferromagnetic trigger with  $g=0.5$  ( $\Delta_{min}^A$ ), with the original minimum energy gaps ( $\Delta_{min}^O$ ). For 999 problems of the minimum energy gap was found to have decreased after adding the antiferromagnetic trigger.

As is clear from Fig. (6.5), for 999 problems, the minimum energy gaps reduce after adding the antiferromagnetic trigger with strength 0.5. It was also found that 923 problems still have a single anti-crossing between the ground and the first excited state, while for the other 77 problems, it increases to 2.

For some cases with small original minimum energy gaps and short annealing time of  $T_A=10$ , non-adiabatic evolution of the state results in a larger overlap of the final state with the ground state. Some of these mechanisms can be the state deviating from the ground state even before the anti-crossing and transferring some of the amplitude back to the ground state, or the presence of 2 sufficiently small and comparable anti-crossings, or a coincidental larger overlap of the final state with the ground state as a consequence of being a superposition state. Thus, when the annealing time is increased to 100 or 1000, the state shifts to the first excited state only at the anti-crossing, and follows it closely. This explains the drop in the percentage of improved cases upon increasing the annealing time after adding the trigger.

To obtain an estimate of the difficulty of the affected problems, Fig. (6.6) shows a scatter plot of the success probabilities after adding the trigger against the original success probabilities, for the three annealing times. (See Fig. 4 in the appendix for the similar success probability scatter plot for the 8-spin problems for all the values of  $g$ .) The points lying above the line  $p^O = p^A$  represent the cases with improved success probability after including the antiferromagnetic trigger. It should be noted that the 439 problems improved by adding antiferromagnetic trigger for  $T_A=10$ , are the ones that have a relatively smaller original success probabilities (harder problems with smaller minimum energy gaps). This suggests that the mechanisms leading to an improvement in the success probability are mostly non-adiabatic in this case.

It should also be noted that for  $T_A=100$  and  $T_A=1000$ , the original success probabilities are already quite high, giving way to another reason for the decrease in the relative success probability with increasing annealing time.

For both  $T_A=100$  and  $T_A=1000$  problem number 402 and 709 have a larger relative success ratio upon adding the antiferromagnetic trigger with  $g=0.5$ . Problem 402 corresponds to the only case where the minimum energy gap increases after adding the trigger, explaining the reason for the increase in the success probability.

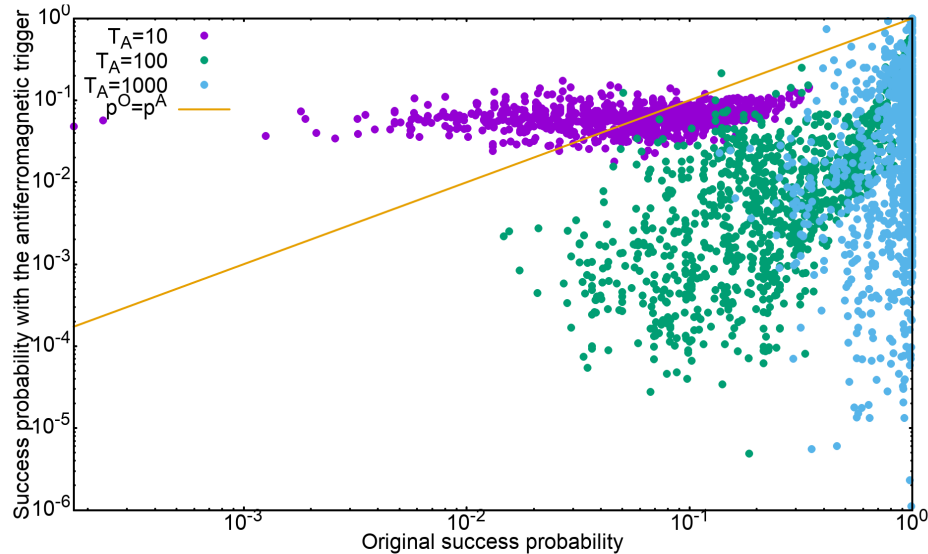


Figure 6.6: A plot of the success probabilities after adding the antiferromagnetic trigger with  $g=0.5$  ( $p^A$ ), with the original success probabilities( $p^O$ ) for annealing time 10, 100 and 1000.

For problem 709, Fig. (6.7) shows the energy gap between the ground state and the first excited state of the Hamiltonian (as a function of the annealing parameter  $s$ ), before and after adding the antiferromagnetic trigger. The inset of the figure also shows the energy gaps for some other problems after adding the trigger. As can be observed from the figure, the shape of the curve after adding the antiferromagnetic trigger to problem 709 is different than both the curve for the original Hamiltonian of this problem and the other problems. The slope in this case, unlike the other cases, is not symmetric about the minimum gap value. While comparing the success probabilities across different problems (and assuming  $p = 1 - \exp(-T\Delta^2/c)$ ), the slope ( $c$ ) for each problem was supposed to have a similar value, and only changes in the minimum gaps were accounted for. Since this assumption breaks down for this case, the Landau-Zener formula no longer holds good for this problem.

Finally, we plot the success probability against the minimum energy gaps for all the problems of the set, before and after adding the antiferromagnetic trigger, for all the three annealing times. The resulting plot is shown in Fig. (6.8). (See Fig. (5(b)) in the appendix for the similar plot for the 8-spin problems for all the values of  $g$ .)

It can be noted from Fig. (6.8) that the original success probabilities mostly follow the Landau-Zener dependence on minimum energy gaps (3.7), although the scattering for  $T_A=10$  is comparatively large. As the annealing time is increased, the scattering becomes less prominent. However, upon adding the trigger, the scattering becomes even larger, so that the points corresponding to  $T_A=10$  appear rather flat. Additionally, the problems with smaller minimum gaps have a higher success probability for  $T_A=10$  than for  $T_A=100$ , due to non-adiabatic evolution of the system in these problems. In this case too the curves become successively less scattered on increasing the annealing time and the general effect of adding the trigger with strength  $g=0.5$  is to shift the points leftwards by reducing the minimum energy gaps.

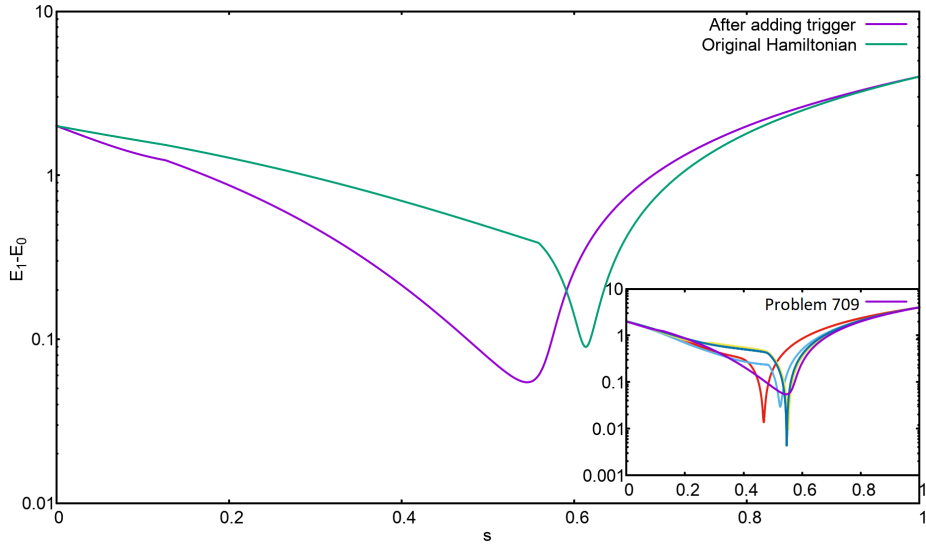


Figure 6.7: A comparison of the minimum energy gaps between the two lowest energy levels as a function of the annealing parameter  $s$ , in the absence and presence of the antiferromagnetic trigger with  $g=0.5$ . The inset shows a comparison with some other problems after adding the trigger.

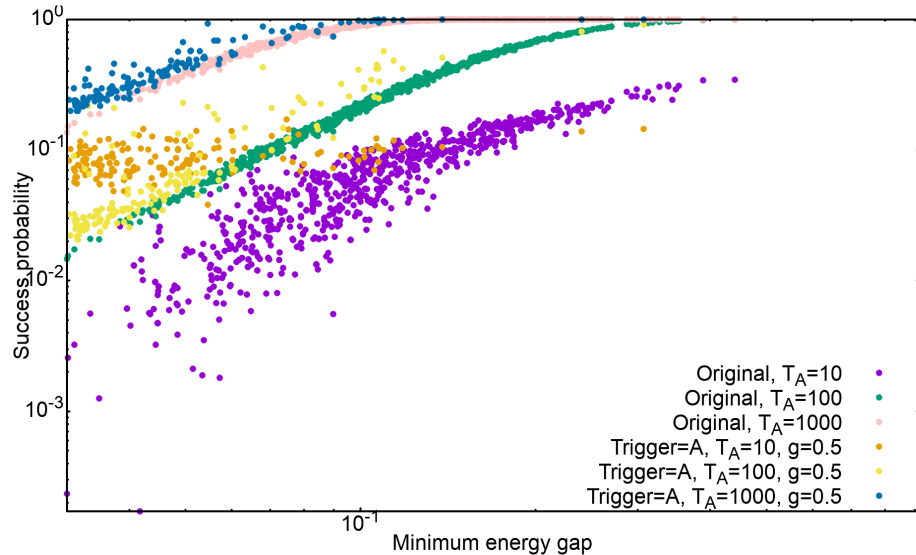


Figure 6.8: Success probability versus minimum energy plot for all the problems belonging to the set of 12-spin SAT problems, for annealing times 10, 100 and 1000, in the absence and presence of the antiferromagnetic trigger.

### 6.3 Trigger strength $g=1$

This section features the same analysis as the last section but with the value of the strength parameter  $g=1$ .

We begin by showing the distribution of the relative success probability after adding the antiferromagnetic trigger with  $g=1$ , for annealing times 10, 100 and 1000, in Fig. (6.9).

We find that 377 problems have an improved success probability after adding the antiferromagnetic trigger for  $T_A=10$ . This number reduces to 215 and 200 upon increasing the annealing time to 100 and 1000 respectively. Moreover, as the annealing time is increased, the largest value of the relative success probability drops from 501 at  $T_A=10$ , to 15.85 at  $T_A=100$ , to 6.31 at  $T_A=1000$ . Again, to obtain more insight about the effects of adding the antiferromagnetic trigger with  $g=1$ , the minimum energy gaps are computed for all the problems of the set after adding the trigger. Figure (6.10) shows the resulting scatter plot between the minimum energy gaps after adding the antiferromagnetic trigger against the original minimum energy gaps.

In this case, 879 problems have smaller minimum energy gaps upon the addition of the trigger. Thus, a decrease in the success probability for most of the cases compared to the original, for all annealing times, seems to be plausible.

Furthermore, for most of the cases the number of energy anti-crossings between the ground state and the first excited state increases to 2, while in one case it was noted to be 4. Table (6.4) shows the number of cases with different number of anti-crossings.

Number of anti-crossings	Number of cases
1	202
2	705
3	92
4	1

Table 6.4: Number of cases with different number of anti-crossings after adding the antiferromagnetic trigger.

To obtain a feeling of the difficulty of the problems which have a relative success ratio greater than one, a scatter plot of the success probabilities after adding the antiferromagnetic trigger against the original success probabilities is shown in Fig. (6.11).

Again, it can be noted that for  $T_A=10$ , the 377 problems that have a higher success probability after adding the antiferromagnetic trigger are limited to the cases with smaller original success probability (smaller minimum gaps). Since adding the trigger reduces the minimum energy gap in most of the cases, the cases with smaller  $p^O$  mostly benefit from a non-adiabatic evolution (shorter annealing time).

To understand the role that the annealing time plays in improving the success probability, the scatter plots for the minimum energy gaps were plotted only for the problems with a relative success probability greater than 1 for a fixed annealing time. Figure (6.12) shows the resulting plots for annealing times of 10, 100 and 1000.

Out of the 377 problems with higher success probability after adding the antiferromagnetic trigger for  $T_A=10$ , 279 problems have a reduced minimum energy gap as a consequence of adding the trigger. These problems can therefore be expected to be benefiting from a non-adiabatic evolution for small annealing time of  $T_A=10$ . On the other hand, for the rest 98 problems, the minimum gaps increase. It was noted that except for 2 cases (problems 325 and 705), all the problems with enlarged minimum gap and improved success probability for  $T_A=10$  also have an improved success probability for  $T_A=100$  and  $T_A=1000$ . This suggests that for these cases, adding the antiferromagnetic trigger increases the minimum energy gap enough to make the evolution closer to adiabatic even for  $T_A=10$ .

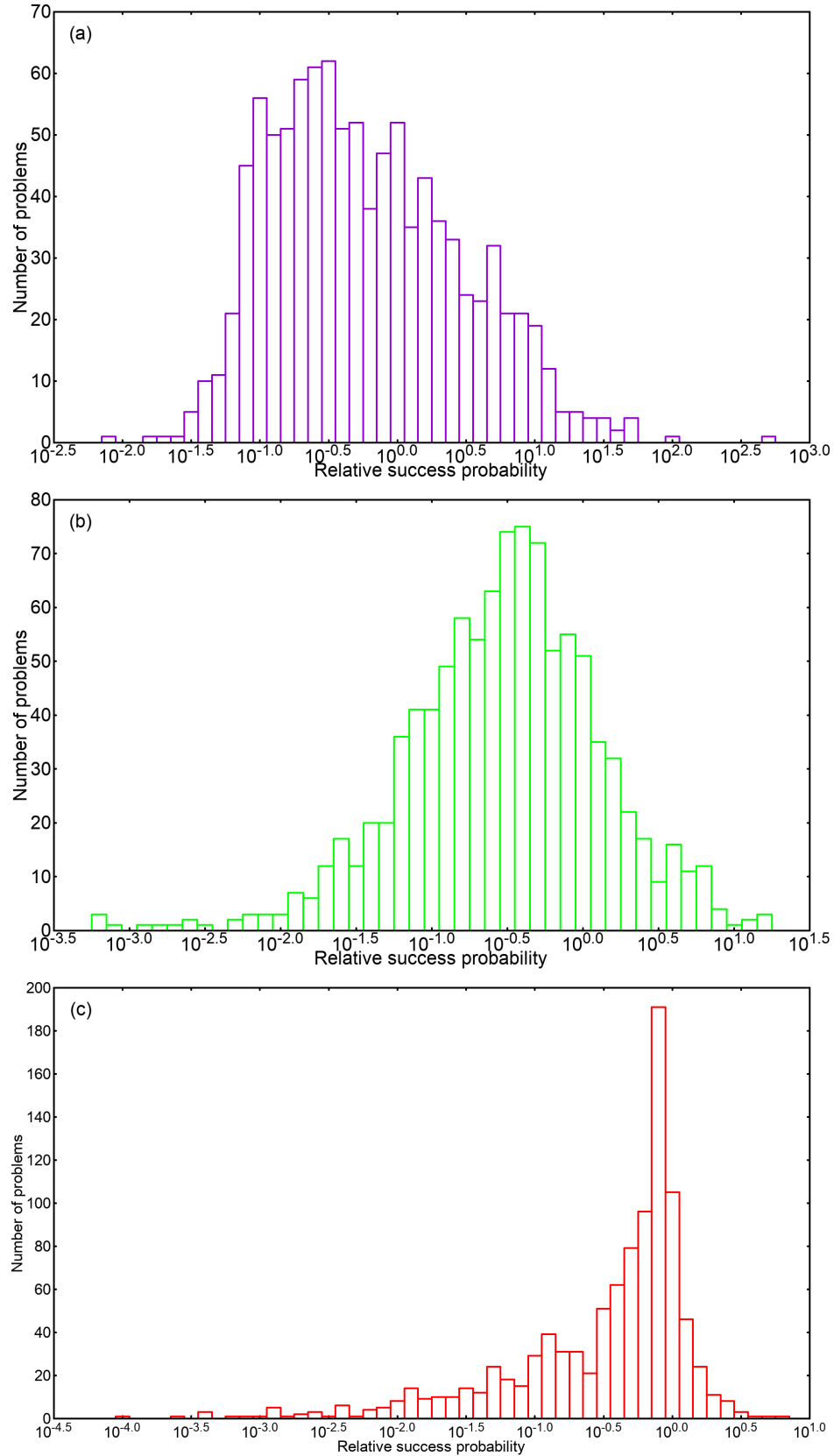


Figure 6.9: Distribution of the relative success probability  $p^A/p^O$  for  $g=1$ . (a):  $T_A=10$ ; (b):  $T_A=100$ ; (c):  $T_A=1000$ .

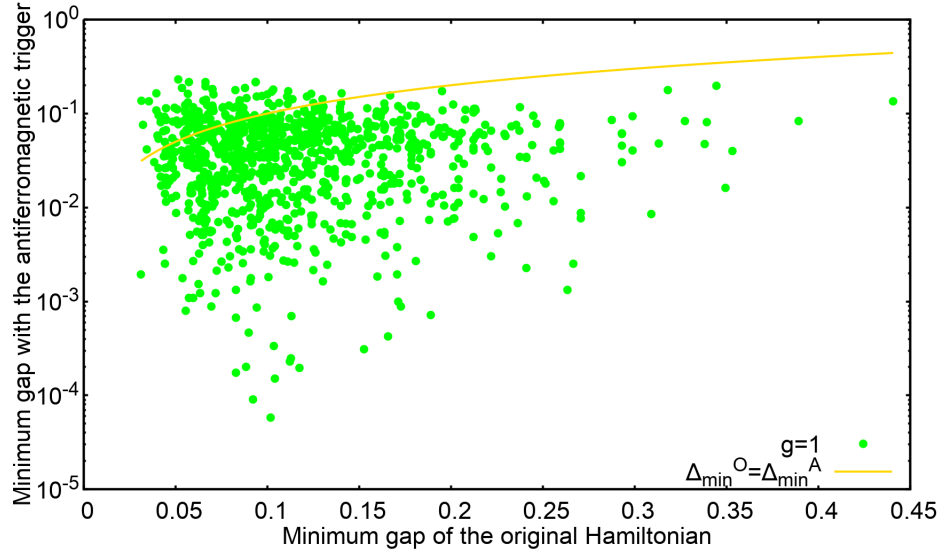


Figure 6.10: A plot of the minimum energy gaps after adding the antiferromagnetic trigger with  $g=1$  ( $\Delta_{min}^A$ ), with the original minimum energy gaps ( $\Delta_{min}^O$ ). For 879 problems the minimum energy gap decreases after adding the trigger.

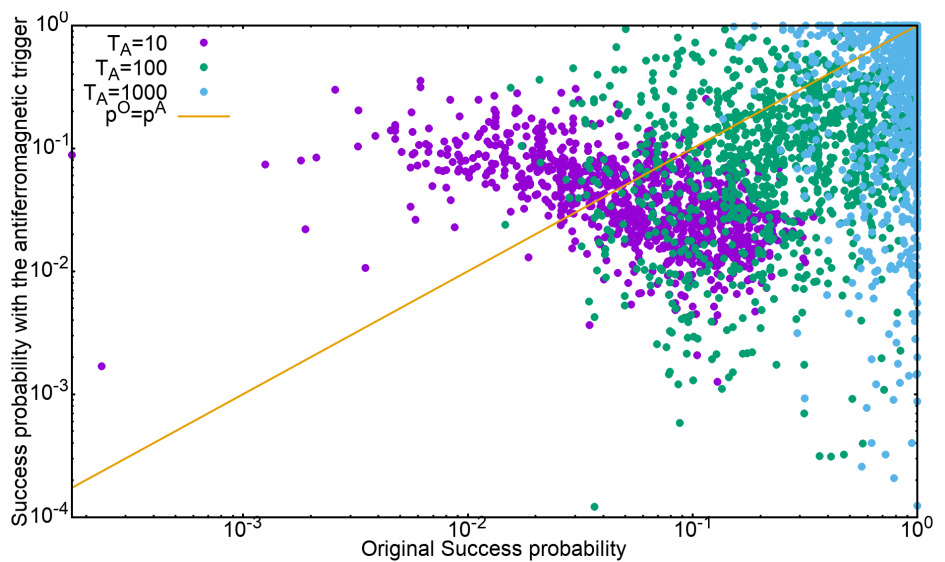


Figure 6.11: A plot of the success probabilities after adding the antiferromagnetic trigger with  $g=1$  ( $p^A$ ), with the original success probabilities ( $p^O$ ) for annealing time 10, 100 and 1000.

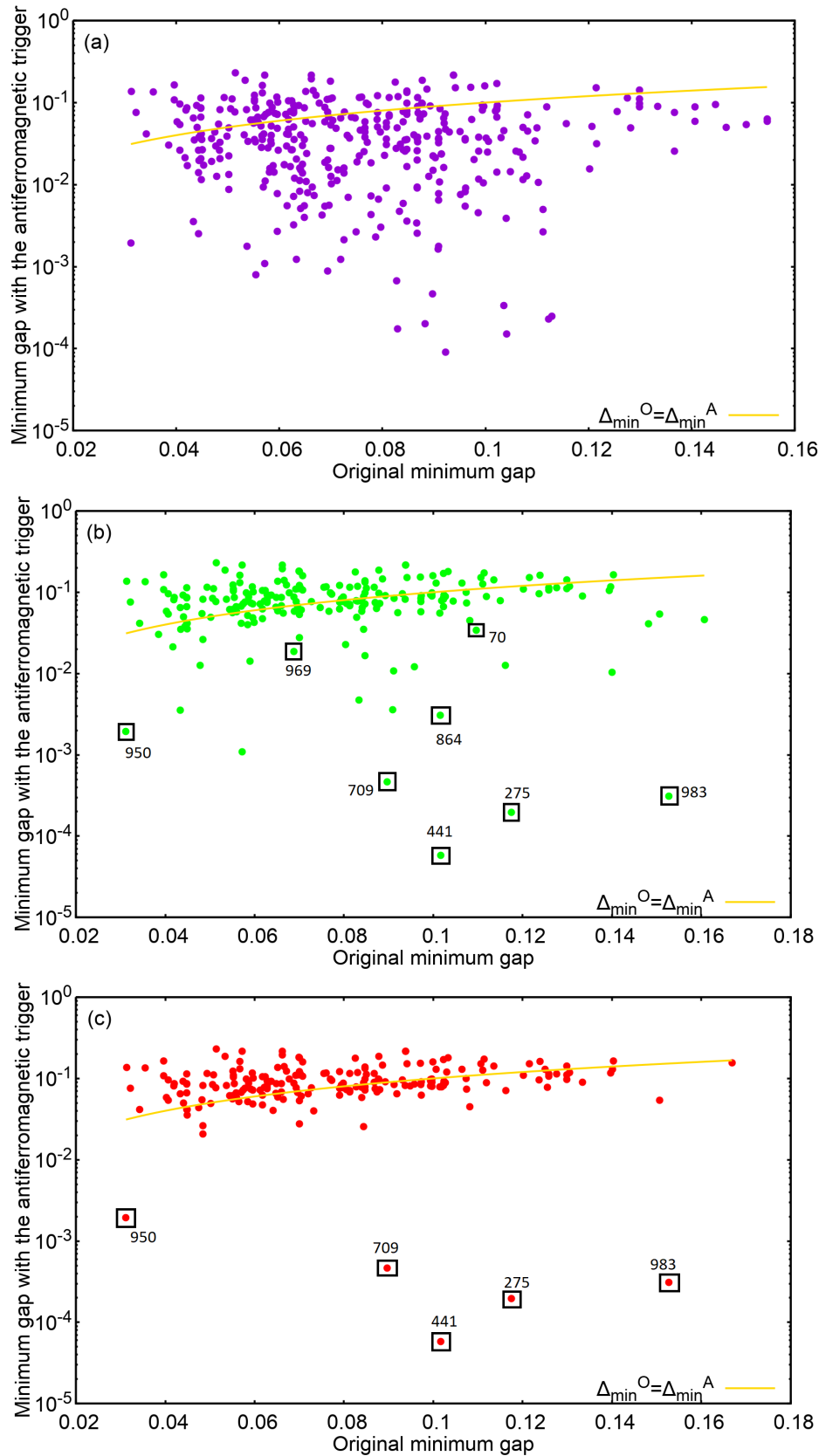


Figure 6.12: Scatter plot of energy gaps  $\Delta^A$  with  $\Delta^O$  for cases with improved success probability after adding the antiferromagnetic trigger with  $g=1$ . (a):  $T_A = 10$ ; (b):  $T_A = 100$ ; (c):  $T_A = 1000$ . For a certain subset of the problems, the corresponding problem number is indicated next to the points.

Additionally, for problems 325 and 705, the relative success probability is greater than 1 for  $T_A=10$  and  $T_A=1000$ , while it is smaller than 1 for  $T_A=100$ . The energy spectra and the mechanism leading to this trend are similar for both these problems. Therefore, Fig. (6.13) shows the energy spectrum and the energy expectation values for the state, before and after adding the trigger for problem 705.

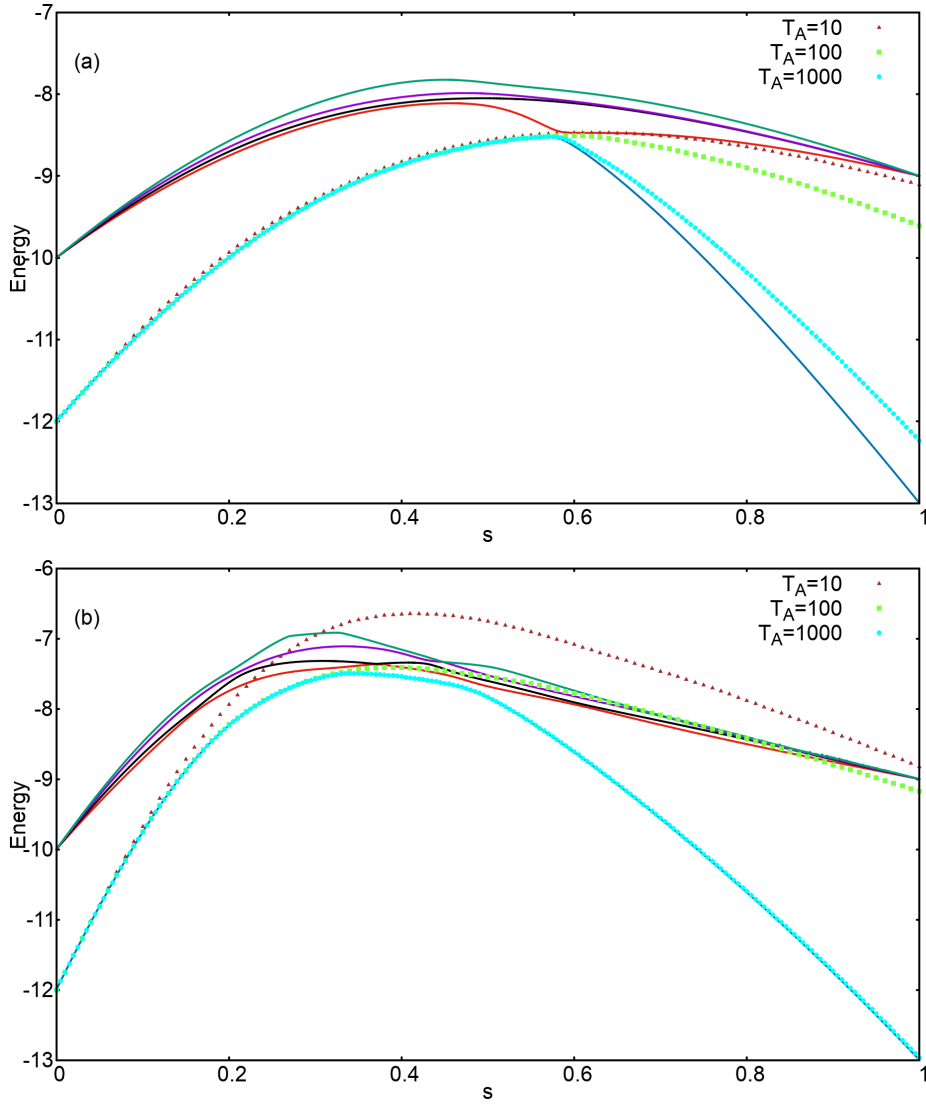


Figure 6.13: Energy spectrum and energy expectation values for the instantaneous state for problem 705. (a): Original Hamiltonian; (b): Antiferromagnetic Hamiltonian.

Although adding the trigger enlarges the minimum gap in these cases, the spectrum of the problem changes in a way such that the first excited state is present in the vicinity of the ground state for a longer time. In this particular case, this gives the system state a chance to transit to the higher energy levels even before the first energy anti-crossing for  $T_A=10$ , and end in a state with a larger overlap with the ground state than in the original case, where it closely follows the first excited state after the anti-crossing. For  $T_A=100$ , and in the presence of the trigger, the state shifts to the higher excited state at the second energy anti-crossing, but this time the overlap of the final state with the ground state is smaller than that in the case of the original Hamiltonian. Finally, an annealing time of  $T_A=1000$  becomes long enough for the evolution to become adiabatic, and since the minimum energy gap is increased after adding the trigger, the success probability in the presence of the trigger becomes larger.

Next, from Fig. (6.12(a) and 6.12(c)) it can be noted that the majority of the problems improved by adding the antiferromagnetic trigger, and choosing the annealing time to be  $T_A=100$  or  $T_A=1000$  correspond to the cases where the minimum energy gaps become larger upon adding the trigger. Out of the 215 (200) problems improved

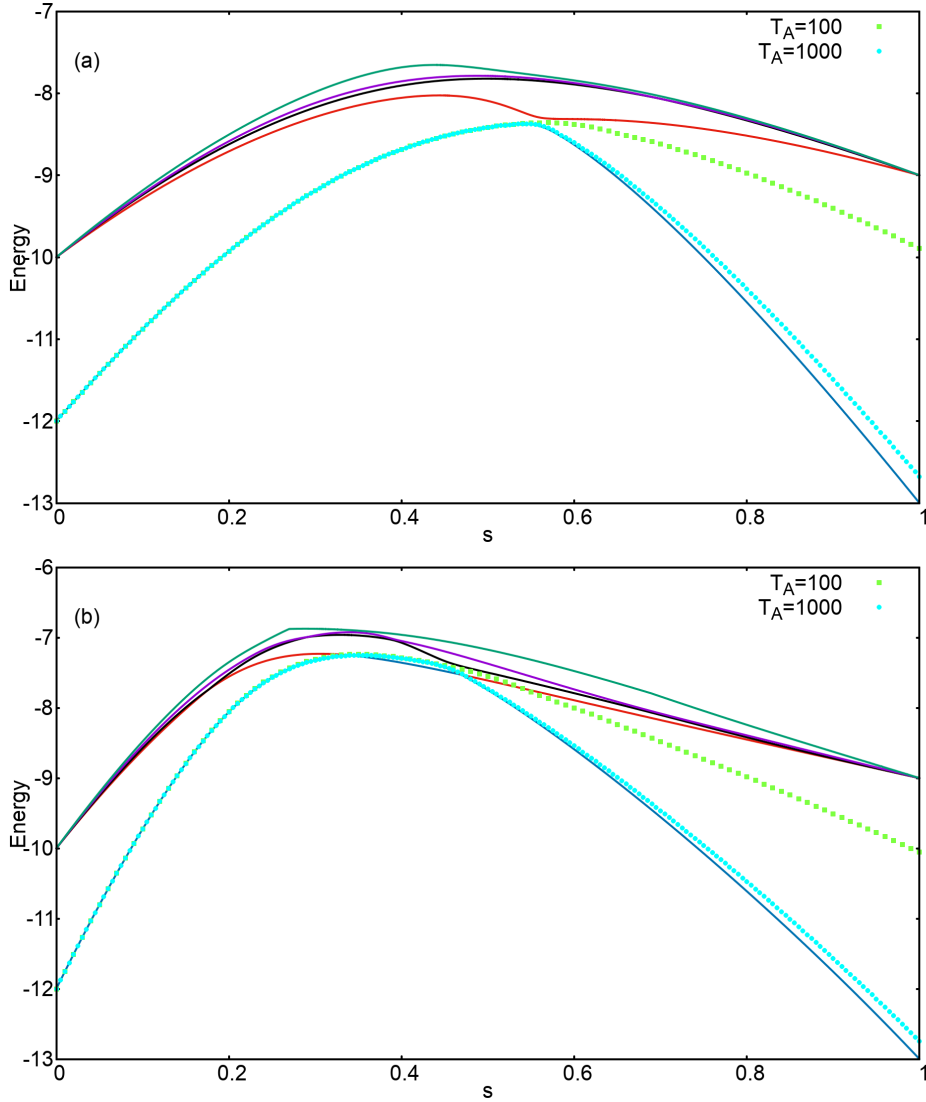


Figure 6.14: Energy spectrum and energy expectation values for the instantaneous state for problem 441. (a): Original Hamiltonian; (b) Antiferromagnetic Hamiltonian.

after adding the trigger for  $T_A=100$  ( $T_A=1000$ ), 117 (121) problems have larger minimum gaps after including the trigger.

Some of the problems with an improved success probability despite of a reduced minimum energy gap were selected and their dynamics was studied. These have been marked in the middle and bottom panel of Fig. (6.12).

It can be noticed that problems 275, 441, 709, 950 and 983 appear in both the figures. The conclusions drawn are the following:

- For problems 70, 275, 441, 709 and 864 the presence of two anti-crossings increases the overlap of the final state with the ground state of the Hamiltonian. Figure (6.14) shows the energy spectrum and the energy expectation values for the corresponding state for the original Hamiltonian, and the Hamiltonian after adding the antiferromagnetic trigger.

After adding the trigger to this problem, for both  $T_A=100$  and  $T_A=1000$ , the system state shifts most of its amplitude to the first excited state at the first anti-crossing. On reaching the second anti-crossing, some of the amplitude of the state comes back to the ground state, thus increasing the success probability in these cases.

- To understand the reasons for an improved success probability in problem 950, the overlap of the state of the system was computed with the three lowest energy states of the instantaneous Hamiltonian, for  $T_A=100$ .

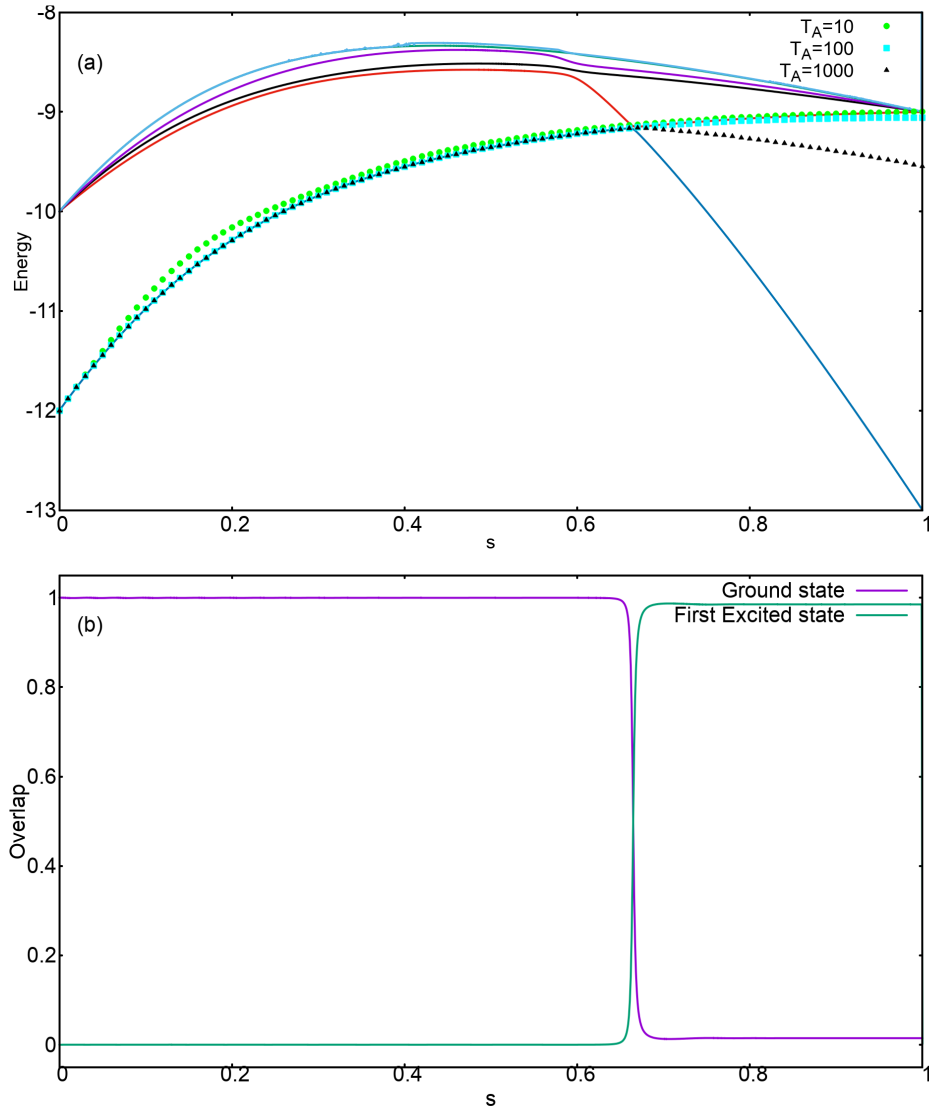


Figure 6.15: Original Hamiltonian in Problem 950. (a): The energy spectra and instantaneous energy expectation values corresponding to  $T_A=100$ , and  $T_A=1000$ ; (b): The overlap of the system state with the three lowest lying energy levels of the instantaneous Hamiltonian for  $T_A=100$ .

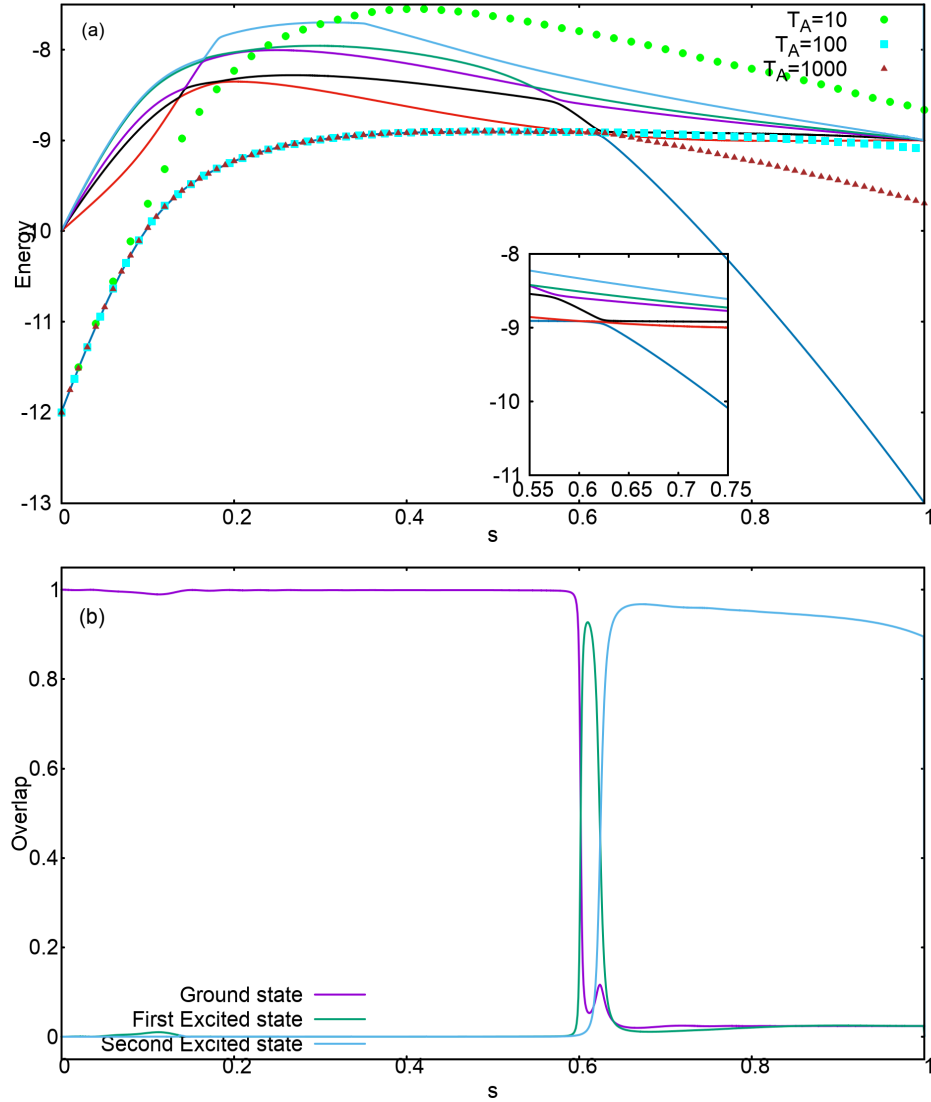


Figure 6.16: After adding antiferromagnetic Hamiltonian to Problem 950. (a): The energy spectra and instantaneous energy expectation values corresponding to  $T_A=100$ , and  $T_A=1000$ ; (b): The overlap of the system state with the three lowest lying energy levels of the instantaneous Hamiltonian for  $T_A=100$ .

As can be observed on comparing Figs. (6.15(a)) and (6.16(a)), the energy spectrum of problem 950 changes significantly upon adding the antiferromagnetic trigger. The minimum energy gap becomes smaller, and the two lowest energy states remain in close vicinity for longer. Unlike the shift of the state of the system to the first excited state at the anti-crossing, and following it closely thereafter in the original Hamiltonian for  $T_A=100$  (see Fig. (6.15(b))), the dynamics of the state becomes more complex after including the antiferromagnetic trigger. It can be noted from Fig. (6.16(b)) that upon adding the trigger the system transits to the first excited state before the second anti-crossing, from where it shifts most of its amplitude to the second excited state. The remaining amplitude in the first excited state comes back to the ground state at the second anti-crossing, improving the success probability. Similar dynamics can be expected to benefit the case for  $T_A=1000$  case as well.

- Again, to understand the exact dynamics in case of problem 969, the overlap of the system state with the three lowest energy levels of the Hamiltonian was computed. As was the case in the original Hamiltonian of problem 950, from Fig. (6.17) it can be observed that the system state shifts most of its amplitude to the first excited state at the anti-crossing, after which it stays close to the first excited state for the rest of the course. This decreases the overlap with the ground state, thus explaining the small success probability.

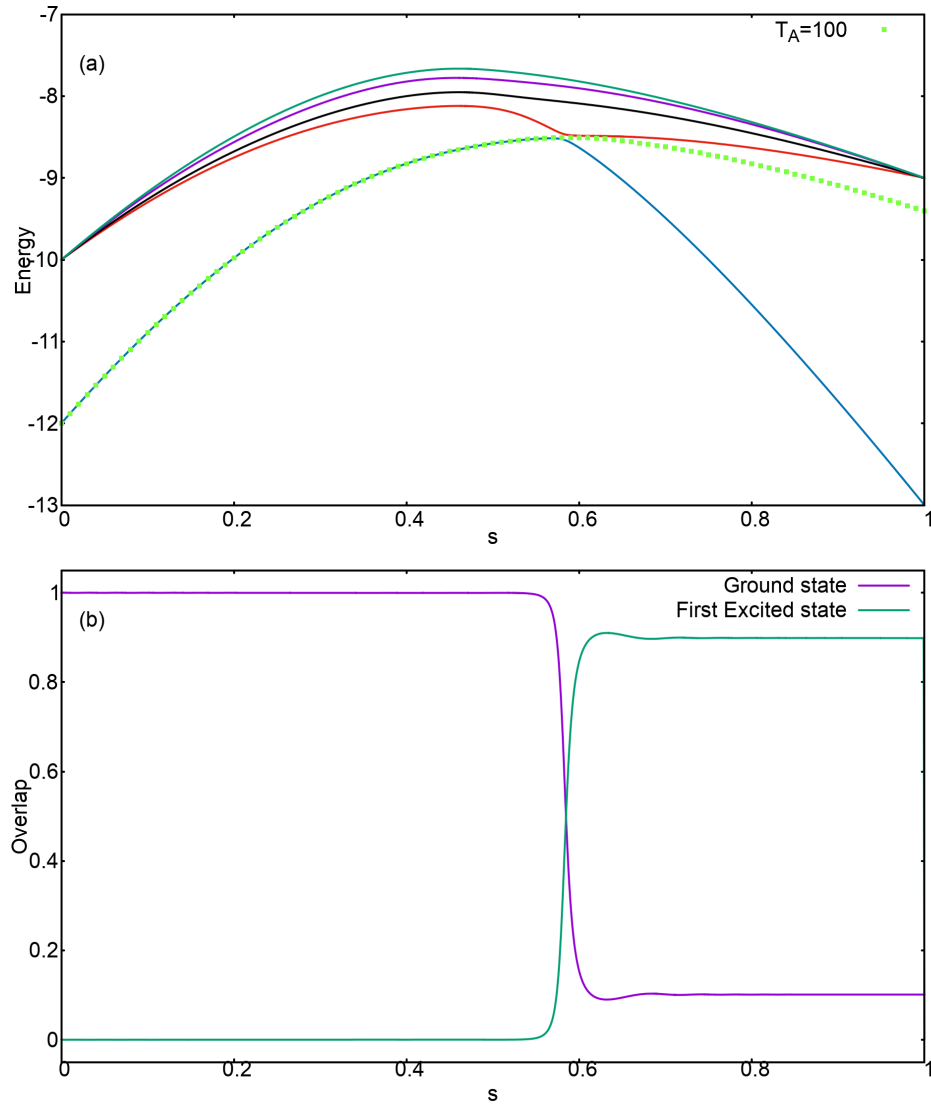


Figure 6.17: Original Hamiltonian in Problem 969. (a): The energy spectra and instantaneous energy expectation values corresponding to  $T_A=100$ , and  $T_A=1000$ ; (b): The overlap of the system state with the three lowest lying energy levels of the instantaneous Hamiltonian for  $T_A=100$ .

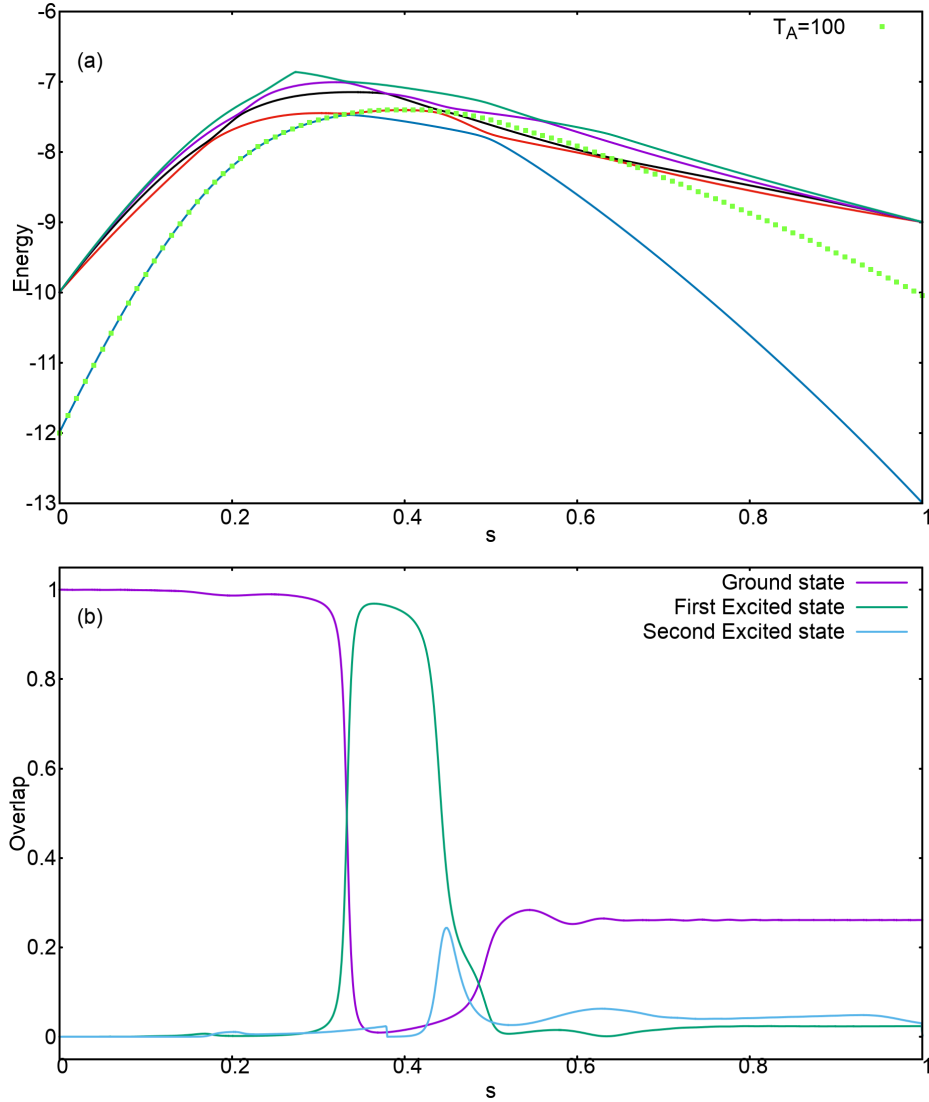


Figure 6.18: After adding antiferromagnetic Hamiltonian to Problem 969. (a): The energy spectra and instantaneous energy expectation values corresponding to  $T_A=100$ , and  $T_A=1000$ ; (b): The overlap of the system state with the three lowest lying energy levels of the instantaneous Hamiltonian for  $T_A=100$ .

Figure (6.18(b)) makes it clear that on adding the antiferromagnetic trigger the system state shifts to the first excited state at the first anti-crossing. It shifts the amplitude further to the close lying higher excited states. However, since the first and second excited states stay close enough for a long time, so that the state continuously exchanges the amplitude between these states, the overlap with these states oscillates. As the state approaches the second anti-crossing, the amplitude present in the second excited state shifts back to ground state.

- Finally, for problem 983, Fig. (6.19) shows the energy gap between the lowest two energy levels as a function of the annealing parameter  $s$ , for the original Hamiltonian, and after adding the antiferromagnetic trigger. The minimum energy gap after adding the trigger becomes wider, so that the ground state and the first excited state stay close for longer. This gives the state a chance to redistribute the amplitude between these states. Therefore, despite the decrease in the minimum energy gap, there is a larger amplitude in the ground state in this case, compared to that in the original Hamiltonian.

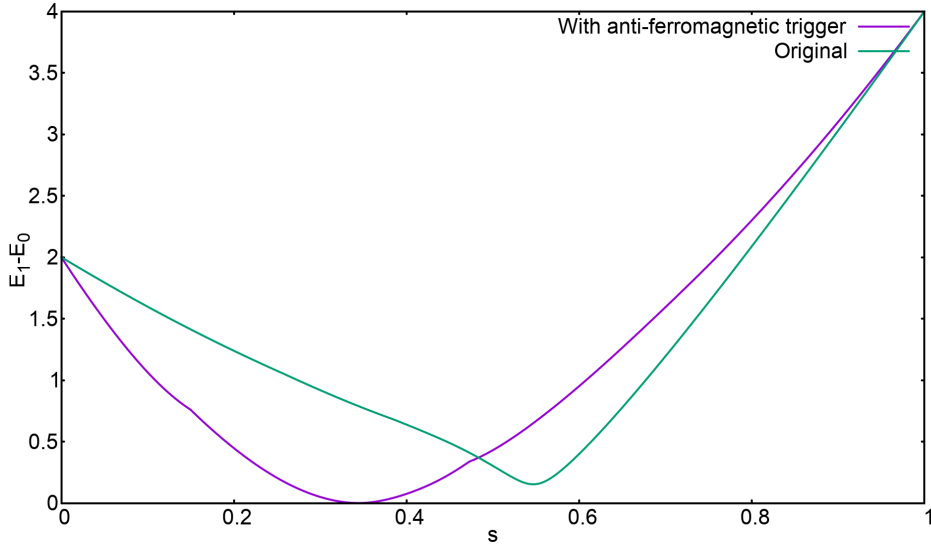


Figure 6.19: Energy gap between the ground state and the first excited state of the original Hamiltonian, and that after adding the antiferromagnetic trigger with  $g=1$ .

Figure (6.20) shows the plot for the success probabilities for different problems against the corresponding minimum gaps.

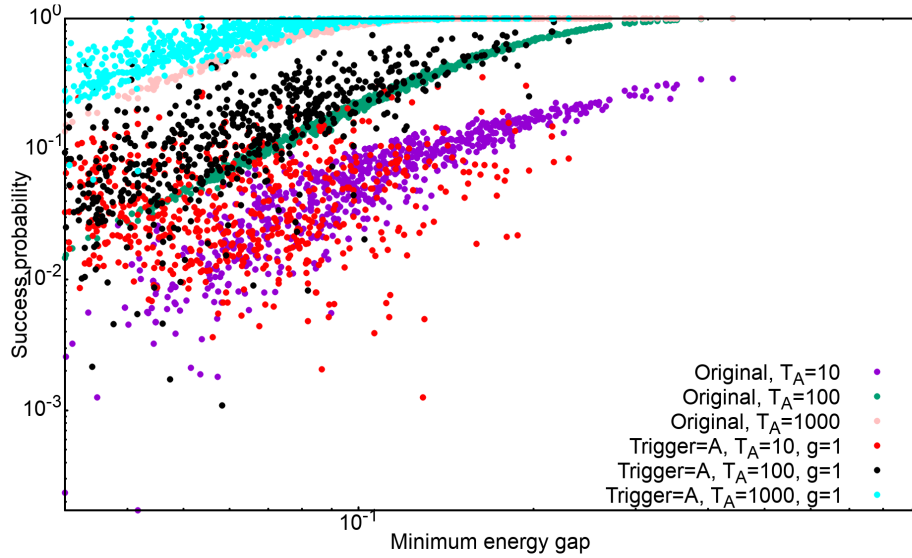


Figure 6.20: Success probability versus minimum energy plot for all the problems belonging to the set of 12-spin problems, for annealing times 10, 100 and 1000, in the absence and presence of the antiferromagnetic trigger.

It can be seen that compared to the success probability versus minimum energy gap corresponding to the Hamiltonian where the antiferromagnetic trigger is added with  $g=0.5$  (see Fig. (6.8)), the scattering in case of adding the antiferromagnetic trigger with  $g=1$  is larger for all the three annealing times. This indicates that the success probability is benefiting through non-adiabatic mechanisms for a larger fraction of problems in this case. One of the plausible reasons for this can be the increased number of energy anti-crossings between the ground state and the first excited state of the Hamiltonian. It can also be observed that unlike in Fig. (6.8), the curves for this case can be more easily distinguished to roughly have the Landau-Zener form, and that the points are not as restricted towards the left as a consequence of adding the trigger. This can be attributed to the presence of cases with enlarged minimum energy gaps as well.

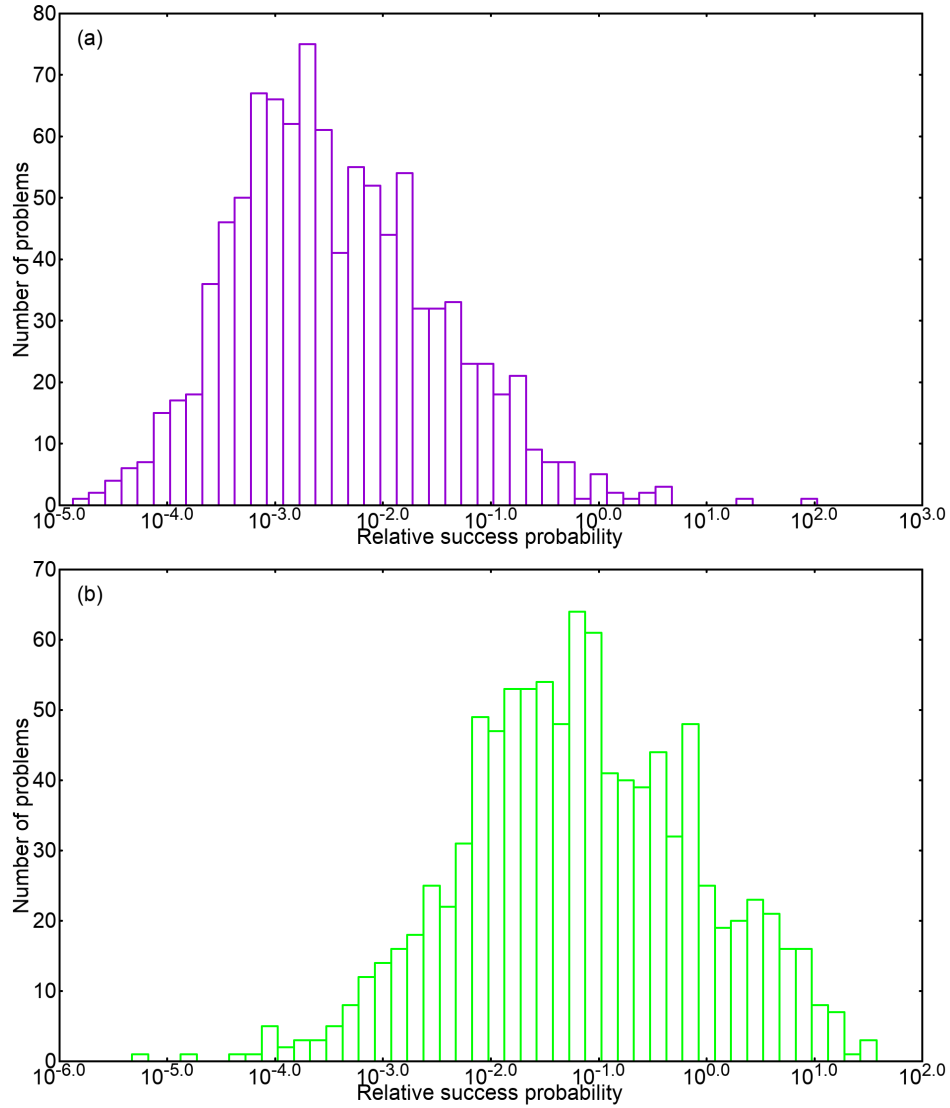


Figure 6.21: Distribution of the relative success probability  $p^A/p^O$  for  $g=0.5$ . (a):  $T_A=10$ ; (b):  $T_A=100$ .

## 6.4 Trigger Strength $g=2$

Finally, in this section the effects of adding the antiferromagnetic trigger with strength  $g=2$  are discussed.

Figure (6.21) shows the distribution of the relative success probability after adding the antiferromagnetic trigger for  $T_A=10$  and  $T_A=100$ . In this case, only 15 problems have an improved success probability after adding the trigger for  $T_A=10$ . Upon increasing the annealing time to 100, this number increases to 158, and to 225 for  $T_A=1000$ . This is in contrast with the observations from the previous sections where the number of the problems with improved success probability is maximal for  $T_A=10$ .

Furthermore, for  $T_A=1000$  the spread of the relative success probability is only from 0.63 to 1.58, i.e. the effect of adding the trigger is only marginal. Additionally, for 448 problems the relative success probability is 1. For this reason the histogram for the distribution of the success probability for  $T_A=1000$  is omitted.

Figure (6.22) shows the scatter plot of the minimum energy gaps after adding the antiferromagnetic trigger ( $\Delta^A$ ) against the original minimum energy gaps ( $\Delta^O$ ), for  $g=2$ . In this case, the minimum energy gaps reduce for 798 problems upon adding the trigger. It can also be noted that with the antiferromagnetic trigger of strength 2 the energy spectrum changes significantly in terms of the number of anti-crossings between the ground and the first energy level, and the proximity of the higher energy levels. Table (6.5) shows the number of cases with different number of anti-crossings.

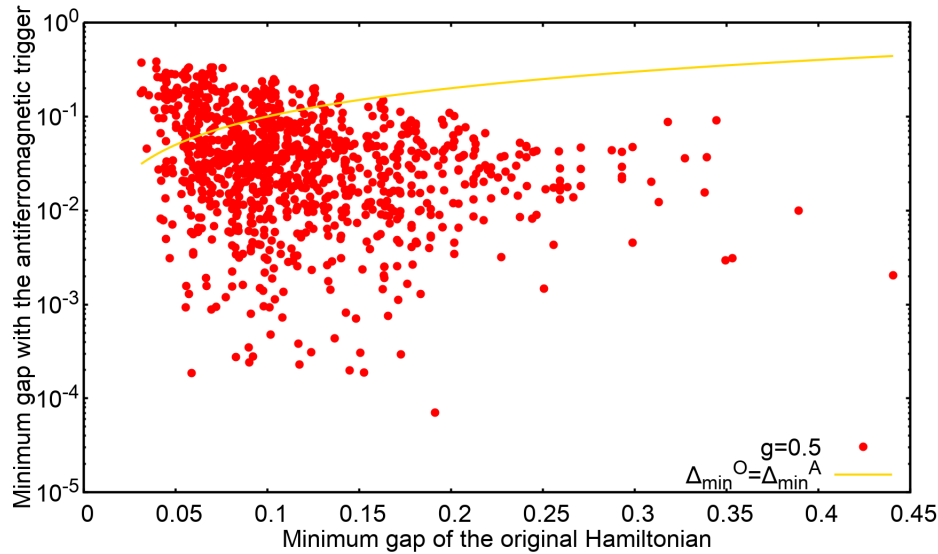


Figure 6.22: A plot of the minimum energy gaps after adding the antiferromagnetic trigger with  $g=2$  ( $\Delta_{\min}^A$ ), with the original minimum energy gaps ( $\Delta_{\min}^O$ ). For 798 problems the minimum energy gap decreases after adding the trigger.

Number of anti-crossings	Number of cases
1	1
2	132
3	439
4	33
5	65

Table 6.5: Number of cases with different number of anti-crossings after adding the antiferromagnetic trigger with  $g=2$ .

Next, to assess the difficulty of problems affected by adding the antiferromagnetic trigger to the Hamiltonian, Fig. (6.23) shows the scatter plot of the success probabilities upon including the antiferromagnetic trigger ( $p^A$ ) with the original success probabilities ( $p^O$ ).

In this case too, the spread of the problems improved by adding the trigger is the largest for  $T_A=10$ . This can be attributed to the small original success probability ( $p^O$ ) for a small annealing time of  $T_A=10$ , or to the non-adiabatic evolution mechanisms leading to a larger overlap with the ground state. In this case the problems with the three largest relative success probabilities corresponding to  $T_A=10$ , have smaller original success probabilities accounting for large improvements (the maximum relative success probability is 93.91). For  $T_A=100$  and  $T_A=1000$  the improvements become successively limited, with maximum relative success probabilities being 41.36 and 7.34 respectively. This is a consequence of increasing original success probabilities for longer annealing times. To understand the role that the annealing time plays in improving the success probability, the scatter plots for the minimum energy gaps are plotted only for the problems with a relative success probability greater than 1 for a fixed annealing time. Figure (6.24) shows the resulting plots for annealing times of 10, 100 and 1000.

From Fig. (6.24), it can be noted that 12 out of the 15 problems with an improved success probability for  $T_A=10$ , have larger minimum energy gaps upon including the antiferromagnetic trigger. It can be seen that all of these problems have an improved success probability for longer annealing times of 100 and 1000 as well. This suggests that adding the trigger widened the minimum energy gap enough for the evolution to become closer to adiabatic even for  $T_A=10$ .

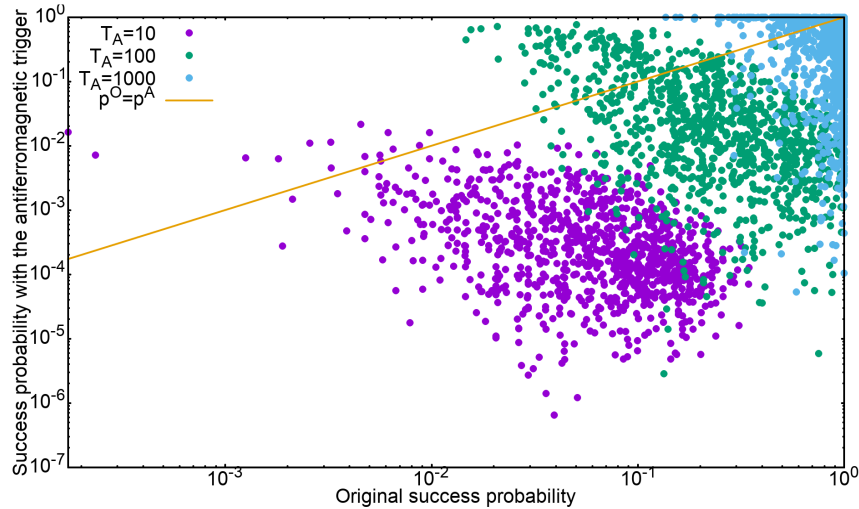


Figure 6.23: A plot of the success probabilities after adding the antiferromagnetic trigger with  $g=2$  ( $p^A$ ), with the original success probabilities( $p^O$ ) for annealing time 10, 100 and 1000.

However, unlike the case in the previous sections, only 3 problems (problem number 478, 693 and 871) with an improved success probability for  $T_A=10$ , have a smaller minimum energy gap after adding the antiferromagnetic trigger. All these problems are benefited from the similar non-adiabatic evolution of the state. The energy spectrum and the instantaneous energy expectation values of the state for the original Hamiltonian and the Hamiltonian after adding the trigger have been shown in Fig. (6.25) for problem 693. For the original Hamiltonian, the state of the system shifts to the first excited state on approaching the energy anti-crossing, and closely follows it thereafter. This makes the overlap of the system state with the ground state negligible. However, in the case where the antiferromagnetic trigger is included, the minimum energy gap reduces, making it feasible for the system to transit to the higher excited levels. Consequently, the system state ends in a superposition state consisting of higher energy levels, which has a larger overlap with the ground state of the Hamiltonian.

In this problem, the success probability after adding the trigger reduces for both  $T_A=100$  and  $T_A=1000$ . For the spectrum with the trigger and  $T_A=100$ , the system state shifts to the first excited state at the first anti-crossing, from where it soon shifts to the higher excited states. Unlike the case for  $T_A=10$ , this time the state follows them closely, resulting in a vanishing overlap with the ground state. For  $T_A=1000$ , on the other hand, the state shifts to the first excited state only on reaching the second anti-crossing. Since the original minimum gap is larger for this problem, the original success probability is larger for this annealing time.

Out of the 158 problems found to have an improved success probability after adding the trigger for  $T_A=100$ , 118 problems also have a larger minimum energy gap as a result of adding the trigger. It can be further noted that all of these cases have a relative success probability greater than 1 for  $T_A=1000$  as well. The energy spectra for some of the remaining 40 cases were studied to understand the evolution of the state. Non-adiabatic mechanisms are responsible for the improvement in the success probabilities in all these cases. For  $T_A=1000$ , 189 out of the 225 cases with an improved success probability upon including the antiferromagnetic trigger, have a larger minimum energy gap after adding the trigger. The energy spectra for some of the remaining 36 cases were also studied, of which 13 problems also have a larger success probability for  $T_A=100$ .

A problem with an interesting dynamics with a larger success probability for both  $T_A=100$  and  $T_A=1000$ , despite of a reduced minimum energy gap, after adding the trigger, is problem 63. To understand the reasons behind the improvement, the overlap of the system state is computed with the three lowest energy states of the instantaneous Hamiltonian. As was the case in the original Hamiltonian of problem 950, from Fig. (6.26) it can be observed that the system state shifts most of its amplitude to the first excited state at the energy anti-crossing, after which it stays close to the first excited state for the rest of the course. This decreases its overlap with the ground state, thus explaining the small success probability.

Figure (6.27(b)) makes it clear that the system state for  $T_A=100$  starts to deviate from the ground state around the first energy anti-crossing. The amplitude shifted to the first excited state immediately transits to the second excited state, and further to the higher excited states. At the second anti-crossing, all of the remaining amplitude of the wave function in the ground state shifts to the first excited state, making the amplitude in the ground state

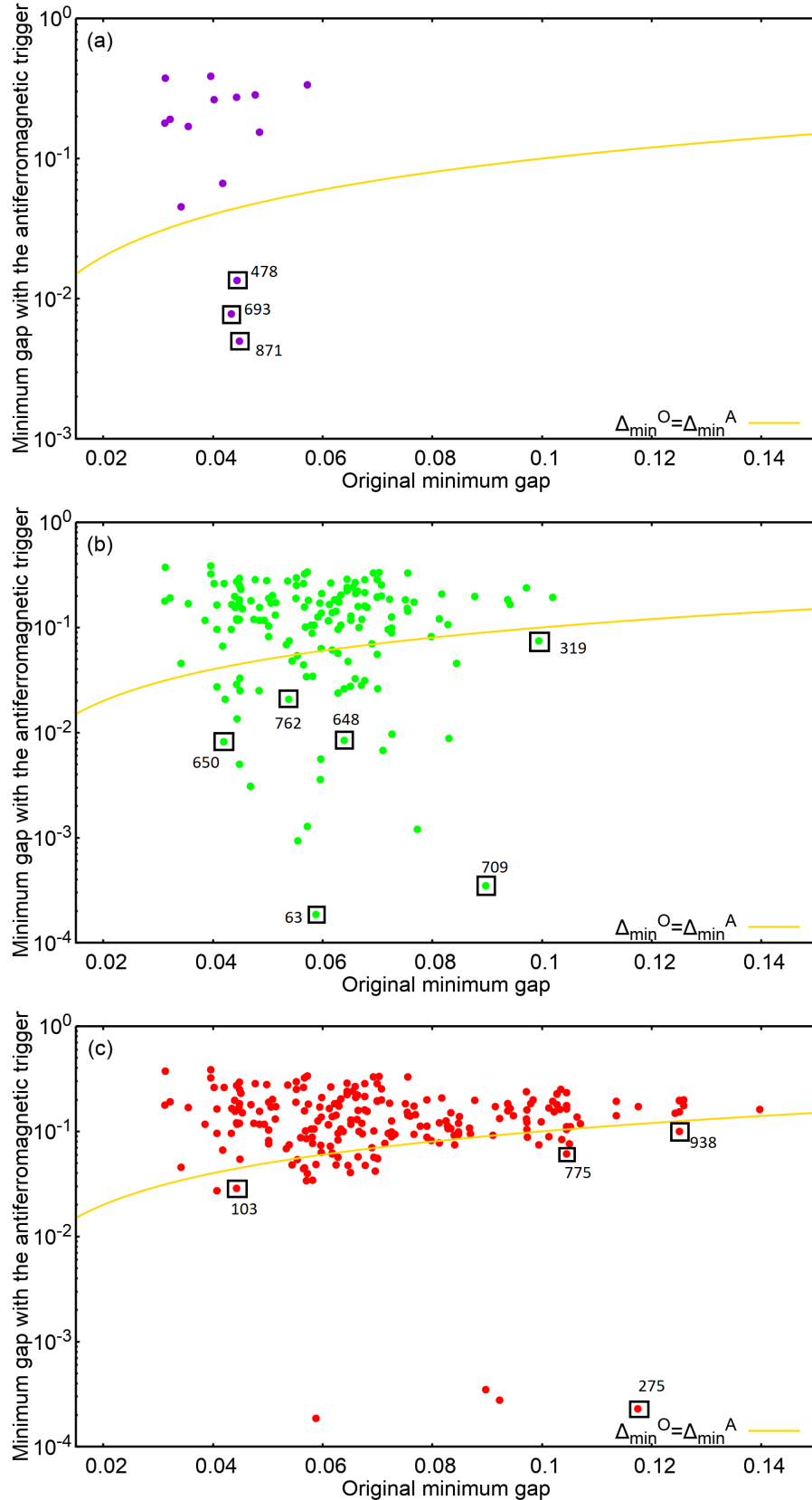


Figure 6.24: Scatter plot of energy gaps  $\Delta^A$  with  $\Delta^O$  for cases with improved success probability after adding the antiferromagnetic trigger with  $g=2$ . (a):  $T_A = 10$ ; (b):  $T_A = 100$ ; (c):  $T_A = 1000$ .

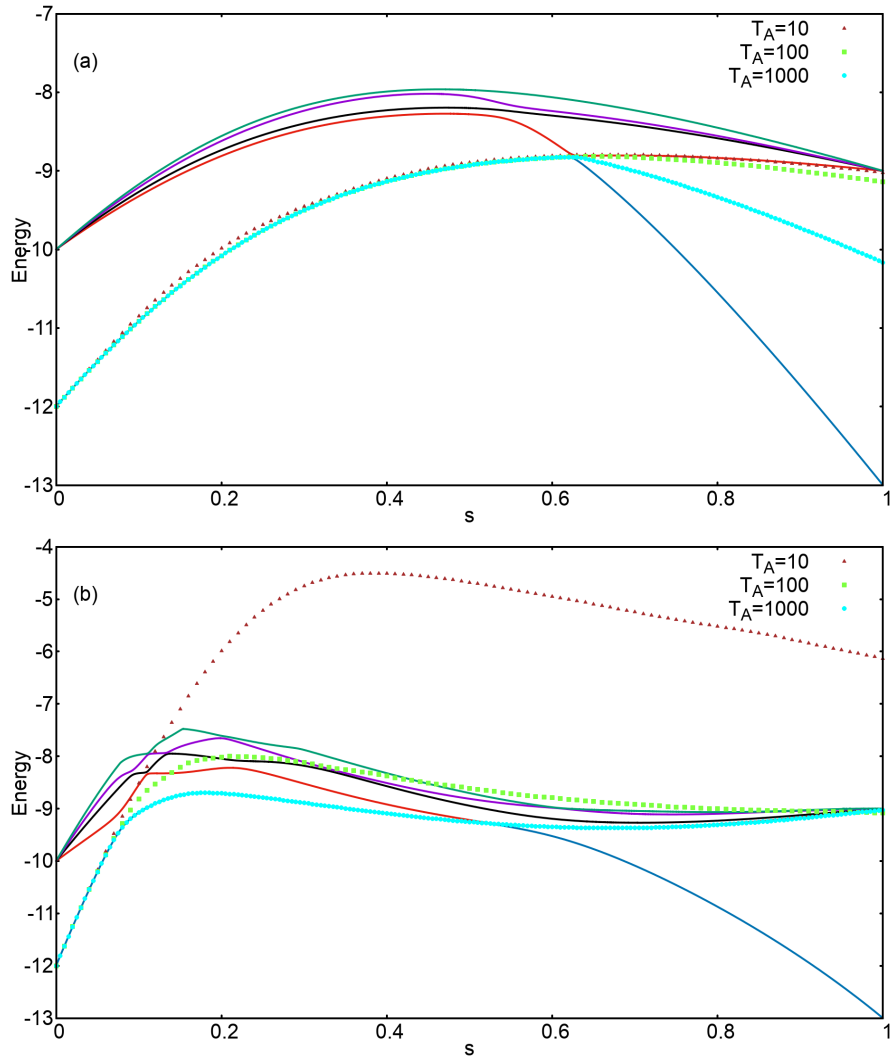


Figure 6.25: Problem 693: Energy spectrum and instantaneous energy expectation values. (a): Original Hamiltonian; (b): Hamiltonian after adding the antiferromagnetic trigger.

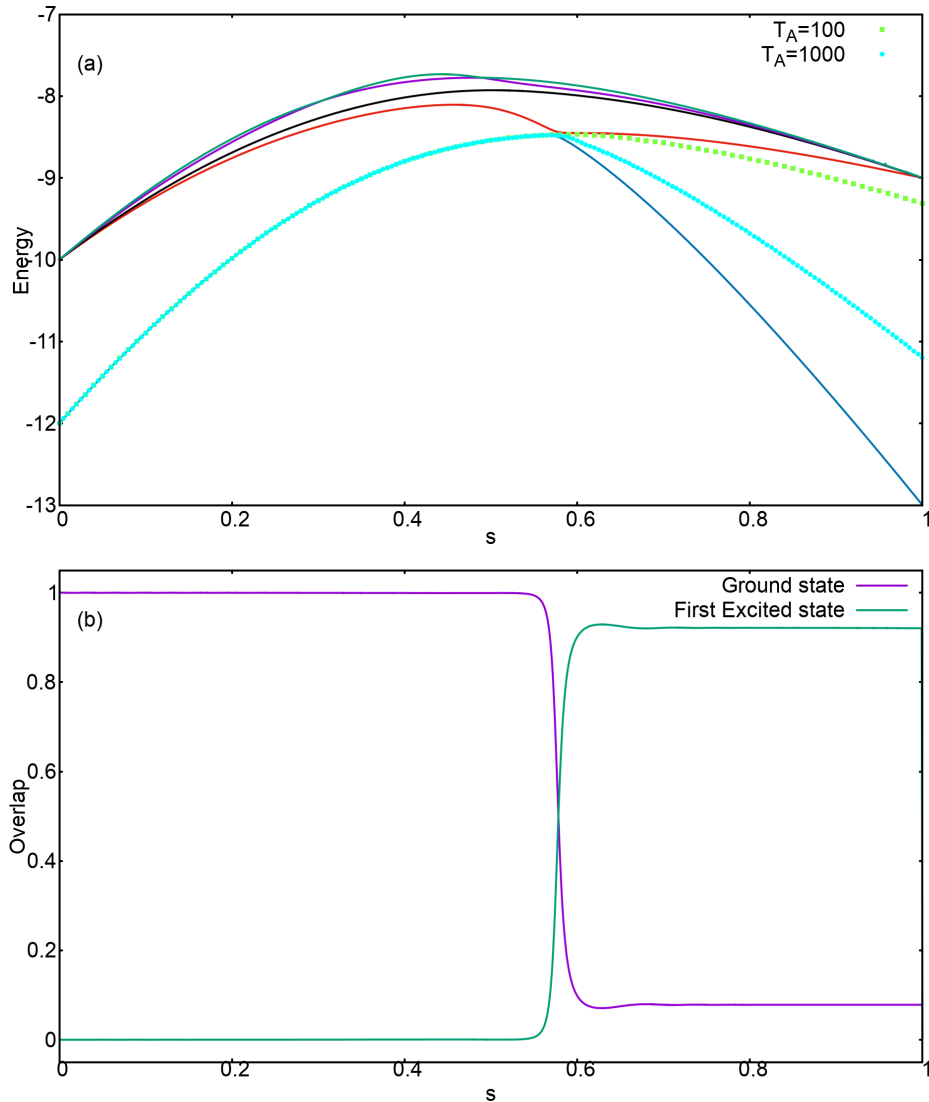


Figure 6.26: For original Hamiltonian in Problem 63: [Top] The energy spectra and instantaneous energy expectation values corresponding to  $T_A=100$ , and  $T_A=1000$ . [Bottom] The instantaneous overlap of the system state with the three lowest lying energy levels of the Hamiltonian for  $T_A=100$ .

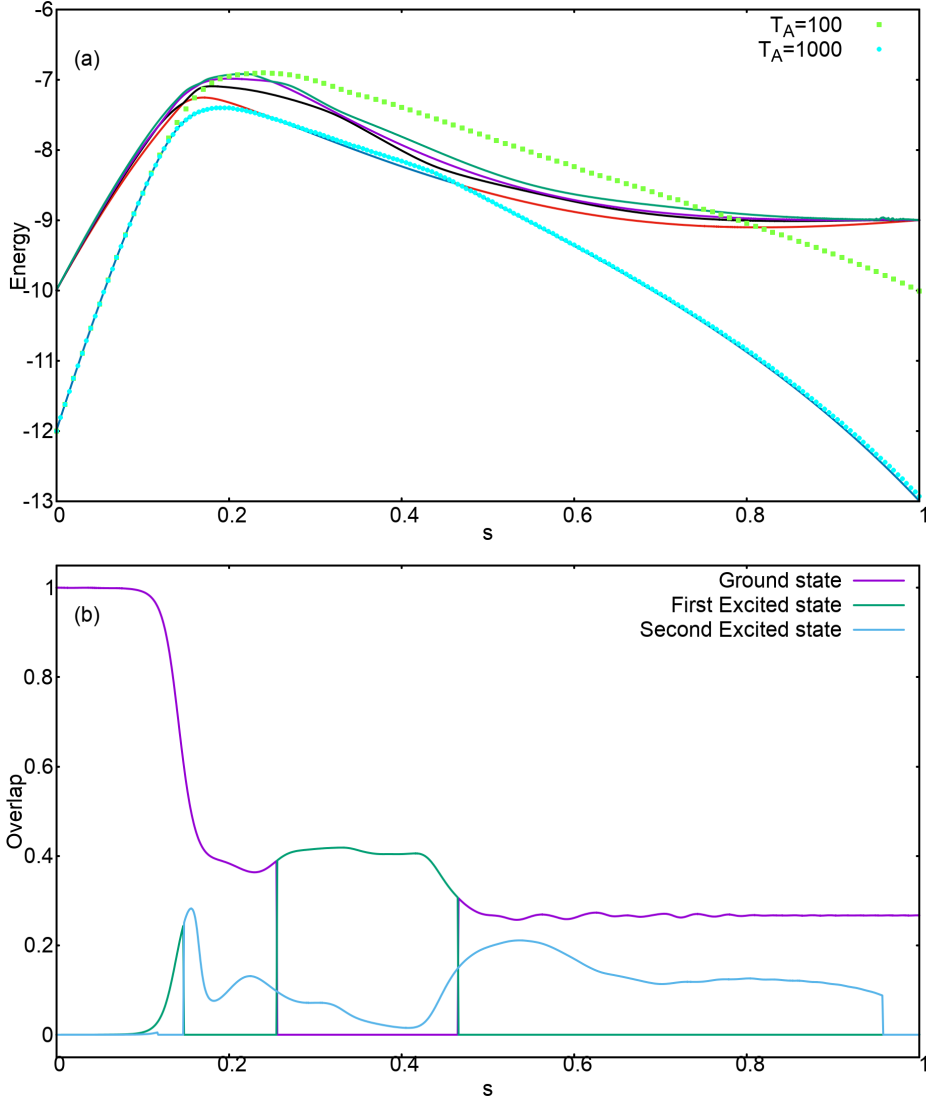


Figure 6.27: After adding the antiferromagnetic Hamiltonian to Problem 63 (a): The energy spectra and instantaneous energy expectation values corresponding to  $T_A=100$ , and  $T_A=1000$ ; (b): The overlap of the system state with the three lowest lying energy levels of the instantaneous Hamiltonian for  $T_A=100$ .

drop to zero. This is suggestive of the fact that the minimum energy gap indeed closes at this point, making it a point of crossing between these energy levels. Another probable point of crossing between these levels occurs around  $s=0.465$ , causing all the amplitude present in the first excited state to transit to the ground state of the Hamiltonian. This results in an improved success probability.

However, no such point of crossing was obtained while computing the minimum energy gaps for this case. This can be a consequence of the limited precision at which the energy spectrum of the time dependent Hamiltonian is computed.

Additionally, as can be observed from Fig. (6.27), for  $T_A=1000$  the system state shifts the full amplitude to the first excited state on reaching the first crossing. This amplitude then comes back to the ground state at the second crossing, explaining the increase in the success probability.

The mechanics of some of the other cases studied is shown in the appendix (see Figs. (7 and 8 in the appendix).

Finally, Fig. (6.28) shows the success probability versus minimum energy gap plot for all the problems of the set, for the original Hamiltonian, and the Hamiltonian after adding the trigger.

Upon adding the antiferromagnetic trigger with  $g=2$ , the scattering of the points of the curves increases compared to that of the original curves, as well as for the curves with the antiferromagnetic trigger with  $g=1$  (see Fig. (6.20)). This indicates that a larger number of problems have a non-adiabatic evolution in this case. This

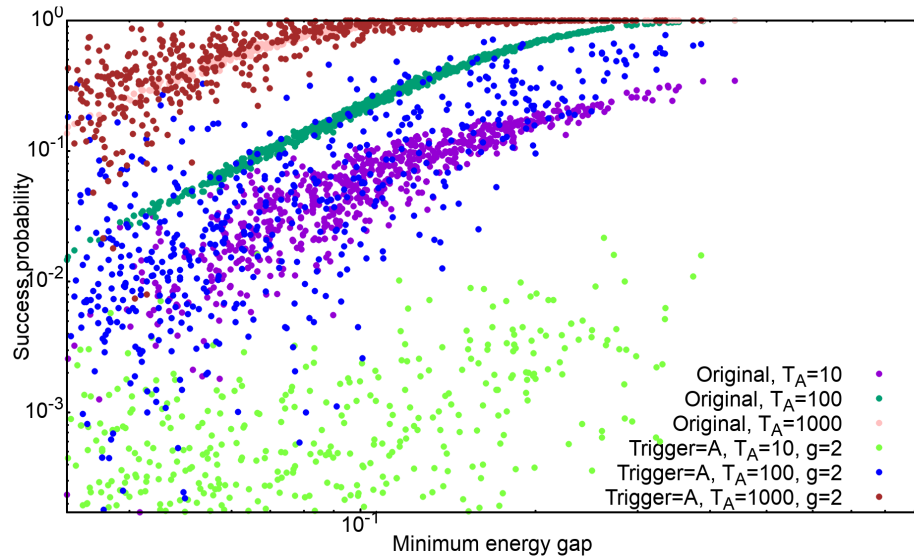


Figure 6.28: Success probability versus minimum energy gap for all the problems belonging to the set of 12-spin SAT problems, for annealing times 10, 100 and 1000, in the absence and presence of ferromagnetic trigger.

can be explained by narrowing of the minimum energy gaps, increase in the number of energy anti-crossings, and distortion of the energy spectra for a majority of the cases. Moreover, compared to Figs. (6.9) and (6.20), the success probabilities after adding the trigger for  $T_A=10$  are much smaller in this case. Lastly, the data points corresponding to the curves after adding the trigger, are not as limited to smaller values of the minimum gap, as there are more problems with an enlarged minimum energy gap in this case.

Thus the consequences of adding an antiferromagnetic trigger are much more complicated than a ferromagnetic trigger, where the minimum energy gaps and the success probabilities are always improved after adding the trigger.

# Chapter 7

## Summary

To solve a SAT-problem by means of quantum annealing, the problem needs to be mapped to the Ising Hamiltonian. The idea of quantum annealing is exploring the energy spectrum of the resulting Hamiltonian by making use of quantum fluctuations induced by the transverse magnetic field in the model. In this work, efforts were made to simulate a quantum annealer to solve 2-SAT problems for a set of 8-spin and 12-spin problems. This requires the time dependent Schrödinger equation to be solved, to obtain the final state of the system under the action of the Hamiltonian. In addition to the two terms commonly used by D-wave for quantum annealing (the initial Hamiltonian and the problem Hamiltonian), a third term, namely the trigger Hamiltonian, was introduced. The objective of this work was to study the effects of including the trigger Hamiltonian on the performance of quantum annealing.

The set of 12-spin 2-SAT problems contained 1000 problems, while that for 8-spin 2-SAT contained 91 problems. There were two types of trigger Hamiltonians employed: a ferromagnetic trigger and an anti-ferromagnetic trigger. Additionally, the strength with which the trigger was added was controlled by means of a variable  $g$ , which was chosen to have values 0.5, 1 and 2, while the annealing time,  $T_A$ , was chosen to be 10, 100 or 1000.

For the 12-spin problems, it was observed that compared to the minimum energy gaps between the ground state and the first excited state of the original Ising Hamiltonian (i.e., in the absence of any triggers), the minimum energy gaps after adding the ferromagnetic trigger were enlarged for all the 1000 problems of the set, for all the three values of  $g$ . Furthermore, for every problem the enlargement of the minimum energy gaps was directly proportional to the strength with which the trigger was added. Consequently, the success probabilities after adding the ferromagnetic trigger for a given  $T_A$ , were larger than the original success probabilities for the corresponding  $T_A$ . This suggests that the evolution of the system state is close to adiabatic in this case, and increasing the strength of the ferromagnetic trigger and the annealing time lead to larger success probabilities.

On the other hand, the effects of adding the antiferromagnetic trigger depend strongly on the strength parameter  $g$ , and the chosen annealing time  $T_A$ , but more so on the problem at hand. For a majority of the problems, the minimum energy gap decreased as a result of adding the anti-ferromagnetic trigger (999 problems for  $g=0.5$ , 879 for  $g=1$ , and 798 for  $g=2$ ). It was also observed that irrespective of the strength with which the anti-ferromagnetic trigger was added, and the chosen annealing time, the success probability of the majority of problems decreased upon including the trigger. Additionally, for larger values of  $g$ , the number of anti-crossings between the ground state and the first excited state also increased. For 12-spin problems, and  $g=1$ , a majority of problems were found to have 2 anti-crossings, while for  $g = 2$  it increased to 3. For  $g=2$ , only a very few problems had a larger success probability for  $T_A=10$ , while the number increased for  $T_A=100$  and  $T_A=1000$ . On the other hand, for  $g=0.5$  and  $g=1$ , the maximum number of cases with improved success probability upon adding the trigger, corresponded to  $T_A=10$ . On increasing the annealing time to 100 and 1000, the number of problems with improved success probability was found to drop in both these cases. This suggests that in most of these cases the success probability increases due to the non-adiabatic evolution of the state. Some of these mechanisms were observed by studying the energy spectrum with instantaneous energy expectation values, or by computing the instantaneous overlap of the system state with a few low lying energy states of the Hamiltonian. It was noted that choosing annealing times small enough for the system state to deviate from the ground state before the anti-crossing, so that some of the amplitude comes back at the anti-crossing, or presence of multiple anti-crossings with small and comparable energy gaps, or a large deviation of the state from the ground state to end in a superposition state with larger overlap with the ground state, can turn out to be advantageous for the success probability.



# **Appendices**



## .1 8-spin Problems

Here, we show some of the important results for the set of 8-spin problems, each consisting of 8 Boolean variables and 9 clauses. Analogous to Fig. (5.4), Fig. (1) shows the scatter plot of the minimum energy gaps after adding the ferromagnetic trigger against the original minimum energy gaps, for all the 8-spin problems. As in the case of the 12-spin problems, all the minimum energy gaps are enlarged as a result of adding the ferromagnetic trigger, for all the three strengths of the trigger. Moreover, the enlargement is directly proportional to the strength of the trigger.

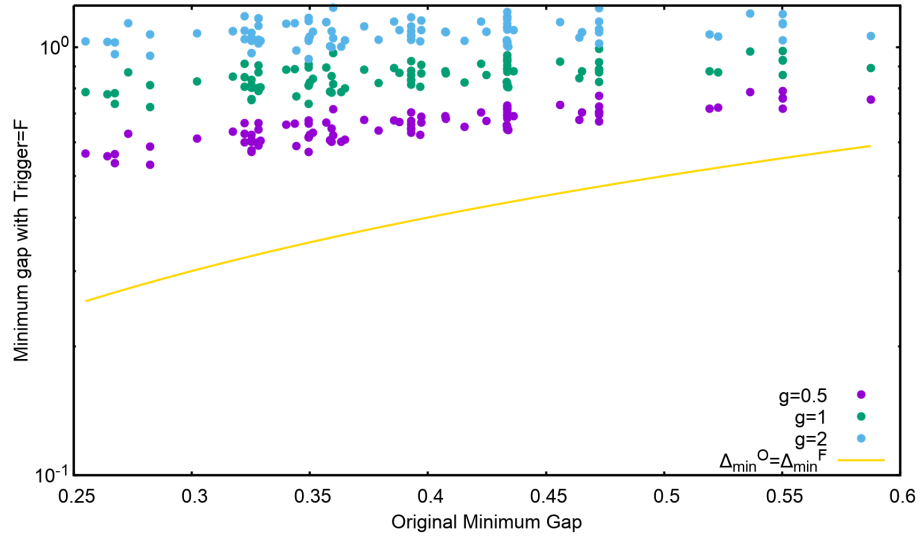


Figure 1: Scatter plot of the minimum gaps upon adding the ferromagnetic trigger with  $g \in \{0.5, 1, 2\}$  against the original minimum energy gaps. The points lying above the solid line represent the problems with an enlarged minimum gap.

The corresponding plot with the antiferromagnetic trigger is shown in Figure (2).

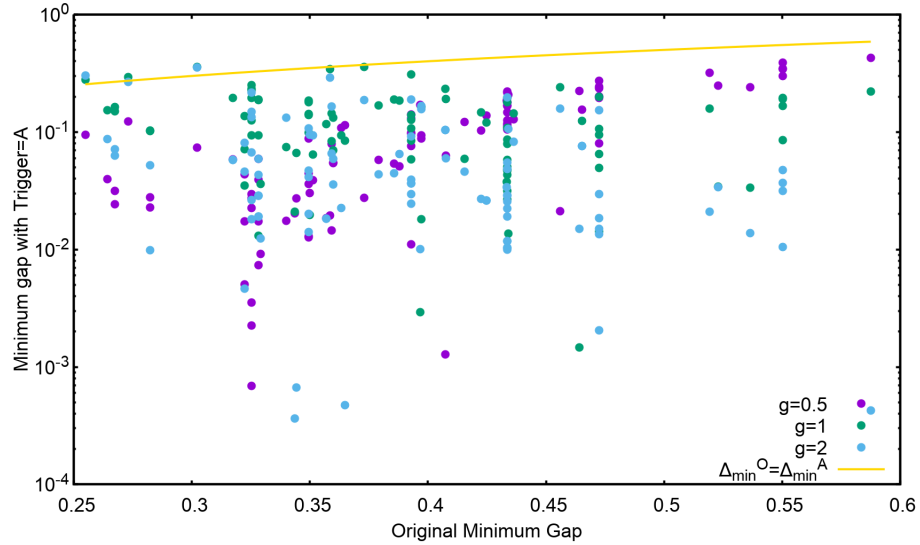


Figure 2: Scatter plot of the minimum gaps upon adding the antiferromagnetic trigger with  $g \in \{0.5, 1, 2\}$  against the original minimum energy gaps. The points lying above the solid line represent the problems with an enlarged minimum gap.

The minimum energy gaps after adding the antiferromagnetic trigger are reduced for almost all the cases. For

$g=1$  and  $g=2$  only two problems have a larger minimum gap after adding the trigger, while for  $g=0.5$ , all the minimum gaps are reduced.

To obtain an estimate of how adding the ferromagnetic trigger affects the success probability of the 8-spin problems, and the range of the affected problems, a scatter plot of the success probability against the original success probability is given in Figure (3). It can be noted that the original success probability in this case, for annealing times of 100 and 1000, is very close to 1, for all the the problems of the set. For this reason the results for only  $T_A=10$  have been shown here.

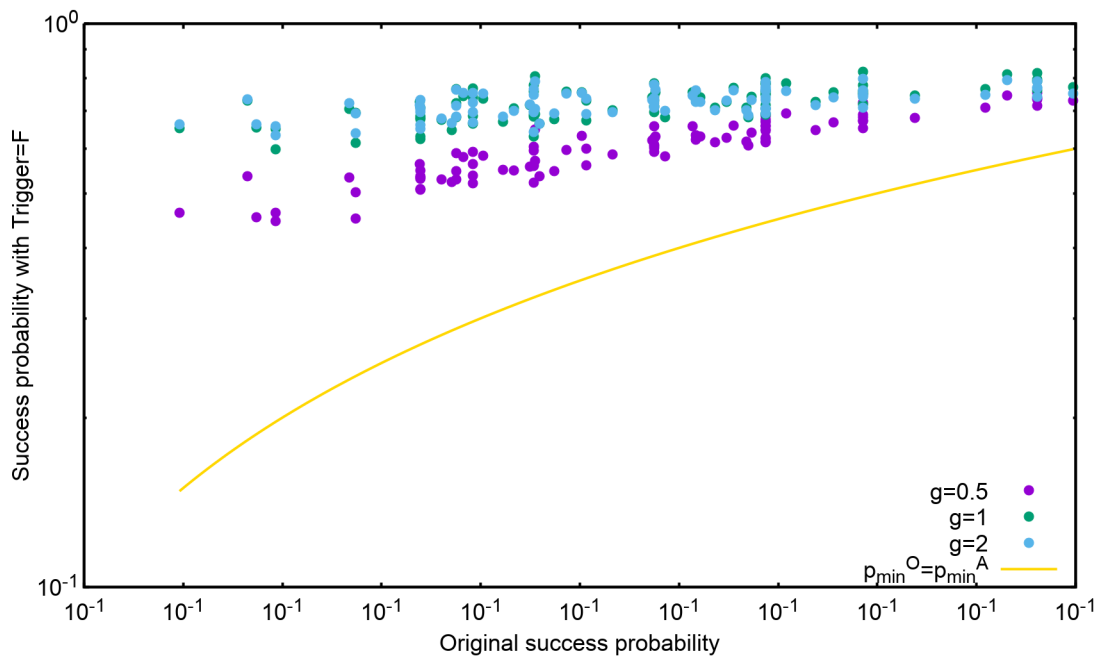


Figure 3: Scatter plot for the success probability after adding ferromagnetic trigger against the success probability of the original Hamiltonian, for  $T_A=10$ , with different strengths. The points lying above the solid line represent the problems with an improved success probability.

From Figure (3) it can be observed that the success probability after adding the ferromagnetic trigger is larger than the original success probability for all the problems. Additionally, on increasing the strength of the trigger, the success probability for a certain problem becomes systematically larger. However, on adding the antiferromagnetic trigger the success probabilities decrease for a majority of the cases (see Figure (4)). Only 3 problems corresponding to  $g=0.5$  and  $g=2$ , and 12 to  $g=1$  have a larger success probability after adding the antiferromagnetic trigger.

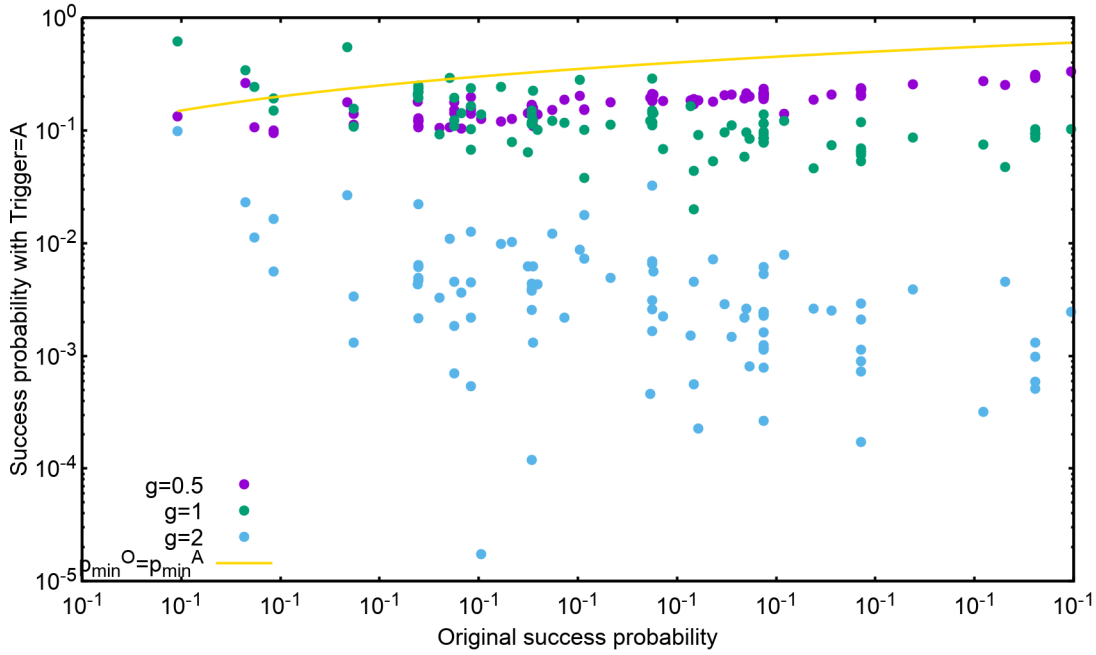


Figure 4: Scatter plot for the success probability after adding antiferromagnetic trigger against the success probability of the original Hamiltonian, for annealing time  $T_A=10$ , with different strengths. The points lying above the solid line represent the problems with an improved success probability.

Finally, a plot of the success probabilities with the minimum energy gaps has been shown before and after adding the triggers, in Figure (5).

The effects of adding the ferromagnetic trigger are very systematic compared to the effects of adding the antiferromagnetic trigger. The minimum gaps become larger with increasing the strength of the trigger, and the success probabilities improve with increasing the annealing time. On the other hand, the overall effect of adding the antiferromagnetic trigger was a significant increase in the scattering of the curves. This trend can be explained on the basis of non-adiabatic mechanisms affecting the success probability for a larger number of problems, since adding the antiferromagnetic trigger reduces the minimum energy gaps for a majority of the problems.

## .2 Modelling the energy levels using effective Hamiltonian approach

For modelling the energy levels after adding the triggers to the original Ising Hamiltonian, the trigger Hamiltonian is regarded as a perturbation to the original Ising Hamiltonian consisting of the initial and the final Hamiltonians, so that

$$H(t) = H_0(t) + H_T(t), \quad (1)$$

where  $H_0$  is the original Hamiltonian, and  $H_T$  is the trigger Hamiltonian.

For this, we will restrict to the first order perturbation theory, and to the lowest lying energy levels of the original Hamiltonian ( $|\psi_0\rangle$  with energy  $E_0$  and  $|\psi_1\rangle$  with energy  $E_1$ ). Then,

$$a'_0 = \langle \psi_0 | H | \psi_0 \rangle = E_0 + \langle \psi_0 | H_T | \psi_0 \rangle = E_0 + a_0, \quad (2)$$

$$a'_1 = \langle \psi_1 | H | \psi_1 \rangle = E_1 + \langle \psi_1 | H_T | \psi_1 \rangle = E_1 + a_1, \quad (3)$$

$$\langle \psi_0 | H(t) | \psi_1 \rangle = \langle \psi_0 | H_T | \psi_1 \rangle = a_2, \quad (4)$$

with  $a'_0$  and  $a'_1$  being the diagonal elements of the effective Hamiltonian. The effective Hamiltonian then becomes

$$H = \begin{pmatrix} a'_0 & a_2 \\ a_2^* & a'_1 \end{pmatrix}$$

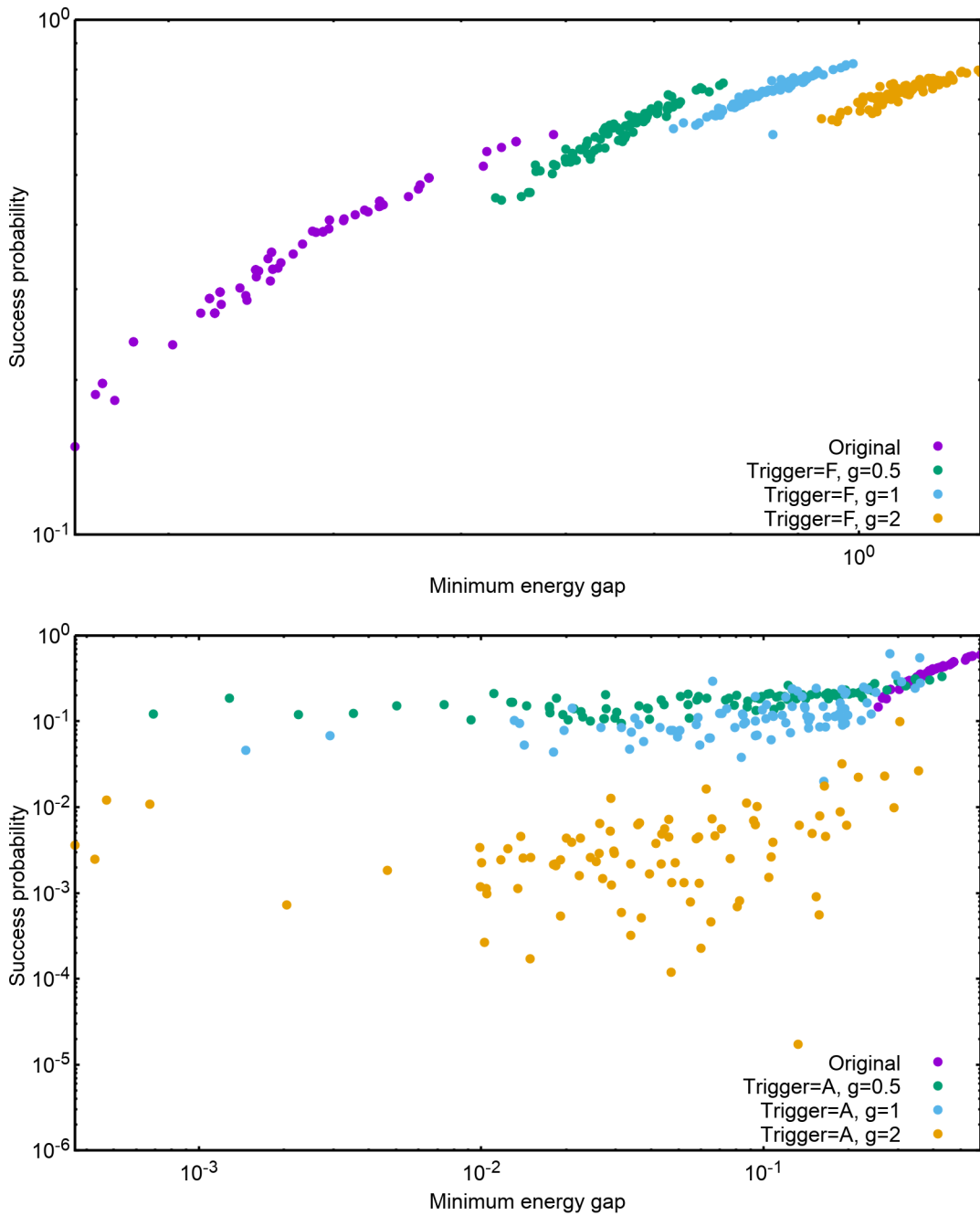


Figure 5: Plot of the success probability versus minimum energy gaps for all the problems belonging to the set for  $T_A=10$ . (a): After adding the ferromagnetic trigger; (b): After adding the antiferromagnetic trigger

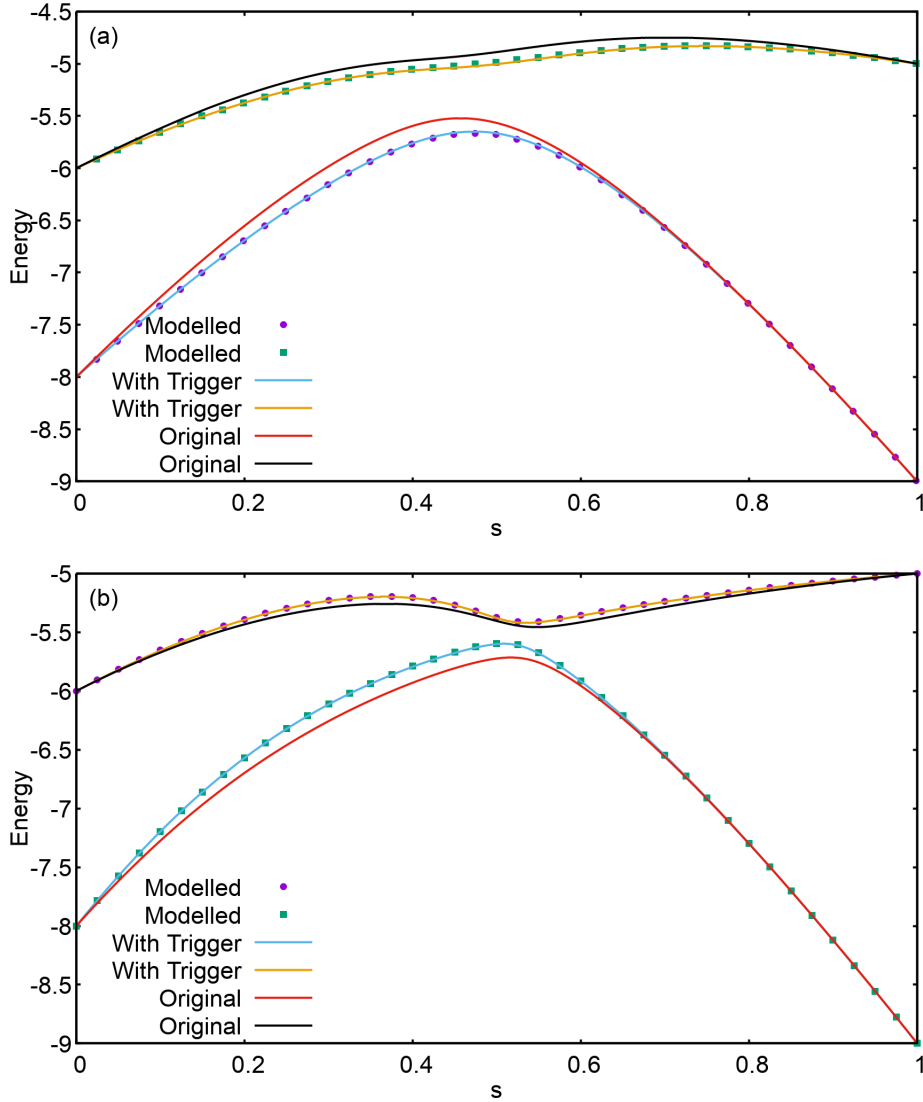


Figure 6: The modelled energy levels after adding the triggers for  $g=0.1$ . (a): Ferromagnetic trigger; (b): Antiferromagnetic trigger. The energy levels obtained for the original Hamiltonian, and the Hamiltonian upon including the trigger Hamiltonian have also been shown.

If  $\Delta_{min}$  is the minimum energy gap between the ground state and the first excited state of the original Hamiltonian, the minimum energy gap between the ground state and the first excited state of the effective Hamiltonian,  $\Delta'_{min}$  is thus given as

$$\Delta'_{min} = \sqrt{(\Delta + a_1 - a_0)^2 + 4a_2^2}. \quad (5)$$

However, in order for the approximation to be valid, the value of the strength parameter,  $g$ , should be small. Thus choosing  $g$  to be 0.1, Figure (6) shows the modelled energy levels for the effective Hamiltonian, for the ferromagnetic and antiferromagnetic triggers. As can be observed from the figure, the effective Hamiltonian model can correctly describe the trend for the change in the minimum energy gap of the original Hamiltonian in both the cases. The energy levels of the Hamiltonian with stronger trigger Hamiltonians, cannot be modelled with only the two lowest lying energy states of the original Hamiltonian, and the higher energy states of the original Hamiltonian also need to be considered. Thus this simple approximation breaks down for higher  $g$  values.

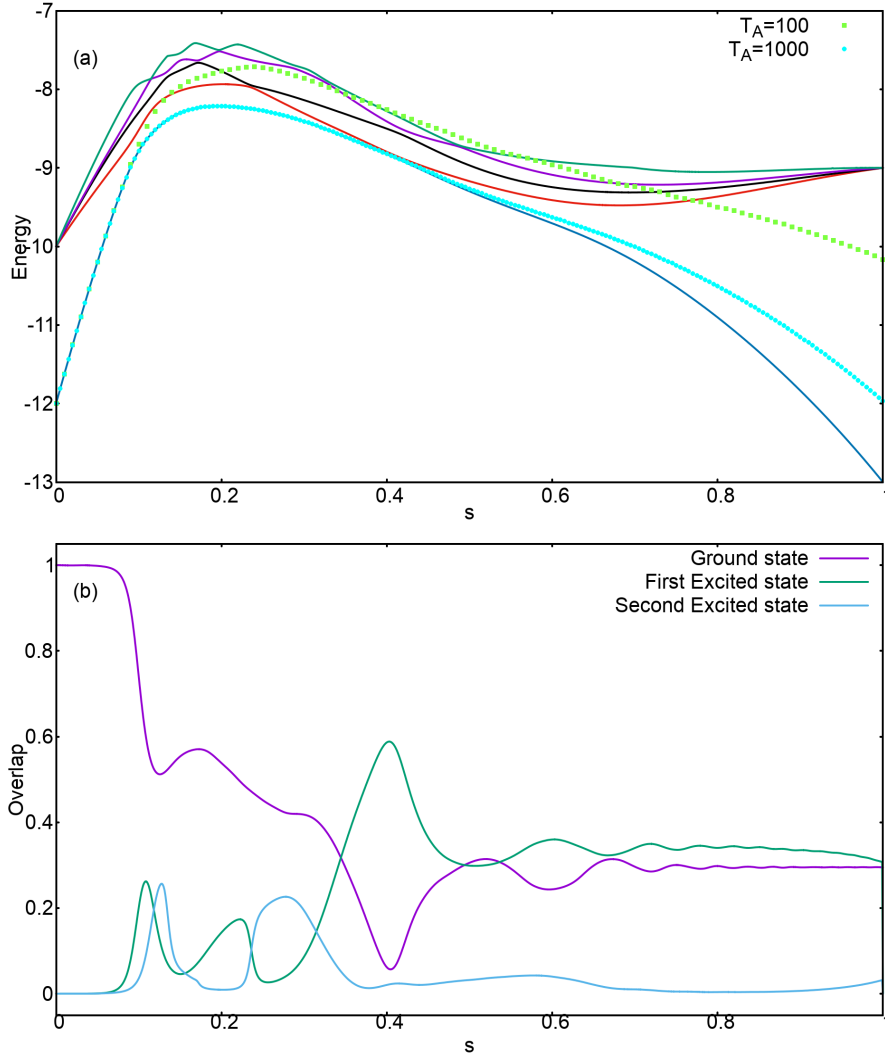


Figure 7: Problem 103: (a): The energy spectra and instantaneous energy expectation values corresponding to  $T_A=100$ , and  $T_A=1000$ ; (b): The overlap of the system state with the three lowest lying energy levels of the instantaneous Hamiltonian for  $T_A=100$ .

### .3 Specific 12-spin problems

Here, the energy spectra with the instantaneous energy expectation values of the state, and the overlap of the state of the system with the three lowest lying energy states of the instantaneous Hamiltonian are shown for some of the problems marked in the middle and bottom panel of Figure (6.24). These are:

- Problem 103, 319, and 705: The main reason for an improvement in the success probability in all of these problems is the proximity of the ground state and the first excited state for a longer time around one of the anti-crossings. The amplitude of the wavefunction of the state that transits to the first excited state at the first anti-crossing, oscillates between these two levels. This leads to a larger overlap of the final state with the ground state of the Hamiltonian. Shown here is the case for problem 103.
- Problem 648 and 709: Both of these cases were found to have two anti-crossings (or crossings). The state of the system shifts most of the amplitude to the first excited state at the first anti-crossing. Most of this amplitude then comes back to the ground state of the Hamiltonian at the second anti-crossing. This explains the improvement in the success probability. Shown here is the case for problem 709.

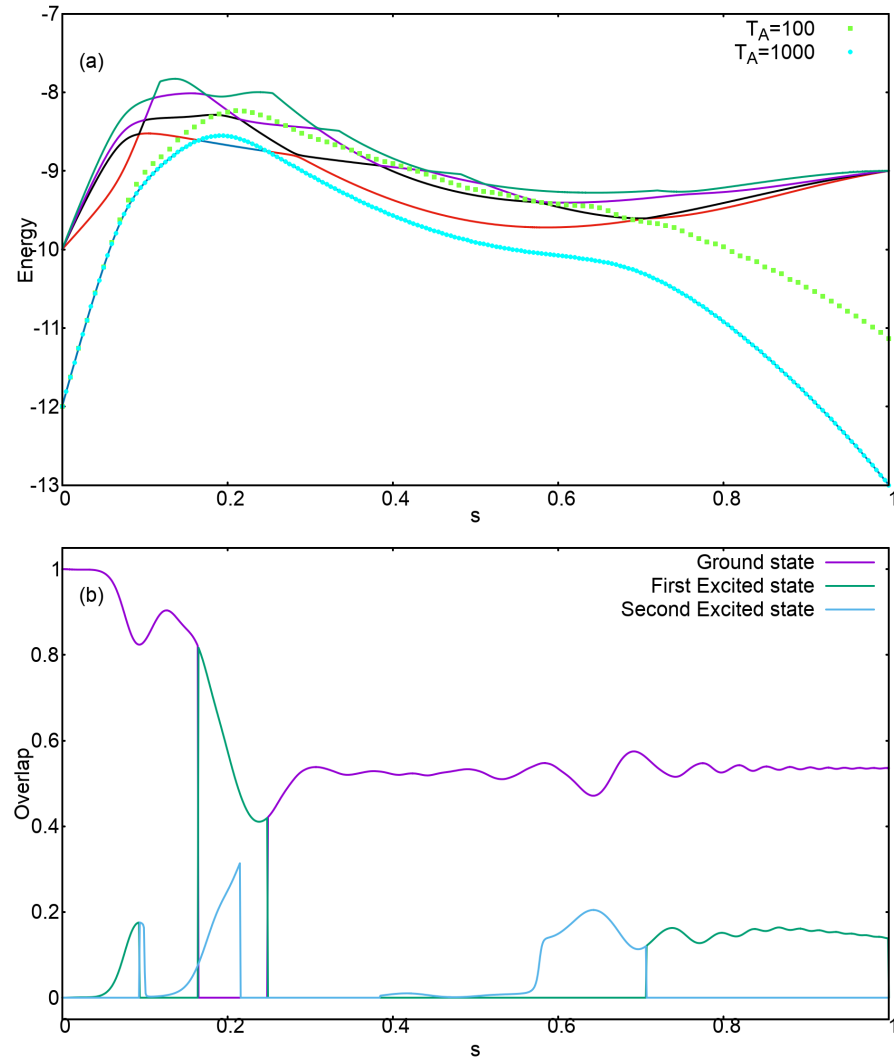


Figure 8: Problem 709: (a): The energy spectra and instantaneous energy expectation values corresponding to  $T_A=100$ , and  $T_A=1000$ ; (b): The overlap of the system state with the three lowest lying energy levels of the instantaneous Hamiltonian for  $T_A=100$ .



# Bibliography

- [1] Tameem Albash and Daniel A. Lidar. Adiabatic quantum computation. *Reviews of Modern Physics*, 90(1), Jan 2018.
- [2] Paul Benioff. Quantum mechanical hamiltonian models of turing machines. *Journal of Statistical Physics*, 29(3):515–546, 1982.
- [3] Richard P Feynman. Simulating physics with computers. *International journal of theoretical physics*, 21(6):467–488, 1982.
- [4] Thaddeus D Ladd, Fedor Jelezko, Raymond Laflamme, Yasunobu Nakamura, Christopher Monroe, and Jeremy Lloyd O’Brien. Quantum computers. *nature*, 464(7285):45, 2010.
- [5] Michael A Nielsen and Isaac Chuang. Quantum computation and quantum information, 2002.
- [6] David Deutsch and Richard Jozsa. Rapid solution of problems by quantum computation. *Proceedings of the Royal Society of London. Series A: Mathematical and Physical Sciences*, 439(1907):553–558, 1992.
- [7] Peter W Shor. Algorithms for quantum computation: Discrete logarithms and factoring. In *Proceedings 35th annual symposium on foundations of computer science*, pages 124–134. Ieee, 1994.
- [8] Lov K Grover. A fast quantum mechanical algorithm for database search. *arXiv preprint quant-ph/9605043*, 1996.
- [9] Philipp Hauke, Helmut G Katzgraber, Wolfgang Lechner, Hidetoshi Nishimori, and William D Oliver. Perspectives of quantum annealing: Methods and implementations. *arXiv preprint arXiv:1903.06559*, 2019.
- [10] Tameem Albash and Daniel A Lidar. Decoherence in adiabatic quantum computation. *Physical Review A*, 91(6):062320, 2015.
- [11] Edward Farhi, Jeffrey Goldstone, and Sam Gutmann. Quantum adiabatic evolution algorithms with different paths. *arXiv preprint quant-ph/0208135*, 2002.
- [12] Elizabeth Crosson, Edward Farhi, Cedric Yen-Yu Lin, Han-Hsuan Lin, and Peter Shor. Different strategies for optimization using the quantum adiabatic algorithm. *arXiv preprint arXiv:1401.7320*, 2014.
- [13] Layla Hormozi, Ethan W Brown, Giuseppe Carleo, and Matthias Troyer. Nonstoquastic hamiltonians and quantum annealing of an ising spin glass. *Physical Review B*, 95(18):184416, 2017.
- [14] Stephen Boyd and Lieven Vandenberghe. *Convex optimization*. Cambridge university press, 2004.
- [15] Ting-Jui Hsu, Fengping Jin, Christian Seidel, Florian Neukart, Hans De Raedt, and Kristel Michelsen. Quantum annealing with anneal path control: application to 2-sat problems with known energy landscapes. *arXiv preprint arXiv:1810.00194*, 2018.
- [16] Neuhaus Thomas. Quantum searches in a hard 2sat ensemble. *arXiv preprint arXiv:1412.5460*, 2014.
- [17] Giuseppe E Santoro and Erio Tosatti. Optimization using quantum mechanics: quantum annealing through adiabatic evolution. *Journal of Physics A: Mathematical and General*, 39(36):R393, 2006.
- [18] Scott Kirkpatrick, C Daniel Gelatt, and Mario P Vecchi. Optimization by simulated annealing. *science*, 220(4598):671–680, 1983.

- [19] Bruno Apolloni, C Carvalho, and Diego De Falco. Quantum stochastic optimization. *Stochastic Processes and their Applications*, 33(2):233–244, 1989.
- [20] Max Born and Vladimir Fock. Beweis des adiabatensatzes. *Zeitschrift für Physik*, 51(3-4):165–180, 1928.
- [21] Edward Farhi, Jeffrey Goldstone, Sam Gutmann, and Michael Sipser. Quantum computation by adiabatic evolution. *arXiv preprint quant-ph/0001106*, 2000.
- [22] Hans De Raedt and K Michelsen. Computational methods for simulating quantum computers. *arXiv preprint quant-ph/0406210*, 2004.
- [23] Hale F Trotter. On the product of semi-groups of operators. *Proceedings of the American Mathematical Society*, 10(4):545–551, 1959.
- [24] Masuo Suzuki, Seiji Miyashita, and Akira Kuroda. Monte carlo simulation of quantum spin systems. i. *Progress of Theoretical Physics*, 58(5):1377–1387, 1977.
- [25] Hans De Raedt and Pedro de Vries. Simulation of two and three-dimensional disordered systems: Lifshitz tails and localization properties. *Zeitschrift für Physik B Condensed Matter*, 77(2):243–251, 1989.
- [26] Hans De Raedt. Product formula algorithms for solving the time dependent schrödinger equation. *Computer Physics Reports*, 7(1):1–72, 1987.
- [27] LD Landau. Zur theorie der energieübertragung i. *Z. Sowjetunion*, 1:88–95, 1932.
- [28] Clarence Zener. Non-adiabatic crossing of energy levels. *Proceedings of the Royal Society of London. Series A, Containing Papers of a Mathematical and Physical Character*, 137(833):696–702, 1932.
- [29] H De Raedt, S Miyashita, K Saito, D Garcia-Pablos, and N Garcia. Theory of quantum tunneling of the magnetization in magnetic particles. *Physical Review B*, 56(18):11761, 1997.
- [30] Seiji Miyashita. Dynamics of the magnetization with an inversion of the magnetic field. *Journal of the Physical Society of Japan*, 64(9):3207–3214, 1995.
- [31] Seiji Miyashita. Observation of the energy gap due to the quantum tunneling making use of the landau-zener mechanism. *Journal of the Physical Society of Japan*, 65(8):2734–2735, 1996.